°Doctor of Philosophy

Environmental controls of vertical motion over the maritime tropics

By

Miguel A. Bernardez

A dissertation submitted in partial fulfillment of

the requirements for the degree of

(Atmospheric and Oceanic Sciences)

at the

UNIVERSITY OF WISCONSIN-MADISON

2023

Date of final oral examination: 6/6/2023

The dissertation is approved by the following members of the Final Oral Committee:

Larissa Back, Professor, Atmospheric and Oceanic Sciences
Daniel Vimont, Assistant Professor, Atmospheric and Oceanic Sciences
Stephanie Henderson, Associate Professor, Atmospheric and Oceanic Sciences
Sam Stechmann, Associate Professor, Math
Angel Adames-Corraliza, Professor, Atmospheric and Oceanic Sciences

Dissertation Declaration and Approval

I, Miguel A. Bernardez, declare that this Dissertation titled 'Environmental controls of vertical motion over the maritime tropics' and the work presented in it are my own.

Miguel A. Bernardez		
Author	Signature	Date

I hereby approve and recommend for acceptance this work in partial fulfillment of the requirements for the degree of :

Larissa Back		
Committee Chair	Signature	Date
Daniel Vimont		
Faculty Member	Signature	Date
Stephanie Henderson		
Faculty Member	Signature	Date
Sam Stechmann		
Outside Member	Signature	Date
Angel Adames-Corraliza		
Faculty Member	Signature	Date

Abstract

Environmental controls of vertical motion over the maritime tropics

by Miguel A. Bernardez

Understanding what controls vertical motion profile shape is fundamental to understanding tropical precipitation patterns. There is not a comprehensive understanding of what controls the top-heaviness of vertical motion in the tropics and through this dissertation I will present novel research towards that task. In the first research chapter, I investigate the two controls which have been proposed in the literature: the thermodynamic profiles of the environment and the dynamics imposed by sea surface temperature (SST) patterns. To fit these two perspectives together, we focus on two regions with distinctly top and bottom-heavy vertical motion: The Western Pacific and the Central Eastern Pacific. The top-heaviness angle is introduced to describe this difference. To study thermodynamic controls on vertical motion profile shape, we use weak temperature gradient (WTG) simulations. We are able to simulate the shape differences between our two regions from the thermodynamics and show that the temperature and SST are the most important for the vertical motion shape differences between our two regions. We show that the qualitative shape differences can be explained using a simple entraining plume model. We hypothesize that the SST gradients lead to a cooler equilibrium lower tropospheric temperature compared with no gradient, this leads to a more conducive thermodynamic environment to bottom-heaviness and the dynamics mechanism controls top-heaviness through the thermodynamics.

In the second research chapter, We present an analysis of observations from the Organization of Tropical East Pacific Convection (OTREC) field campaign. We find that moisture and temperature anomalies are related to the top-heaviness angle. To characterize the moisture profile variability, we introduce a new metric called the moisture dipole coefficient (MDC). We use it in conjunction with the saturation fraction (SF) to show they describe the amount of vertical motion and top-heaviness of vertical motion. We also demonstrate a correlation between the MDC and a measure of dry static stability, which indicates an evolution of moisture and vertical motion profiles such that the atmosphere is driven towards a critical moisture profile that is set by the temperature profile. A simple model of an entraining plume is used to demonstrate how thermodynamic profiles lead to top-heaviness variations and vice versa leading to a balance, which we call vertically resolved moisture quasi-equilibrium (VR-MQE). Finally, the authors show that the process of VR-MQE is not well represented in the forecast model used during the field program.

In the third research chapter, Weak Temperature Gradient (WTG) modeling using a small cloud resolving model (CRM) admits multiple equilibria depending upon the initial model conditions. A new kind of equilibrium is presented here which undergoes a periodic and steady state oscillation which is emergent from static boundary conditions. The periodic oscillation is shown to be a vertical motion moisture mode generated by the interaction between vertical motion and radiation. A simple two-mode model based on decomposing the vertical motion profile is able to describe the oscillation.

Acknowledgements

This dissertation and research would not have been possible without the support of many, many people. Thanks first to Amanda for keeping me from foundering on metaphoric icebergs midway through my journey. I also give deep thanks to my parents, Juan and Tracy, for supporting me through it all and always being there when I needed help. Special thanks to my brother, Rafael, for coming with me to Madison and helping me get established here.

I also need to acknowledge the tremendous effort and patience that Larissa Back gave to support me through the years of research that is included in this dissertation. She propelled me past the many research speed bumps, put up with the long meetings, and made sure that I was was communicating my ideas effectively. Thanks also to the freedom to explore my varied research interests, while also helping to reign in those vary same tendencies when they became too wild. I would also like to thank Ángel Adames-Corraliza for keeping the fire of my research interests stoked and helping to instill a genial nature back into the department. I would also like to thank the rest of the members of my committee - Dan Vimont, Stephanie Henderson, and Sam Stechmann - who tolerated my often cumbersome explanations to help me chisel away the marble block revealing the statue underneath. The professors of AOS have also provided tremendous support and teaching and I'd like to specially thank Elizabeth Maroon, for supporting WXchallenge and being a driving force in the department, Jon Martin and Michael Morgan, for bringing enthusiastic curiosity and humor to department functions, and Grant Petty, for his passion and dedication and always answering my questions. I also need to thank Michael Notarro for being easy to assist as a teacher. Pete Pokrandt for helping tame the computers that I needed for my research and for his calm during some of the more anxious moments.

I also need to thank my friends and fellow grad students. Thanks to Zoe, Kelton and Juliet for being a needed social outlet during the depths of despair during the pandemic. Thanks to Maggie and Julia for being wonderful class mates and setting an example of

how to make it through graduate school. And most importantly thanks to Vijit for being the best lab-mate that one could hope for. Thanks to Andrew for keeping me going to the gym, always being inviting and welcoming, and driving me to be a better person. Thanks to Megan and Luke for all of the game nights, dinners, softball games, and for including me in your family Christmas when I couldn't make it home. Thanks to Rachel and Seth for helping to make the last few years easy enough to actually finish.

This is absolutely non-comprehensive and the words cannot convey the depth of my feelings towards everyone who helped my achieve my dreams. Thank you!

Contents

List of Figures

List of Tables

Abbreviations

CRH	**C**olumn **R**elative **H**umidity
CRM	**C**loud **R**esolving **M**odel
CWV	**C**olumn **W**ater **V**apor
DE	**D**riven **E**quilibrium
DSE	**D**ry **S**tatic **E**energy
ECMWF	**E**uropean **C**enter (for) **M**edium **R**ange **F**orecasting
EOF	**E**mpirical **O**rthogonal **F**unction
GCM	**G**lobal **C**limate **M**odel
GCM	**G**eneral **C**irculation **M**odel
II	**I**nstability **I**ndex
IFS	**I**ntegrated **F**orecasting **S**ystem
ITCZ	**I**nter**T**ropical **C**onvergence **Z**one
LCL	**L**ifted **C**ondensation **L**evel
LHS	**L**eft **H**hand **S**ide
MDC	**M**oisture **D**ipole **C**oefficient
MJO	**M**adden-**J**ulian **O**scillation
MSE	**M**oist **S**tatic **E**nergy
MQE	**M**oisture **Q**uasi **E**equilbrium
OTREC	**O**rganization (of) **T**ropical **E**ast **P**acific **C**onvection
RCAE	**R**adiative **C**onvective **A**dvective **E**equilbrium
RCDE	**R**adiative **C**onvective **D**ynamic **E**equilbrium

RCE	**R**adiative **C**onvective **E**equilbrium
RH	**R**elative **H**umidity
PCA	**P**rincipal **C**omponent **A**nalysis
POD	**P**rocess **O**riented **D**iagnostics
SF	**S**aturation **F**raction
SWTG	**Spectral**hat **W**eak **T**emperature **G**radient
VR-MQE	**V**ertically **R**esolved **M**oisture **Q**uasi **E**equilbrium
WRF	**W**eather **R**esearch (and) **F**orecasting (model)
WTG	**W**eak **T**emperature **G**radient

Physical Constants

latent heat of vaporization	L_v	=	2.5e6 (J/g)
specific heat capacity	c_p	=	1004 (J/kg/K)
gravitational acceleration	g	=	9.81 (m/s/s)

Chapter 1

Introduction

The goal of this dissertation is to add to our understanding of vertical motion and what controls the shape of its profile. The nature of vertical motion is to entwine complicatedly with other atmospheric phenomena, always lurking in the shadows of our ignorance of deep convection. Maritime tropical vertical motion, and importantly the shape of its vertical profile, is important to the distribution of moisture in the atmosphere (Masunaga and Mapes, 2020, Peters and Bretherton, 2006), differences in radiative heating (Back et al., 2017), the general circulation (Riehl, 1950) and the distribution of rain (Sobel and Bretherton, 2000). It is central to how both mass and energy are constrained and is connected to both the dynamics and thermodynamics being affected by the radiational heating, surface heat fluxes, and thermodynamic state (Raymond, 2000, Raymond and Flores, 2016, Raymond et al., 2014), while also by horizontal convergence and large-scale circulation (Back and Bretherton, 2009a,b). In this dissertation, I will explore some of

the different ways that vertical motion is important to the tropical system, explain what is currently known about it and its controls, and share research that I have conducted to improve our understanding of what controls vertical motion, with the goal of improving our understanding of all of the different aspects of the tropical system that vertical motion touches, and improve our ability to forecast weather and climate conditions.

Before I work on fitting the puzzle piece of vertical motion profile shape into the mosaic of the tropical atmosphere, I will lay out the properties of the vertical motion shape and its distribution that I am interested in describing. Vertical motion profile shape is deceptively simple as it tends to only have two modes of variability, although that does not stop many people from only looking at the 500 hPa velocity. The two modes of variability can be represented using the velocity in two different levels (Ahmed and Neelin, 2018), the gravest gravity modes (Mapes, 1993), or using principal component analysis to explain the most variability (Back and Bretherton, 2009a). For the last example, I find that a vast majority ($> 85\%$) of the variance can be explained by the first two modes (Back et al., 2017, Inoue et al., 2020a). I am investigating the shape of the vertical motion and not the magnitude, and in analogy to a transform to polar coordinates this can be captured using the angle between the two modes, called the top-heaviness angle. The relationship between the top-heaviness angle and the shape of the profile of vertical motion is shown in figure (3.1). Angles near zero are ascending profiles with a peak in the middle of the atmosphere. As the angle increases or decreases, the vertical motion profile becomes more top or bottom-heavy respectively. As the angle moves towards positive or negative 180 degrees, the vertical motion profile becomes descending.

The color map used in this figure was made expressly to highlight the important features of the vertical motion. Green, which is the easiest for the human eye to see, highlights the areas of the atmosphere that are descending leaving the rest of the area to be ascending. Within the ascending region, the difference between top and bottom-heavy vertical motion is shown with a red-blue color difference. The transition between two different kinds of ascending motion smoothly transitions through purple, which highlights the smooth transition that vertical motion undergoes between top and bottom-heavy vertical motion. The effect can be seen in figure (2.1), which shows the mean vertical motion profile shape, through the top-heaviness angle, for the 40-year climatology. The intertropical convergence zone (ITCZ) is highlighted against the surrounding descending air shown in green. Within the ITCZ, I can see distinct regions of top or bottom-heavy vertical motion, with the Eastern and Western Pacific showing a distinctly different top-heaviness angles. These are the two regions of interest in the first research chapter and will be used as exemplars in order to improve the description of the controls of top-heaviness.

With the basic nature of tropical vertical motion profile shape laid out, I move onto the current understanding of the controls found in the literature. A suspiciously convenient starting point for understanding this distribution of the top-heaviness angle, and the importance of top-heaviness variability to the atmosphere, is the weak temperature gradient (WTG) approximation framework. The WTG approximation assumes that horizontal gradients of temperature are small because they are quickly redistributed by gravity waves. Unlike the mid-latitudes, where rotation allows for cold and warm fronts to form, the tropics show very weak temperature gradients (Sobel and Bretherton, 2000,

Sobel et al., 2001). This leaves the vertical motion as the main force keeping the atmospheric temperature profile from changing with time. The controls of top-heaviness are the controls of the profile of heating and of the persistence of temperature anomalies.that are

A convenient measure of the temperature is the dry static energy (DSE), which is the sum of the thermal and gravitational potential energy of air $s = c_p T + gz$. s is the DSE, T is the temperature of air, Cp is the specific heat capacity of dry air, g is the gravitational acceleration rate, and z is the altitude. The DSE is only altered by heating or pushed around by the winds, which can be seen in the budget equation:

$$\frac{\partial s}{\partial t} + \vec{v} \cdot \nabla_h s + \omega \frac{\partial s}{\partial p} = Q_1.$$

The first term on the left hand side (LHS) of the equation is the time-tendency of DSE, the second term is the horizontal advection which can be ignored thanks to the WTG approximation, and the last term is the vertical advection term. The RHS balances this through the apparent heating which combines the vertical eddy transport, radiation, and the evaporation or condensation of moisture, called the latent heating (Yanai et al., 1973). I also ignore the time-tendency of DSE because the time-scale of interest is much larger than the temperature relaxation time-scale. WTG also means I can ignore the horizontal advection term leaving our budget equation as:

$$\omega \frac{\partial s}{\partial p} = Q_1$$

.

Ostensibly predicting vertical motion is down to predicting the profile of apparent heating. The profile of apparent heating is difficult to predict in part because important processes operate at scales that I am currently unable to feasibly resolve. This is exemplified by our large global climate models (GCMs) requiring a parameterization for microphysics, radiation, clouds, aerosols and other constituents, surface fluxes, turbulence, and finally a deep convection parameterization to calculate the vertical motion (Bechtold et al., 2008). These parameterization seek to cleverly simplify the complex atmospheric processes and create a computing task of tractable size. For the purpose of understanding vertical motion the parameterizations can be split into two groups, the moist convection scheme and the other schemes that have an effect on moist convection. Next I will lay out what I understand of these two groups and how they relate to the vertical motion shape that is the subject of my research.

The latent and radiative components of the apparent heating are both highly dependent upon the moisture in the atmosphere, dropping the first breadcrumb of the path to vertical motion. The radiative heating differences which are controlled by the moisture through the clouds, rain, and ice shading the surface from solar shortwave heating and through the much higher and colder cloud tops radiating less heat to space (Bony and Emanuel, 2005, Johnson and Ciesielski, 2000). The shortwave shading cools the surface and does not directly impact the atmospheric heat budget and the long-wave heating effects act as a source of anomalous heating and affects the vertical motion.

The latent heating of condensation and evaporation of moisture is much more clearly a function of the moisture. The more moisture there is in the atmosphere, the greater the tendency for moisture to condense and fall out as rain (Bretherton et al., 2004, Raymond, 2000). While the simple relationship between moisture and precipitation has been well-established, the details of the relationship and how it affects vertical motion is not well established. I know that in analogy to the speed of light, it would take an infinite amount of energy to completely saturate the atmosphere, which would also come at the limit of infinite precipitation (Raymond, 2000).

These two important factors to the vertical motion shape are dependent on moisture which indicates that the variability of vertical motion should be closely tied to moisture variability. The distribution of column moisture in the tropics, just like the variability of vertical motion, tends to follow a bimodal distribution with a set of columns that are dry and a set of columns that are moist and precipitating (Mapes et al., 2018). The margin between the dry and moist regions tends to shape and is maintained in part by the vertical motion (Masunaga and Mapes, 2020). When considering the time-evolution of moisture, and thus convection and vertical motion, the atmosphere follows a cyclical recharge-discharge pattern where moisture in the column increases along with precipitation until a critical point where convection becomes active enough that the moisture decreases and precipitation ceases (Maithel and Back, 2022).

Vertical motion plays an important role in these processes and in the determination of the

distribution of moisture. This interaction between moisture, convection, and vertical motion is generally studied and understood through a concept called the gross moist stability (GMS) (Neelin and Held, 1987, Raymond et al., 2009). The GMS is essentially a measure of how much the energy of the atmosphere will change during and for a given amount of convection, and is defined as the ratio of a measure of a variable that is conserved moist adiabatically to a measure of the precipitation. In this work I use the vertical advection of DSE as the measure of precipitation and MSE as the variable moist adiabatically conserved. Related quantities are usually labeled as "adjective"+GMS (e.g. vertical GMS) and are defined as the ratio of sources of a variable that is moist adiabatically conserved (e.g. vertical advection of MSE) to the same measure of precipitation, which provides an idea of how convection and precipitation responds to that particular convective forcing (Inoue et al., 2020a, Inoue and Back, 2017). The GMS is a useful metric because, as the original authors (Neelin and Held, 1987) put it, "provides a convenient way of summarizing our ignorance of the details of the convective." Assuming that the GMS can be determined a priori, it is able to predict the amount of precipitation that will result from an amount of convective forcing. One question this research seeks to help answer is about how to determine the GMS related to vertical motion.

Expounding on the details of convection that the GMS summarizes, I next look at the relationship between moisture and latent heating. Two key atmospheric levels of importance when considering moist processes are the -10 C and -40 C temperature levels, which are important to how ice forms and has large impacts on both latent heating (Romps and Kuang, 2010) and radiative heating (Dai and Bloecker, 2019). Other specifics like the

presence of cloud condensation nuclei or the mass of liquid and frozen water that can be suspended in air are important for determining how much moisture will condense or freeze, which can affect the vertical motion (Abbott and Cronin, 2021). Additionally the evaporation of rain as it falls is important for the large-scale moisture profile and driving circulations through processes like downdrafts and cold pool formation (Tompkins, 2001).

A way of circumventing the need to directly simulate the messy and complicated conversion of latent to sensible heat is to use the moist static energy (MSE), which is the combination of DSE and moisture: $h = s + L_v q_v$. Here h is the MSE, Lv is the latent heat of vaporization, and qv is the specific humidity. The MSE is an important metric because it is conserved moist adiabatically, including precipitation. The available potential energy to convection and vertical motion is also proportional to MSE anomalies. The WTG approximation and the DSE remaining fairly constant in time means that variations in MSE are supplied mostly by the moisture profile. This is revealed by the budget of MSE:

$$\frac{\partial h}{\partial t} + \vec{v} \cdot \nabla_h h + \omega \frac{\partial h}{\partial p} = Q_{rad} + Q_{surf} + \frac{\partial \omega' h'}{\partial p}.$$

Like the DSE budget, the first term on the LHS is the tendency of MSE, the second term is the horizontal advection of MSE, and the third term is the vertical advection of MSE. The RHS has radiative heating and the heat fluxes from the surface, and the vertical eddy transport of MSE.

When I apply the WTG approximation, the MSE budget equation becomes:

$$L_v \frac{\partial q_v}{\partial t} + \omega \frac{\partial h}{\partial p} - Q_{rad} = -L_v \vec{v} \cdot \nabla_h q_v + Q_{surf} + \frac{\partial \omega' h'}{\partial p}.$$

The tendency and horizontal advection of MSE becomes the tendency and horizontal advection of moisture. Additionally the radiation and horizontal advection of MSE have been moved to the opposite side of the equal sign in order to group them with like terms. The radiation varies with changes in the vertical motion and MSE, so I can combine their effects, which is an accurate reflection of real world variability (Back and Bretherton, 2009a, Masunaga et al., 2021).

Whether the vertical advection of MSE alone leads to an increase in MSE is dependent on the top-heaviness of vertical motion. This is because the top-heaviness changes the level where the circulation associated with vertical motion switches from converging to diverging. This is called the level of non-divergence and is located at the level where the vertical speed is maximized. Air above this level is exported out of the atmospheric column and air below this level is imported. The minimum of MSE is in the middle of the atmosphere and whichever layer, diverging (above) or converging(below), which overlaps with the middle of the atmosphere will tend to be smaller. This means bottom-heavy vertical motion tends to import MSE and act to amplify convection and top-heavy vertical motion tends to export MSE and reduce convection.

The radiational heating and vertical advection of MSE can be combined into an effective

vertical advection of MSE and its effect on the amplification of convection is captured by the effective GMS. Changes in the effective vertical advection tend to be small as the changes in radiation balance changes in vertical advection due top-heaviness of vertical motion, which causes the effective GMS to be near zero (Inoue et al., 2020a, Inoue and Back, 2015b). I do not know to what extent this balance exists, for what scales it can be assumed to hold true, and under what conditions I can apply the condition. Regardless of our understanding of the balance between radiation and vertical MSE advection, it means that do not lead to MSE differences that I can use to predict future atmospheric states.

The horizontal advection of moisture, and the other heating terms on the RHS of the MSE budget alter the MSE and lead to convective amplification and decay. The horizontal advection of moisture is the driver of convective variability on daily time-scales (Inoue et al., 2020a) and can often be predominantly determined by processes that are independent of the vertical motion and occur outside of the column of interest (Wang et al., 2016), so I can treat some of the horizontal advection as a convective forcing that is independent of the vertical motion.

The longer timescales, where the atmosphere is essentially in a steady state and I am not concerned with the evolution, are constructed from an ensemble of the convective evolution. By understanding how the ensemble is controlled, I can constrain the possible behaviors of the atmosphere and develop diagnostics for testing how well a particular

convective parameterization is able to represent vertical motion. There are two mechanisms that have been proposed to understand the controls of vertical motion over these longer time-scales: the underlying distribution of SSTs (Back and Bretherton, 2009a,b, Lindzen and Nigam, 1987, Sobel and Neelin, 2006) and the environmental thermodynamics (Raymond and Flores, 2016, Raymond et al., 2015, 2009). The underlying SST determines surface heat fluxes and drives near surface convergent flows (Back and Bretherton, 2009a). The environmental thermodynamics helps to determine the profile of latent heating. These two mechanisms are not mutually exclusive and must be reconciled to deepen our understanding of top-heaviness. With the characters and stage set, I can tell the story of tropical convection as it currently stands and highlight what I do not yet know.

The atmosphere state begins with some initial moisture profile and some amount of convective forcing which is trying to increase the moisture. As the amount of moisture in the column builds, the vertical motion and precipitation both also increase. The increase in precipitation acts as a negative moisture tendency until it matches the moisture tendency provided by the convective forcing. The effective vertical advection does not have much of an effect in convective amplification or decay, which is convenient for not driving a snowball effect. The convective forcing then drops away and the precipitation drains the moisture out of the column, which completes the recharge-discharge cycle.

This story is a good description of how convection operates in the tropics, however I do not understand many of the details of this process. The details of how and why

vertical advection and radiation tend to balance, the predictability of the top-heaviness which helps drive this balance and redistributes moisture, and a simple way of explaining top-heaviness are all still needed. This can be seen in the difficulty that I have in parameterizing deep convection which leads to biases in the climatological distribution of precipitation (Dai, 2006), the large disagreement between model representations of vertical motion shape and latent heating profiles (Hagos et al., 2010), and difficulty forecasting tropical cyclones (Emanuel and Zhang, 2016). In order to improve these areas, and more, I must develop a comprehensive theory of tropical vertical motion. Three ways to gain a deeper understanding are: computer simulations that are able to resolve the details of convection, a study of observations which I know to contain the details, and a simple analytical math model built upon the first principles which can tell us what details are the most important. The research presented here looks to progress our understanding of what controls top-heaviness using all three methods.

In the first research chapter, I investigate two mechanisms that have been proposed in the literature to control the top-heaviness using a cloud resolving model with a parameterization for vertical motion provided by the WTG approximation. The CRM simulates convection and the WTG parameterization calculates the vertical motion that is needed to counteract the heating from convection. This allows us to simulate the response of vertical motion to different environmental factors. I simulate the climatology of two regions with distinctly top and bottom-heavy vertical motion profiles in order to test whether I can simulate the top-heaviness differences and to understand what aspects of the two mechanisms are driving the observed vertical motion shape differences. The two

mechanisms that I am investigating are a dynamic mechanism where the top-heaviness is determined by the distribution of surface conditions and a stability mechanism where the top-heaviness is due to differences in the large-scale atmospheric stability. The model is not able to explicitly represent the dynamic mechanism, which additionally lets us determine if the dynamic mechanism needs to be explicitly imposed or if it acts through the stability mechanism.

The second research chapter investigates observations of vertical motion and its environment from a field campaign which observed the Eastern Pacific and Western Caribbean. The climatologically bottom-heavy vertical motion in these regions is not as well studied as the top-heavy vertical motion in the Western Pacific over the warm pool and is not as well represented in our modeling efforts. I characterize the vertical motion that was observed during the field campaign, along with the thermodynamic environment that it exists in. This allows us to develop diagnostic criteria for model representations of the processes involved in the determination of top-heaviness. I compare the observational data to a forecast model of the same area and time to demonstrate the processes are not currently well represented and show the need for the process oriented diagnostics that are developed.

In the final research chapter, I present modeling results demonstrating a steady state oscillation in a WTG framework which resembles, and is, a vertical moisture mode. WTG modeling is prone to a behavior called multiple equilibria, where the model will move towards either a dry equilibrium or a moist equilibrium depending on the initial conditions

of the model. The new equilibrium state that I present is a moist, precipitating state that is entirely distinct from the usual moist equilibrium. The vertical motion, moisture, and precipitation oscillate in tandem consistent with a mode of variability called a moisture mode. Moisture modes are characterized by an adherence to WTG, column energy variability which is driven primarily by moisture variability, and a tight coupling between precipitation and moisture. They are an essential aspect of the tropical weather system, however they are traditionally associated horizontal, not vertical advection. In order to better understand these periodic oscillations and vertical moisture modes, I use a simple model based on the two mode decomposition of vertical motion. This simple model is able to explain the oscillation and acts as a linearization of the complexities of convection. If the linearizability can be established, and the coefficients of the model solved before running a WTG simulation, the two mode model represents a powerful tool for comparing different representations of convection.

In the final concluding chapter, I will give an overview of the results that are presented herein. The impacts of these results and the conclusions that I draw will be presented along with a discussion of the important questions that remain unanswered.

Chapter 2

Integrating thermodynamic and dynamic views on the control of the top-heaviness of convection in the Pacific ITCZ with weak temperature gradient simulations

2.1 Introduction

I have trouble simulating the tropical rainfall distribution because it entails interactions between many different systems across a multitude of scales, from cloud clusters (Yanai

et al., 1973) to large-scale features like the Madden-Julian Oscillation (MJO) (Madden and Julian, 1971) to the slowly evolving climatological state (Riehl and Malkus, 1958). Vertical motion plays a central role in this problem and to the tropical rainfall distribution because it is directly tied to latent heating from rain through the dry static energy (DSE) budget(Handlos and Back, 2014, Yanai et al., 1973). The shape of the vertical motion profile in particular, is essential to how the tropical system behaves across a range of timescales and waves (Back and Bretherton, 2006, Gjorgjievska and Raymond, 2014, Inoue et al., 2020b, Inoue and Back, 2015a, Kang et al., 2009, Schumacher et al., 2004, Sherwood et al., 2014).

Despite the importance of vertical motion profile shape to the tropical atmosphere, our understanding of the underlying processes that determine this shape is incomplete (Back et al., 2017, Hagos et al., 2010). In this work, I examine and integrate 2 mechanisms that have been proposed for how vertical motion is controlled. Our limited understanding of the controls and of the vertical motion profile shape to the tropics make it a natural target for creating process oriented diagnostics (PODs) that can help us understand vertical motion and improve our diagnosis of simulations of vertical motion. Our goal in this work is to develop our understanding, which can then be used to create process-oriented diagnostics and ultimately improve our models and our ability to project and forecast what will happen in the tropics.

In this research, I focus on the causes of the difference between a region with climatological top-heavy vertical motion where maximum vertical velocity is in the upper troposphere,

versus a region with bottom-heavy vertical motion where the maximum vertical motion occurs in the lower troposphere. I use the regions found by Back and Bretherton (2006) to have consistently top-heavy or consistently bottom-heavy vertical motion: the Western and Central-Eastern Pacific boxes (shown in figures 2.1 and 2.2). These regions are chosen because reanalyses and AGCMs agree on whether they are top-heavy or bottom-heavy (see Back and Bretherton (2006)), while in many other regions and times throughout the tropics there is much less agreement between models and different observationally derived products. Figure (2.1a) shows the top and bottom-heavy vertical motion profiles which are a result of the different conditions between the two regions. Both of our chosen regions have similar amounts of rainfall, column water vapor, and horizontal moisture transport and yet they achieve this energetically in different ways due to the different vertical motion shapes (Back and Bretherton, 2006). Throughout the rest of this chapter, I will refer to variables from the Central-Eastern Pacific as bottom-heavy and I will refer to the variables from the Western Pacific as top-heavy, so the top-heavy SST is the SST from Western Pacific box.

Figure (2.1 c) shows the climatological pattern of top-heaviness throughout the tropics using a new measure that I have created called the top-heaviness angle. This top-heaviness angle is an extension of the top-heaviness ratio created by Back et al. (2017), which utilizes the first two modes of a vertical decomposition of the vertical motion. The first two modes when the vertical motion is decomposed into a set of empirical orthogonal functions are responsible for greater than 85% of the vertical motion variability (Back and Bretherton, 2009a, Back et al., 2017). The ratio of the second to the first mode provides a compact

representation of the top-heaviness which has been normalized by magnitude of vertical motion. The top-heaviness angle is found by taking the arctangent of this ratio, which gives an angle representation of the top-heaviness. The top-heaviness angle has the benefit of being well defined for for all vertical motion, as opposed to defined for either upward or downward vertical motion. The legend for the top-heaviness angle and the colormap that I use to visualize it are shown in figure (2.1b). Angles near zero represent strongly ascending regions, while angles near 180° represent descending regions. Positive angles near zero represent more top-heavy profiles and negative angles near zero represent more bottom-heavy profiles.

Previous research has identified two mechanisms that control the climatological distribution of top-heaviness shown in figure 2.1. The first mechanism depends partially on surface convergence caused by the distribution of SSTs, which I call the dynamic mechanism (Back and Bretherton, 2009a,b, Duffy et al., 2020, Lindzen and Nigam, 1987). The second mechanism, which I call the stability mechanism, focuses on the role of the large-scale thermodynamics (Raymond et al., 2015, Raymond and Sessions, 2007, Sessions et al., 2019).

The dynamic mechanism describes the top-heaviness using the surface conditions, specifically the distribution of SSTs and the laplacian of SST, which indicates where the gradients of SST are the largest, are shown in figure (2.3). The SSTs in the top-heavy box are around 2K higher and the gradients of SST in the bottom-heavy box are much greater.

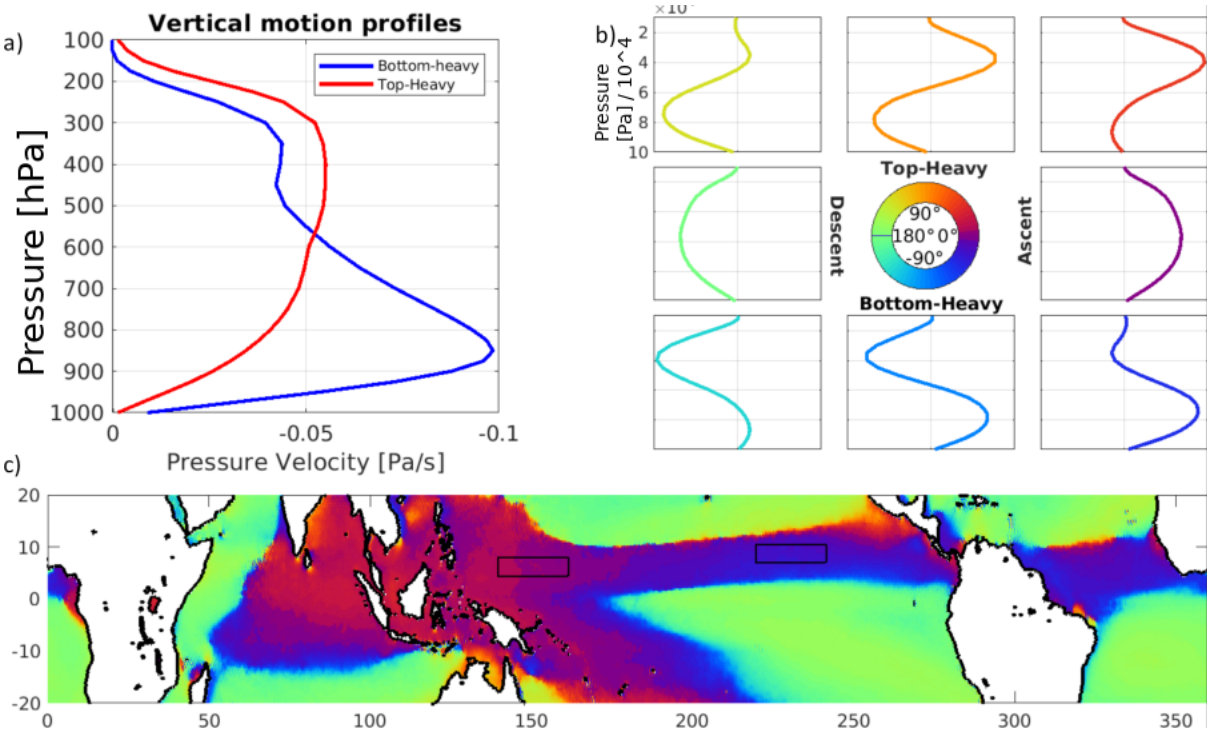

FIGURE 2.1: Geographic variability of vertical motion in the tropics is shown with the top-heaviness angle, along with the vertical motion from the top and bottom-heavy boxes that I am studying and a legend to understand the top-heaviness angle. (a.) Top and Bottom-heavy vertical motion profiles from the two indicated boxes, which serve as the regions of interest for this study. (b.) Color legend showing variability of vertical motion shape according to top-heaviness angle. (c.) Map of the variability of vertical motion shape shown using the top-heaviness angle over the tropics for the ERA5 climatology between 2007-2017.

The dynamic mechanism begins with a surface convergence that is caused by SST gradients, diagrammed in figure (2.2)(Lindzen and Nigam, 1987). SST gradients lead to boundary layer temperature gradients which lead to bent isobars in the boundary layer. In association with friction, these bent isobars lead to a convergent flow and vertical motion near the surface. Back and Bretherton (2009a) found that in the bottom-heavy box, the monthly and longer time-averaged surface convergence, and thus lower tropospheric vertical motion, is primarily due to the SST gradients on these timescales. Their companion paper Back and Bretherton (2009a) argued that the greater top-heaviness of

vertical motion in the top-heavy box, compared to the bottom-heavy box, is attributable to the difference in relative SST in the two regions (Back and Bretherton, 2009b). A higher SST is correlated with a greater atmospheric potential energy, which is associated with deeper and thus more top-heavy vertical motion. The magnitude of the SST and its gradients can be used to create a simple model that predicts the distribution of vertical motion shape and precipitation in reanalysis and GCMs (Back and Bretherton, 2009a,b, Duffy et al., 2020). The (Back and Bretherton, 2009a) model clearly has strong explanatory power, but the precise way that the SST and its gradients exerts control over the top-heaviness, from the perspective of the thermodynamics, has not been determined and a goal of this research is to elucidate the subject.

The stability mechanism describes how vertical motion is controlled by the large-scale thermodynamic environment and predicts bottom-heaviness as a consequence of having a more stable temperature profile. The reason for this is an implicit relationship to plume buoyancy, but the details of this have not been studied in depth. I investigate this further in section 4. The stability mechanism was first uncovered and explained using a simplified model of large-scale vertical motion where stabilizing the large-scale environmental temperature led to the vertical motion becoming more bottom-heavy (Raymond and Sessions, 2007, Sessions et al., 2015). In contrast, when the large-scale temperature is destabilized, the vertical motion becomes more top-heavy. These simulations indicated the existence of the stability mechanism, which was then supported by observations from several field campaigns (Gjorgjievska and Raymond, 2014, Raymond et al., 2014, Sessions et al., 2019).

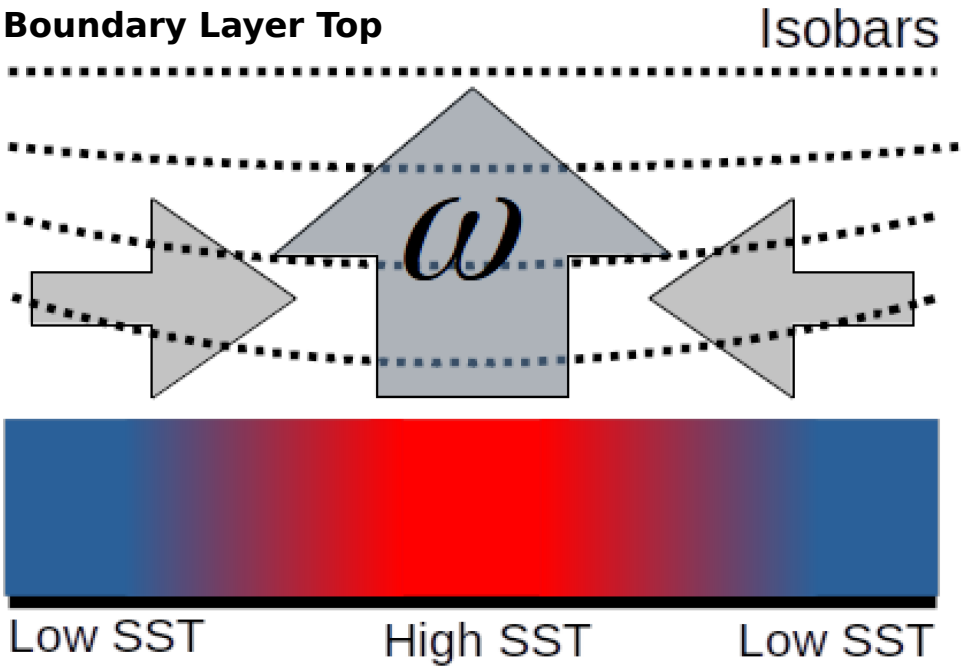

FIGURE 2.2: Schematic of the SST gradient driven surface convergence and how it generates vertical motion. Horizontal SST gradients imprint on the boundary layer. In association with friction, these pressure gradients generate convergent winds. These convergent winds are associated with upward vertical motion in order to satisfy mass continuity. This process is important to regions with bottom-heavy vertical motion according to the dynamic mechanism.

Both of these mechanisms offer an explanation for bottom-heavy vertical motion, and both mechanisms have unanswered questions that leave holes in our understanding. Whether the dynamic mechanism acts through influencing thermodynamic profiles is still unknown. The stability mechanism's role in the climatological top-heaviness has not been previously demonstrated and additionally does not provide an answer to why the top and bottom-heavy boxes have similar amounts of rainfall and column moisture while having different vertical motion profiles.

I use simulations that parameterize vertical motion using the weak temperature gradient (WTG) approximation, which is the same parameterization which helped uncover the

stability mechanism. I use a particular implementation of the WTG approximation called the spectral WTG (SWTG) parameterization that has been shown to reproduce vertical motion from observations as well as the stability mechanism (Herman and Raymond, 2014, Wang et al., 2016). I am using reanalysis data instead of observations to simulate climatological vertical motion profiles, because they are the most continuous and accurate data available on climatological timescales. I wish to understand the mean behavior, so I use time-independent boundary conditions from the climatology values. I simulate the environments and resulting vertical motion from our top and bottom-heavy boxes in order to answer the following questions:

- Can the top-heaviness differences between our two regions be simulated from the SST, temperature, and horizontal moisture advection or do I need to additionally impose the dynamic mechanism?
- If so, what are the most important thermodynamic factors in determining vertical motion shape and its geographic variability?
- Can I connect the vertical motion shape to the environment using a simple entraining plume model?
- How can I reconcile the dynamic and stability mechanisms in light of the results I obtain?

The paper is laid out as follows: In the next section I will discuss the details of the WTG model that I use and the initial simulations of the two regions. Following that I will

explore the sensitivity of the top-heaviness to different aspects of the thermodynamics in order to uncover the most important aspects. After this I will use a simple model of an entraining plume in order to explain the thermodynamic controls of vertical motion. Finally I will discuss how the two mechanisms are linked together and propose a unified mechanism for the control of top-heaviness.

2.2 Weak Temperature Gradient Simulations

2.2.1 WTG parameterization

The WTG approximation, at its most basic, is that horizontal temperature gradients, and thus horizontal temperature advection, can be ignored because they are much smaller than the other important factors (Sobel et al., 2001). The small Coriolis force in the tropics means temperature anomalies are quickly redistributed by gravity waves which leaves horizontally homogeneous temperatures. When there is no horizontal advection of temperature vertical advection becomes the primary balance for diabatic heating which makes the WTG approximation incredibly useful as a simplifying assumption to the virtual temperature budget equation:

$$\frac{\partial \theta_v}{\partial t} + \vec{v} \cdot \nabla \theta_v = Q. \tag{2.1}$$

In this equation, θ_v is the temperature, $\vec{v}$ is the 3D wind velocity vector, and Q is the diabatic heating. I simplify by first neglecting the horizontal advection term using the

WTG approximation. I also assume the time tendency is zero because I am considering the mean behavior. This makes the new thermodynamic equation:

$$W\frac{\partial\theta_v}{\partial z} = Q. \tag{2.2}$$

The vertical motion is an important aspect of the diabatic heating, which makes forecasting in the tropics is a tricky affair without something like our small domain cloud resolving model (CRM) which simulates the diabatic heating. I use the temperature change that results from this heating to calculate the WTG vertical motion. Specifically, I replace the diabatic heating in the above equation with the difference in virtual potential temperature between the model domain mean, $\overline{\theta_v}$, and, θ_v^b, the prescribed profile divided by a characteristic relaxation time scale τ. I then solve for the vertical motion, giving us our WTG velocity equation:

$$W_{WTG} = \frac{\overline{\theta_v} - \theta_v^b}{\tau(\partial\theta_v/\partial z)}. \tag{2.3}$$

The model advects temperature and moisture vertically according to this WTG vertical velocity, driving the model evolution towards equilibrium.

I use a particular implementation of the WTG parameterization, called spectral WTG (SWTG), that decomposes the vertical motion into a series of vertical modes and their amplitudes. Each of these modes individually redistribute anomalies at a characteristic time-scale determined by the mode. The temperature anomaly that each mode relaxes is found by projecting the total temperature anomaly onto the mode. Putting this together,

the SWTG velocity is found using:

$$W_{SWTG} = \sum_j \langle \frac{\overline{\theta_v} - \theta_v^b}{\tau_j(\partial\theta_v/\partial z)}, \Omega_j \rangle \frac{\Omega_j}{\langle \Omega_j, \Omega_j \rangle}. \tag{2.4}$$

Where τ_j is the mode specific relaxation time, Ω_j are the vertical modes, and $\langle\rangle$ indicates a mass-weighted column integral. This method of parameterizing the vertical velocity is more realistic and provides better results with fewer assumptions than earlier implementations (Herman and Raymond, 2014).

2.2.2 Horizontal Moisture Advection

I still have to consider the horizontal transport of moisture in and out of the domain, even though the horizontal advection of temperature is negligible. There are four methods of moisture transport that have been used in previous WTG simulations: moisture relaxation (Sobel et al., 2007), lateral moisture entrainment (Raymond and Zeng, 2005), moisture ventilation (Raymond and Fuchs-Stone, 2021) and imposed moisture advection (Sobel and Bretherton, 2000, Wang et al., 2016). The first three of these methods represent aspects of horizontal moisture transport that are locally forced. However, a considerable amount of horizontal moisture transport can be driven by non-local processes which are outside of the scope of our model (see Appendix A of Wang et al. (2016)).

As a result, I choose to use the fourth method and impose the profile of horizontal advection from the reanalysis. The horizontal moisture advection is calculated using

$$Q_{qhadv} = -v_h \cdot \nabla q_v, \tag{2.5}$$

where q_v is the specific humidity, v_h are the horizontal winds, and Q_{qhadv} is the horizontal moisture advection.

The horizontal moisture advection can influence the vertical motion profile and the balance between moisture and vertical motion (Sessions et al., 2016, Wang and Sobel, 2012). The other methods are attempts to parameterize the horizontal moisture advection. However, imposing the horizontal moisture advection that existed in balance with the vertical motion is the simplest way to achieve our goal. I also do not have to worry about imposing a large-scale moisture profile that corresponds to what is occurring in adjacent columns to the area of interest.

2.2.3 Handling Dry Equilibrium Simulations

Another important consideration when running WTG simulations is the tendency for it to go to either a moist or dry equilibrium depending on many different factors, but importantly the initial profile of moisture (Raymond et al., 2009, Sessions et al., 2015). The dry equilibrium becomes unrealistically dry and the resulting vertical motion may also become non-physical. When a simulation enters the dry equilibrium, rather than use the dry equilibrium vertical motion output, I use a vertical velocity that I calculate

	Rain (mm/day)	top-heaviness $\phi_{TH}(^\circ)$	surface latent heat flux SLH (w/m^2)	column radiative heating $\langle Q_r \rangle (w/m^2)$
DYNAMO	8.89	9.42	103.0	not available
DYNAMO DE	9.73	N/A	110.7	-68.8
Top-heavy	9.63	1.55	131.2	-75.7
Top-heavy DE	8.6	N/A	145.0	-63.0
Bottom-heavy	8.29	-24.5	126.5	-89.1
Bottom-heavy DE	10.6	N/A	110.7	-78.7

TABLE 2.1: Data from reanalysis and observations alongside the data from the DE simulations. Shown are the rain in mm/day, the top-heaviness angle, the surface latent heat flux and column radiative heating.

assuming it balances the radiative cooling. I calculate the velocity from the DE simulation temperature by dividing the radiative heating profile by the DSE stratification at each level.

2.2.4 Model setup

I generate our simulations in essentially the same way as Wang et al. (2016) with the modification that our boundary conditions are time-invariant and I run to a steady state, instead of simulating a discrete time-series. The weather research and forecasting model (WRF) model (version 3.5.1) (Skamarock et al., 2008) is used as the basis for our WTG model. The model has a lower bound of the mean SST, doubly periodic lateral boundary conditions, and an implicit damping scheme is used as the upper boundary condition (Klemp et al., 2008). I use a domain size of 64x64x23 km with a grid size of 1km. I use 60 stretched vertical levels with 10 levels in the first kilometer. The WTG relaxation time scale that I use for the gravest mode is 1 hour.

In addition to the large scale temperature which is integral to the WTG parameterization,

I also impose the large-scale profile of horizontal winds and relax the domain average wind profiles towards the large-scale winds, with a relaxation time of 1 h. The parameterization of the microphysics is done using the Morrison two-moment scheme (Morrison et al., 2009). The parameterization of the interactive radiation uses the RRTMG long-wave scheme and the Goddard shortwave scheme (Iacono et al., 2008) with a constant solar insolation of $370 w/m^2$ (Chou and Suarez, 1999, Matsui et al., 2007, Shi et al., 2010). I parameterize subgrid scale eddies using the three-dimensional Smagorinsky first-order closure scheme and an implicit vertical diffusion scheme is used to ensure numerical conservation of moisture. Everything else that I have not mentioned is kept the same as Wang et al. (2016).

The SWTG parameterization allows us to simulate the vertical velocity profiles as a function of the large-scale temperature profile. Due to the mismatch between real-world physics and the model physics, I cannot compare the profiles of temperature directly to each other. I solve this issue by using a model analogue for the large-scale temperature instead of using reanalysis temperature profile. Many previous WTG simulations, especially simulations of steady states, have used radiative convective equilibrium (RCE) states as the primary source of the environmental temperature profiles (Anber et al., 2015, Daleu et al., 2015, Raymond and Sessions, 2007, Wang et al., 2013). However, the presence of large-scale vertical motion alters that temperature profile relative to RCE (Singh et al., 2019a). To deal with this issue, I run the model with the vertical motion from reanalysis in place of the WTG parameterization and recover the large-scale temperature

profile that is in balance with this vertical motion profile. This is similar to the methods used by Edman and Romps (2015) and Wang et al. (2016).

I call these simulations the driven equilibrium (DE) simulations, because I allow the observed advection to drive our model to an equilibrium that is equivalent to the reanalysis climatology. There is a discrepancy between the DE temperature profile and the profile that I want to use caused by the presence of the large-scale vertical motion. This can be seen if I rewrite the WTG velocity equation as

$$\theta_v^b = \overline{\theta_v} - \tau\omega\frac{\partial\theta_v}{\partial p} \tag{2.6}$$

The DE simulation outputs $\overline{\theta_v}$ and I wish to use θ_v^b in our simulations. I solve for θ_v^b using the above equation and use it in the SWTG simulations as the large-scale temperature profile.

In addition to the temperature profile, I also take the moisture and radiative heating profile from the DE simulations. I use the moisture profile to initialize the model and I use the radiative heating profile instead of interactively simulating it, which helps to avoid dry equilibrium cases (Sessions et al., 2016).

2.2.5 Model Validation

I first validate that our configuration of the model is able to simulate mean vertical motion profiles. I recreate the original DYNAMO simulations from (Wang et al., 2016)

with data from northern sounding array (version 1) (Ciesielski et al., 2014, Johnson and Ciesielski, 2013). To do this I remove the time-dependence from the model input and replace it with its average. The results of the validation DYNAMO simulation along with the later simulations are found in tables (2.2 and 2.3). I found that the time-independent boundary conditions are able to generate vertical motion profiles that are similar to the time-dependent simulations and to the observations. This gives us confidence that the model is able to produce the long-term mean vertical motion from a mean thermodynamic environment.

I next test that our model produces the vertical motion shape response to the large-scale temperature anomalies that is the basis for the stability mechanism (Raymond and Sessions, 2007, Sessions et al., 2015). I test this by adding two temperature perturbations, which I have taken from the previous research, to the large-scale temperature profile and simulating vertical motion profile response. The results, which can be seen in figure (2.7), show that when I apply a stabilizing temperature anomaly, the vertical motion transitions from top-heavy/neutral to bottom-heavy. The reverse occurs when I apply a destabilizing temperature anomaly; this leads to a stratiform vertical motion profile that is extremely top-heavy. I used an interactive radiation scheme in these simulations, which contrasts with the other simulations in this chapter. This choice has been shown to be unimportant to the mechanism that I am testing (Sessions et al., 2016).

The model displays the correct vertical motion response to the temperature anomaly, but the response of the moisture profile is not consistent with what has previously been

seen in Raymond and Sessions (2007), Sessions et al. (2015). In their work, they saw a correlation between the stability and column moisture, with greater stability leading to greater column moisture. While I do see a moisture profile response for all three profiles, they have nearly identical column moisture. I discuss the reasons for this further in section (7).

Base Simulation	Radiation source	SST source	Stability source	Moisture Advection source
1. DYNAMO	interactive	average	time-independent	time-independent
2. DYNAMO	interactive	average	stable	time-independent
3. DYNAMO	interactive	average	unstable	time-independent
4. Top-Heavy	top-heavy	top-heavy	top-heavy	top-heavy
5. Top-Heavy	top-heavy	bottom-heavy	top-heavy	top-heavy
6. Top-Heavy	top-heavy	top-heavy	bottom-heavy	top-heavy
7. Top-Heavy	top-heavy	top-heavy	top-heavy	bottom-heavy
8. Top-Heavy	bottom-heavy	top-heavy	top-heavy	top-heavy
9. Bottom-Heavy	bottom-heavy	bottom-heavy	bottom-heavy	bottom-heavy
10. Bottom-Heavy	bottom-heavy	top-heavy	bottom-heavy	bottom-heavy
11. Bottom-Heavy	bottom-heavy	bottom-heavy	top-heavy	bottom-heavy
12. Bottom-Heavy	bottom-heavy	bottom-heavy	bottom-heavy	top-heavy
13. Bottom-Heavy	top-heavy	bottom-heavy	bottom-heavy	bottom-heavy

TABLE 2.2: The list of simulations that were run along with where the data came from and how it differs between runs.

2.3 Top/Bottom-heavy simulations

2.3.1 Reanalysis

I start with a test to see how well I can simulate the vertical motion from the thermodynamic differences between our two regions. I use the ERA-5 reanalysis as the source of our climatology data. I utilize data on both pressure levels and single levels (Hersbach et al., 2019a,c) over the time span of 2007-2017. The top and bottom-heavy boxes that

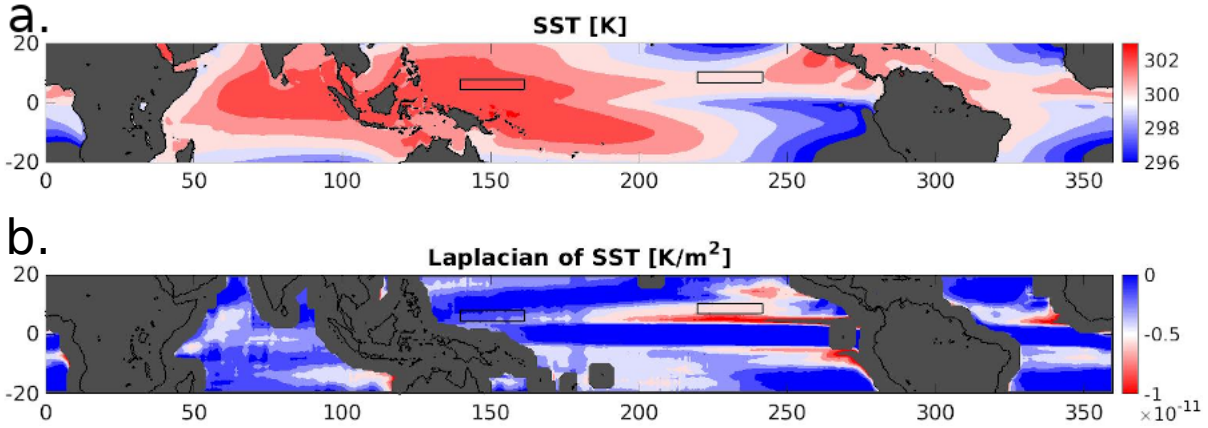

FIGURE 2.3: Map of the surface characteristic variability important to setting the vertical motion profile shape according to the dynamic and stability mechanism. (a.) map of the SST [K] for the 10 year ERA5 climatology. (b.) The laplacian of SST of the above plot, areas with negative values, colored here in red, are areas where the SST pattern will drive convergence $[K/m^2]$.

I am studying from Back and Bretherton (2006) have bounds of 5-7.5 °N 140-160°W for the top-heavy region and 7.5-10°N 120-140°E for the bottom-heavy region. I construct our long term mean by averaging daily data. The thermodynamic profiles that I use to run the model are temperature, water vapor mixing ratio, horizontal winds, profiles of vertical velocity and horizontal moisture advection. The water vapor mixing ratio profiles are only used to generate the horizontal moisture advection profiles and to initiate the DE simulations.

The horizontal moisture advection that I impose in our simulations is calculated using a center difference method on pressure levels from daily data, which is then averaged to the 11 year climatology. Both profiles act as drying terms in the moisture budget. However, they have distinct vertical profiles, see figure (2.4 d). The bottom-heavy box has almost all of its advection concentrated near the surface. The top-heavy box, meanwhile, has a profile of moisture advection that is fairly consistent through the depth of the troposphere.

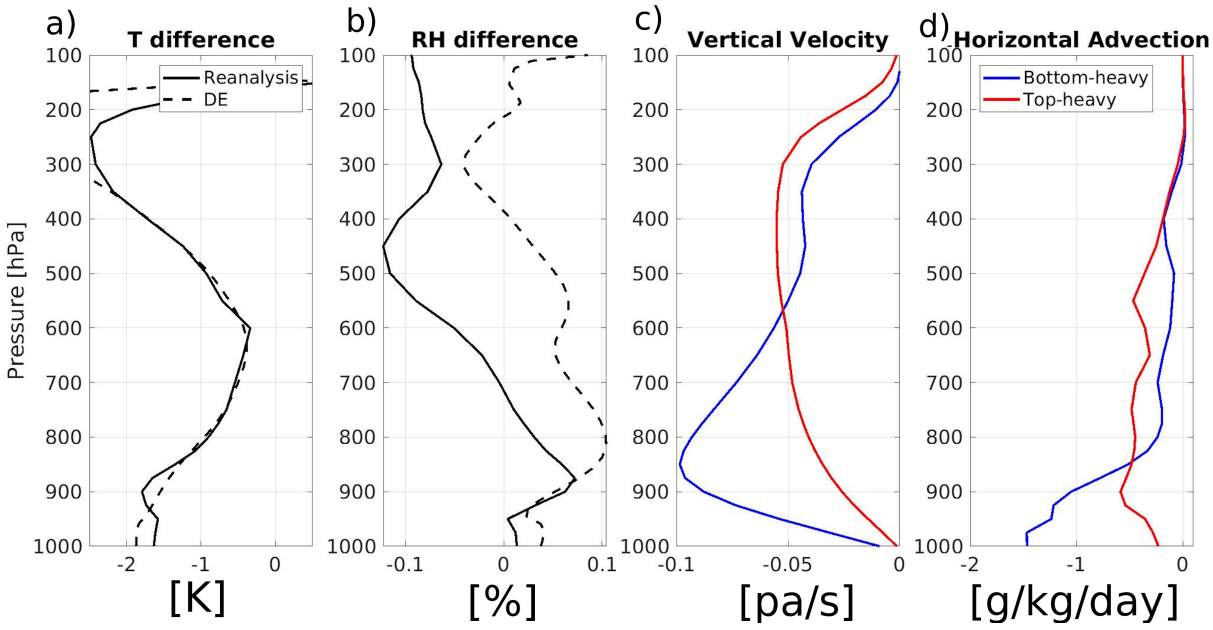

FIGURE 2.4: The large-scale thermodynamic environment used to simulate the vertical motion shape from reanalysis and DE simulations. (a.) Temperature difference between the bottom-heavy box and top-heavy box for both reanalysis and the DE simulations. The negative values show that the top-heavy box is warmer throughout the column. (b.) This shows the RH differences between the top and bottom-heavy boxes from both reanalysis and the DE simulations. (c.) Vertical motion profiles, in units of $[Pa/s]$, for our two regions. (d.) Horizontal moisture advection calculated using daily data before taking the average.

The difference in temperature profiles between the two boxes is shown in figure (2.4a). The bottom-heavy box is 2K cooler than the top-heavy box at both the surface and near the tropopause. The SST in the bottom-heavy box is also around 2K cooler than the top-heavy box, which is the likely reason for much of the difference in temperature profiles. The bottom-heavy box has a slightly higher relative humidity in the lower troposphere where there is more vertical motion. Meanwhile, the top-heavy box has greater relative humidity in the upper troposphere where it begins to have greater vertical motion. Also shown in figure (2.4) are the equivalent temperature and moisture differences that our model produces, which are discussed in the following section.

2.3.2 Driven Equilibrium simulations

The driven equilibrium (DE) simulations are our model's analogue to climatology. These profiles have alternatively been called radiative convective dynamic equilibrium (RCDE) by Singh et al. (2019a) and radiative convective advective equilibrium (RCAE) by Romps (2021). Table 2.1 shows the DE results along with the observation and reanalysis that the model is trying to replicate. The table shows measures which are important to the energy budget including the rainrate, the column radiative heating, the surface latent heat flux, and our newly introduced top-heaviness angle to measure the vertical motion profile shape.

I produce our own estimates of precipitation consistent with the vertical advection that I am interested in, which allows us to compare the precipitation between different sources and to combat potential biases in the estimates. Taking the column integrated DSE budget equation along with the WTG assumptions, no storage or horizontal advection of DSE, and assuming that surface sensible heat fluxes are negligible, DSE storage or horizontal advection allows us solve for precipitation:

$$P = \langle \omega \frac{\partial s}{\partial p} \rangle - \langle Q_R \rangle \tag{2.7}$$

Here P is the precipitation, s is the DSE, and $\langle Q_R \rangle$ is the column integrated radiative heating. These precipitation estimates are a useful metric for comparing how close the models are to each other and to the real world. If a model is accurately representing

physics the estimate of precipitation should match with the observed precipitation. The values that I calculate for each of the data sets and the DE simulations can be found in table 2.1.

Figure (2.4a and b) also shows the differences in temperature and moisture between the top and bottom-heavy boxes for the DE simulations,along with the reanalysis profiles. The DE simulation is able to capture the lower tropospheric temperature differences well between the two regions. The upper troposphere shows disagreement between the DE temperature profile and reanalysis, which is most likely caused by the model's artificial lid. Overall there is a close match between the temperature profile differences in reanalysis and our DE simulations.

The moisture differences are much more significant, showing a bottom-heavy box that is relatively too moist compared to the top-heavy box throughout the column. The Bottom-heavy box has a greater relative humidity than the top-heavy box throughout a much more significant portion of the atmosphere. This is reflected in the precipitation rates differences, which can be seen in 2.1. The bottom-heavy DE simulation has greater rain than the top-heavy DE simulation, which is the reverse of what I see in reanalysis.

I also show variables relating to column energy, surface latent heat flux and radiation, in table (2.1). The DE simulations capture the relative differences in radiative heating between the two regions well, with both columns producing less radiative cooling than reanalysis. The surface latent heat flux differences between the top and bottom-heavy domain are also similar to reanalysis but the differences are much larger. This surface

heat flux difference explains around half of the column MSE difference implied from the different rainrates.

The DE simulations match the reanalysis closely enough that our model provides useful results and I move on to addressing our primary research questions. The importance of the minor differences between the DE simulation and the reanalysis are beyond the scope of the current research. Our next step is to simulate the vertical motion profiles to see if the WTG parameterization captures the vertical motion differences.

2.3.3 SWTG top/bottom-heavy simulations

The simulated vertical velocity profiles from the top and bottom-heavy simulations, presented in figure (2.5), show that the climatological vertical motion profile shapes, and importantly, bottom-heavy vertical motion, can be simulated using the thermodynamic profiles as boundary conditions. Table (2.2) shows all of the simulations and their parameters and table (2.3) shows the same model output variables as table (2.1) with the addition of the saturation fraction (SF), which is the ratio of the column integrated moisture to the column integrated saturation moisture, which is also known as the column relative humidity (Bretherton et al., 2004). The simulation of the bottom-heavy box, simulation 9, produced vertical motion with a top-heaviness angle of $-46°$, see table (2.3). The simulation of the top-heavy box, simulation 4, has a vertical motion profile similar to the reanalysis profile, although not as top-heavy, with an angle of $0°$ compared to $15°$ in reanalysis.

Simulation	Rain (mm/day)	ϕ_{TH} (°)	SLH (w/m^2)	$\langle Q_R \rangle$ (w/m^2)	SF
1.	8.4	6.1	120.3	-69.2	0.84
2.	14.0	-43.0	150.2	-144.6	0.84
3.	9.3	62.9	99.6	-36.0	0.84
4.	7.8	0.2	143.4	-61.9	0.81
5.	0	153.4	188.8	-64.4	0
6.	29.8	23.4	183.0	-61.6	0.88
7.	5.9	-2.2	151.4	-61.9	0.81
8.	8.9	-6.5	140.7	-80.8	.81
9.	6.1	-46.3	104.9	-80.7	0.83
10.	27.8	24.7	192.0	-80.2	0.89
11.	0	167.4	165.9	-81.2	.04
12.	11.3	-13.4	91.7	-80.6	.86
13.	5.04	-44.9	110.9	-62.14	.813

TABLE 2.3: The rain, top-heaviness, surface heat fluxes and radiation for the previously listed simulations.

The precipitation rates that the SWTG simulations produce are lower than both the reanalysis and DE rain rates (table 2.1). Both simulations have similar deviations from the reanalysis rainrate which come primarily from differences in the vertical motion profile shape. In the bottom-heavy simulations, the difference between the reanalysis surface heat flux and the SWTG surface heat flux explains approximately 1/4 of the precipitation deviation. I also find the previously argued for negative correlation between top-heaviness and column moisture; the top-heavy box has a lower SF than the top-heavy box. Despite this, I do not see the previously seen correlation between the precipitation and top-heaviness (Raymond et al., 2015, Raymond and Sessions, 2007, Sentić et al., 2015, Sessions et al., 2015). I explain the reason for this difference further in section (7).

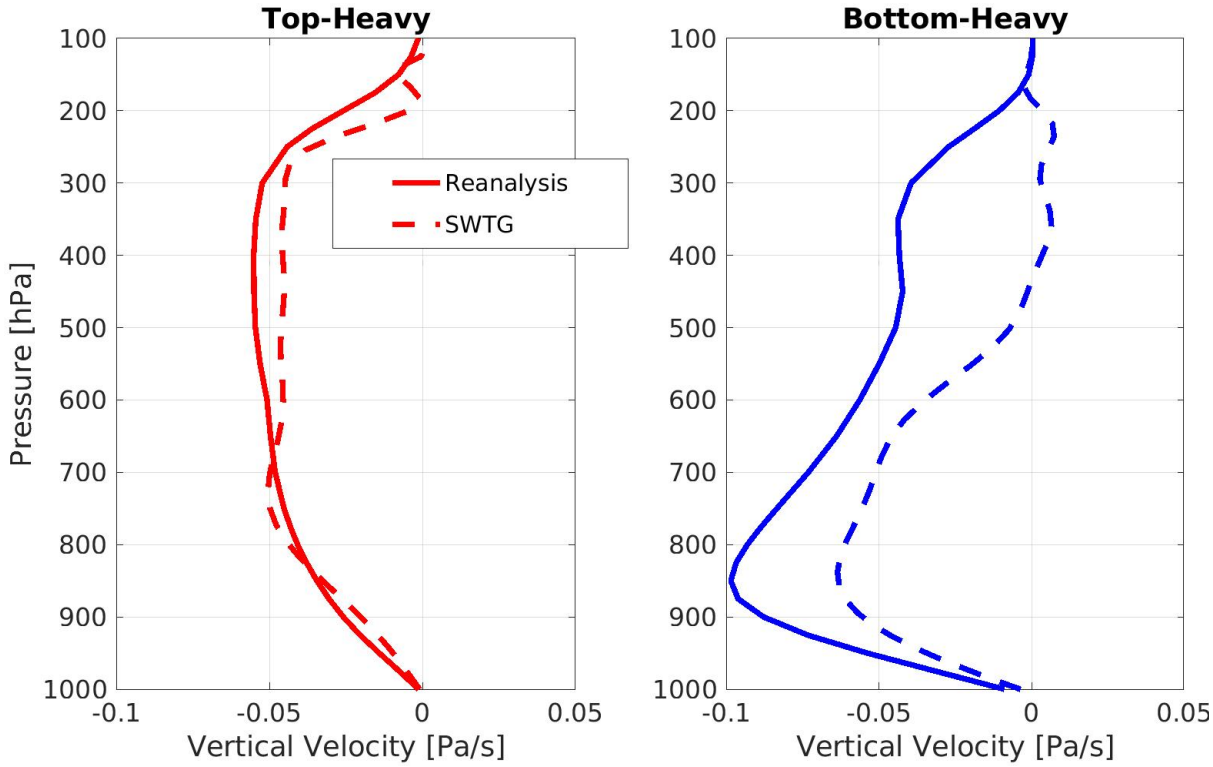

FIGURE 2.5: Vertical motion profiles simulated in top and bottom-heavy domains show that the thermodynamic environment alone can determine top-heaviness qualitatively correctly in simulations. The solid lines are the climatology profiles from ERA5 reanalysis. The dashed lines are the cases with imposed radiation, where I use the profile of radiative heating from the DE simulations. And the dash-dotted lines are from the simulations with radiation computed interactively.

The ability of the model to simulate both bottom and top-heavy vertical motion demonstrates that the vertical motion shape is primarily controlled by large-scale thermodynamics. This compels us to ask what parts of the thermodynamic environment are most responsible for the vertical motion shape.

2.4 Thermodynamic sensitivity tests

I next run sensitivity tests in order to determine which aspects of the thermodynamics are the most important to vertical motion profile shape. In each sensitivity simulation,

I start with the initial and boundary conditions for either the basic top or bottom-heavy simulation domain and switch one of the following parameters: the large-scale temperature profile, the moisture advection profile, the underlying SST, or profiles of radiative heating. I then take an average of the vertical motion from each simulation that has a parameter in common, which gives us four profiles of vertical motion from each. I then difference the profiles from the two boxes in order to get the effective change caused by the difference between the boxes.

The effect on the vertical motion profile from the differences are shown in figure (2.6 A). I pick a parameter and average all of the vertical motion profiles from the simulations with that top-heavy parameter and bottom-heavy parameter and then subtract these profiles. For the stability sensitivity I switch the sign of the resulting vertical motion profile so that it represents a change from the top-heavy box to the bottom-heavy box, so that the sensitivity profiles represent an increase in stability.

The four parameters equate to eight additional tests sensitivity simulations whose result can be seen in tables (2.2 and 2.3) as simulations 5-8 for the top-heavy cases and 10-13 for the bottom-heavy ones. There were two cases that entered into the dry equilibrium: simulation 10 which is the bottom-heavy box with the top-heavy temperature profile and simulation 5 the top-heavy box with the bottom-heavy SST. Both cases that went to the dry equilibrium had the lower, bottom-heavy SST and the more unstable, top-heavy temperature profile. I do not use the vertical motion profiles from these simulations, since

they are non-physical, and instead use the vertical motion profile that is in balance with the radiative heating profile.

The two largest vertical motion profile changes came from the SST and the stability difference between our two regions, simulations 6 and 9 respectively. The vertical motion response from increasing the SST has very little change in vertical motion lower in the atmosphere and a large increase above the freezing level in the upper troposphere. The stability on the other hand, increases the vertical motion everywhere it is cooler, both the upper and lower troposphere. The moisture advection resembles the stability response with an increase in both the upper and lower troposphere. However the effect is much smaller than both of the others.

The results show that the radiative heating differences act as a feedback mechanism for vertical motion and convection and not as a primary forcing. The sensitivity of the vertical motion shape to the profiles of radiation is significantly smaller than either the stability or SST sensitivity effects. There is a small increase in the amount of vertical motion in the lower troposphere and decrease in the upper troposphere. This means the profile of radiative heating is contributing very slightly to the top-heaviness differences between the two boxes. The difference in radiative heating between the two simulated profiles is $10w/m^2$ on average, which is one third the difference in the surface latent heat fluxes.The vertical velocity that would balance the radiative heating differences is an order of magnitude smaller than the radiation sensitivity vertical velocity that is shown in figure (2.6) so this is not playing a significant role.

The differences in horizontal moisture advection is also much smaller than to the SST and temperature profile. The horizontal advection from the top-heavy box induces greater vertical motion but does not affect the vertical motion profile shape much. This can partially be attributed to the differences in the vertical distribution of the moisture transport, because mid-level moistening is more effective than low level moistening in invigorating convection (Wang and Sobel, 2012). Another potential explanation for the lack of effect is that the column averaged horizontal advection of moisture is not significantly different between the two imposed profiles. If I were to choose two boxes with significantly different amounts of horizontal moisture advection, I might see a larger effect. The distinction between how the vertical motion profile shape and amplitude are altered by differences in both the vertical structure and the amplitude of horizontal moisture advection should be addressed by future research.

I deduce that the bottom-heavy vertical motion in the Central Eastern Pacific, from the perspective of the thermodynamics, is due primarily to a combination of higher stability and lower SST, while the top-heavy vertical motion in the Western Pacific is due to a combination of high SSTs and low stability. The high stability cases with warm SST from the sensitivity tests became extremely top-heavy with vigorous convection. This is consistent with the dynamic mechanism, which predicts that high SST will lead to top-heavy vertical motion profiles. The fact that the more stable simulations have higher humidity and rainfall is also consistent with the stability mechanism. However, the stability mechanism predicts bottom-heavy vertical motion in this case, which is not what I see in the simulations. Additionally, the dynamic mechanism says that the surface

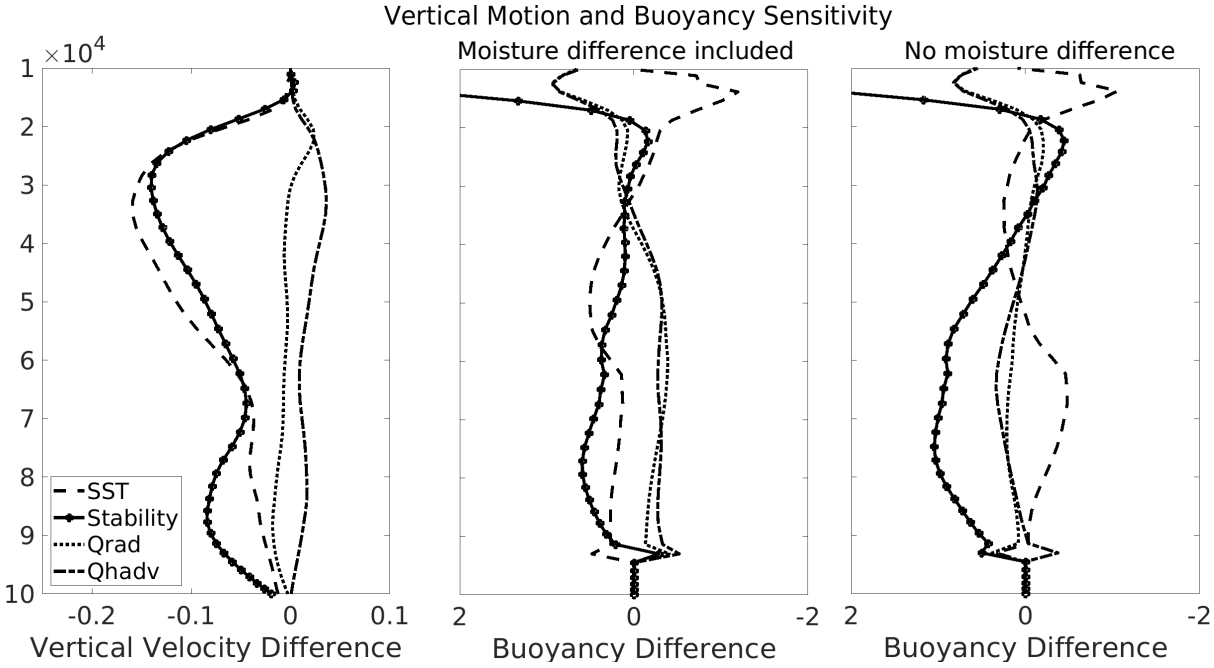

FIGURE 2.6: The average vertical motion shape (panel a) and plume buoyancy response (panels b and c) to thermodynamic variable differences between the top and bottom-heavy simulations. The vertical motion and plume buoyancy changes are most sensitive to SST and temperature profile variations and less sensitive to radiation and horizontal moisture advection. The sign of the stability change profiles have been reversed, which means it represents a change from the top-heavy to the bottom-heavy variable in question. The other three profiles, SST, radiation, and lateral moisture advection, represent a change from bottom-heavy to top-heavy. (b.) The plume buoyancy sensitivity with the RH differences between the two domains included. (c.) The plume buoyancy differences calculated using the mean RH profile so that the differences are due only to temperature differences.

convergence due to SST gradients is essential but it is not explicitly present in our model, although it may be affecting the temperature profile I input as discussed in section 6.

2.5 An Entraining Plume Perspective

To understand how the control of SST and the temperature profile on vertical motion top-heaviness works, I turn to an entraining plume model. These models have a rich and storied history in tropical meteorology, and recently have been used to understand column-integrated water-vapor precipitation relationships (Abbott and Cronin, 2021, Adames et al., 2021, Ahmed and Neelin, 2018, Singh and Neogi, 2022, Singh and O'Gorman, 2013, Singh et al., 2019a), as well as the basis for one of the first convective parameterizations (Arakawa and Schubert, 1974). However, they have never been applied to the shape of the vertical motion profile. Hence this is a novel endeavor in which I believe that even qualitative relationships are a step forward from the existing knowledge-base. Our goal in this work is to understand why, from the perspective of a rising parcels buoyancy, more stable temperature profiles lead to more bottom-heavy vertical motion profiles. In the following section I will discuss our plume model and what it tells us about the thermodynamic controls of top-heaviness. Then, I turn to how I can reconcile the stability mechanism and dynamic mechanism.

2.5.1 Entraining Plume Buoyancy

Following previous work, I use a simple entraining plume model that follows a parcel leaving the boundary layer. The plume starts its journey with the surface value of MSE and begins to rise, after it reaches the lifted condensation level (LCL), it begins to lose MSE due to dry air entrainment according to:

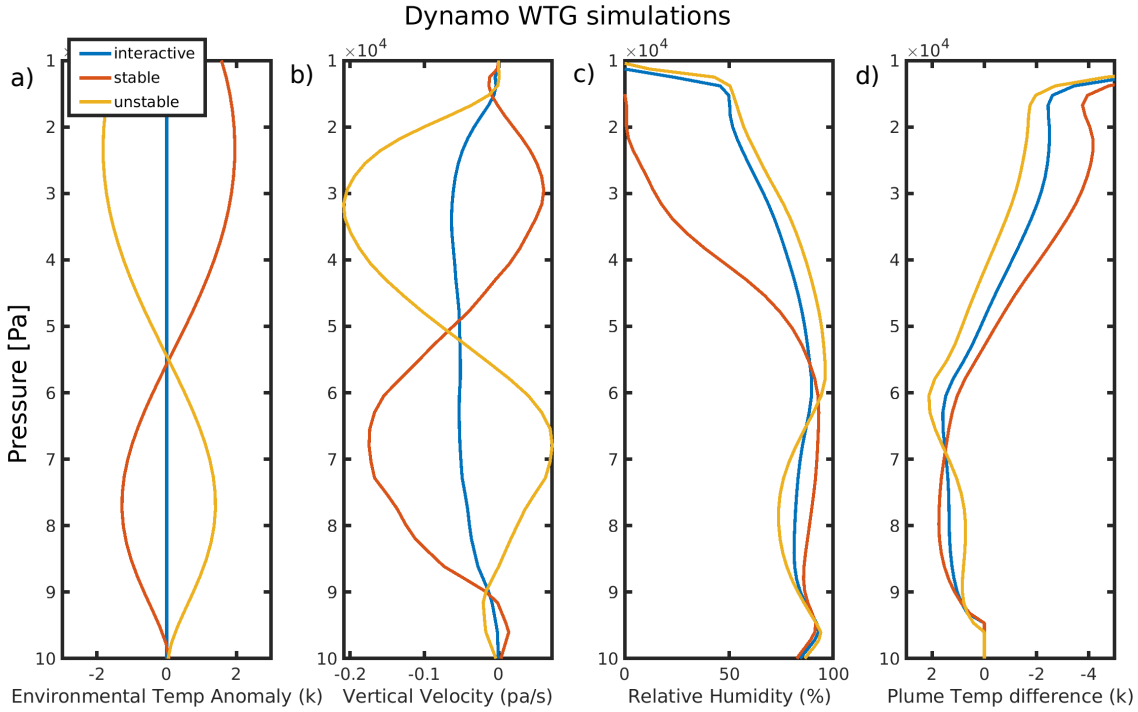

FIGURE 2.7: Figure showing test of stability mechanism using variations of the time-mean DYNAMO data and interactive radiation. (a.) The temperature anomalies that are added to the large-scale temperature profiles in order to (de)stabilize them. (b.) The resulting vertical motion profiles. (c.) The relative humidity of all three cases. (d.) The difference in temperature between an entraining plume and the surrounding environment, which measures the buoyancy that a parcel feels and is related to the vertical motion that I simulate. The x-axis has been reversed so that the sign better matches the vertical motion.

$$\frac{\partial h_p}{\partial p} = \epsilon(h_p - h_e) \tag{2.8}$$

Here h is the MSE, the p and e denote the parcel and environment respectively. ϵ is the rate that environmental air is entrained. I use a constant rate of 0.25 [km-1], because it is simple to analyze and performs qualitatively best for the several rates that I looked at. This assumption could be refined in various ways beyond the scope of our study. I integrate this equation from the lifted condensation level (LCL) to the top of

the atmosphere in order to calculate the plume MSE.

I use the difference between the plume MSE and the environmental saturation MSE to calculate the plume buoyancy profile, which is directly related to the large-scale vertical velocity as I will discuss shortly. The difference between the plume temperature and the environment temperature is our measure of buoyancy. I calculate the temperature of the plume, and its difference to the environment, using a Taylor series approximation of the saturation moisture centered at the environmental temperature:

$$h_p^* - h_{env}^* = c_p \left(T_p - T_{env}\right) + L_v \left(q_p^* - q_{env}^*\right) = \left(T_p - T_{env}\right) \left[c_p + L_v \frac{\partial q^*}{\partial T}\bigg|_{T_{env}^*}\right] \tag{2.9}$$

h is the MSE, T is the air temperature, and q is the specific humidity. c_p is the specific heat capacity, L_v is the latent heat of vaporization, the subscripts env and p correspond to the environment and plume respectively and the the star superscript represents saturated quantities. I calculate the plume buoyancy by solving this equation, at each level, for the difference in temperature between the plume and the environment.

The plume buoyancy is directly related to the in-cloud vertical motion which is in turn related to the large-scale vertical motion that I am trying to understand. Traditionally, buoyancy is thought to accelerate in-cloud updrafts, but recent research has indicated that buoyancy is directly correlated to the in-cloud vertical motion because plumes rise in a high drag, high friction environment (Hernandez-Duenas et al., 2019, Romps and

Öktem, 2015). This means I can qualitatively use the plume buoyancy profile as a proxy for the in-cloud vertical velocity.

The connection between the large-scale vertical motion and the in-cloud mass flux is possible because the large-scale vertical motion is composed of the in-cloud mass flux along with the between cloud subsidence, and cloud fraction according to:

$$\overline{\omega} = \alpha W_u + (1 - \alpha) W_d \tag{2.10}$$

Here ω is the large-scale vertical motion, W_u is the in-cloud updraft velocity which I represent with the plume buoyancy, and W_d is the between cloud subsidence velocity which is determined by radiative cooling, and α is the cloud fraction.

The in-cloud mass flux changes directly correlate with the large-scale vertical motion as long as the other changes due to the cloud fraction and subsidence rate changes are small. The subsidence velocity is not expected to change dramatically, because that would require a large change in the between cloud radiational cooling rate. Cloud fraction changes could cause in-cloud vertical velocity at each level to not correlate with large-scale vertical motion, but for the purposes of this work I neglect that effect. Further refinements to our conceptual model that are beyond the scope of this work could be made by relating cloud fraction at each level to humidity at that level.

The simulations that validated the WTG model's representation of the stability mechanism provide an excellent test case for whether the entraining plume model can describe

why the more stable case has a more bottom-heavy vertical motion profile, and I find that it does. The simulations of interest are simulations 1-3, and the only difference between the three simulations were the temperature anomalies that I added, shown in Figure (6a), which created large differences in the WTG velocity. I calculate the plume buoyancy for each of these simulations and show these in figure (2.7 d) along with the WTG vertical motion, relative humidity, and the temperature anomaly.

The differences between the buoyancy profiles is qualitatively similar to the differences between the vertical motion profiles. The test case with the stabilizing anomaly, the orange line in Figure (6a), shows a more bottom-heavy vertical motion profile in the SWTG simulations (Figure 6b.) and the entraining plume buoyancy profile is more bottom-heavy than the control case (Figure 6a.). The destabilizing anomaly leads to a more top-heavy vertical motion profile in the SWTG simulations and the entraining plume has a more top-heavy buoyancy profile. The simplicity of the model and its assumptions means I do not expect a close quantitative match, and the closeness of the qualitative match shows the model works well for our purposes and supports our idea that the plume model provides a useful explanation of what I observed in the cloud resolving model simulations.

2.5.2 Sensitivity Results

The entraining plume has shown good qualitative results and captures the stability mechanism, so I next turn the model to the sensitivity simulation results to better understand the reason for our top-heaviness difference. I calculate the temperature profiles used in the

buoyancy calculations by averaging the domain mean temperature from every simulation with the chosen common parameter. For instance, if I am interested in the effect of the bottom-heavy temperature I average all of the simulations that used the bottom-heavy temperature profile, which gives us the temperature profile differences attributable to using the bottom-heavy temperature profile in WTG simulations. I calculate the moisture profile using the RH from either the basic top or bottom-heavy simulation along with the temperature profile that I just calculated. I additionally wish to test the effect of only the temperature differences, so I also calculate the buoyancies using the mean RH from the two basic simulations.

I am further interested in the relative effect between the top and bottom-heavy box, so I subtract the two cases giving us the effect due to switching a variable. I select the order of subtraction in order to highlight a particular change. For the stability I choose the order so that it represents a change from the top-heavy to bottom-heavy and for the rest I choose the order so that it is a change from bottom to top-heavy.

Figure (2.6 b) shows the plume buoyancy difference with the effect of moisture included. I have flipped the sign from normal convention so that it aligns with pressure velocity changes. The two largest buoyancy effects, in line with the vertical motion, are due to changes in the SST and stability. The qualitative difference between the vertical motion profiles and buoyancy profiles are strikingly similar, with an increased bottom-heaviness due to stability changes and an increased top-heaviness due to SST changes. The upper troposphere effects are much more pronounced and exaggerated due to the SST changes.

The other two effects that I test, moisture advection and radiation, seem to drive a negative buoyancy anomaly that is very small.

When I remove the effects of differing RH profiles between the two boxes, I see distinct buoyancy changes (figure 2.6 c). The stability create the largest increase the plume buoyancy, however the SST shows negative buoyancy changes. The difference between the two buoyancy affects still resembles the vertical motion profile difference that I see, more buoyancy near the surface in the stability case and less buoyancy in the upper troposphere, but the profiles are much less similar when moisture is not included.

The effect of the SST on the buoyancy are only be seen when the RH differences are included because the WTG parameterization precludes the existence of the temperature profile changes that would be needed in order to change the buoyancy. The stability sensitivity also became more bottom-heavy. This is consistent with the stability validation results, which showed that the stability changes led to moisture changes which act to reinforce the buoyancy and therefore top-heaviness differences. When a temperature change instigates a buoyancy change the effect is also moderated by the moisture and therefore an accurate moisture parameterization is essential to capturing the buoyancy and vertical motion profile that result.

The simple entraining plume model that I have presented here has captured how aspects of both the stability and dynamic mechanisms operate. Changing the stability of the atmosphere affects the top-heaviness by changing the buoyancy that plume's feel as they rise. Higher SSTs drive greater vertical motion by increasing the starting energy and

buoyancy that a plume feels. I now move on to reconciling our two mechanisms into a more cohesive understanding of what controls climatological top-heaviness.

Figure (2.8) shows a visualization of the changes the SST, stability and moisture have on the buoyancy and thus the vertical motion. The toy model is created by initializing the environment with a starting temperature and constant lapse rate. The moisture is then determined by a constant RH value for the boundary layer and the free troposphere. The temperature and moisture changes are created by increasing the MSE, in the case of the moisture, and the MSE and saturated MSE, in the case of the temperature, by 2K equivalent, in a small layer lower in the atmosphere. The SST change is accomplished by increasing the MSE that the plume starts with by 2K.

The moisture increase, see figure (2.8 a), leads to an increase in the buoyancy above where the moisture is changed. The temperature increase, see figure (2.8 b), has two effects, the first is identical to the the moisture increase, because I have increased the temperature while maintaining the RH constant. The second effect is a local decrease in the buoyancy because the saturated MSE of the environment has increased, which means the latent energy of the parcel goes into achieving saturation instead of being excess buoyancy. Increasing the SST, see figure (2.8 c), leads to an increase in the buoyancy throughout the column.

This toy model demonstrates the basic changes on buoyancy and vertical motion due to idealized changes in the thermodynamic state. The real atmosphere operates in a similar, albeit more complicated, fashion and the toy model provides a simplified explanation of

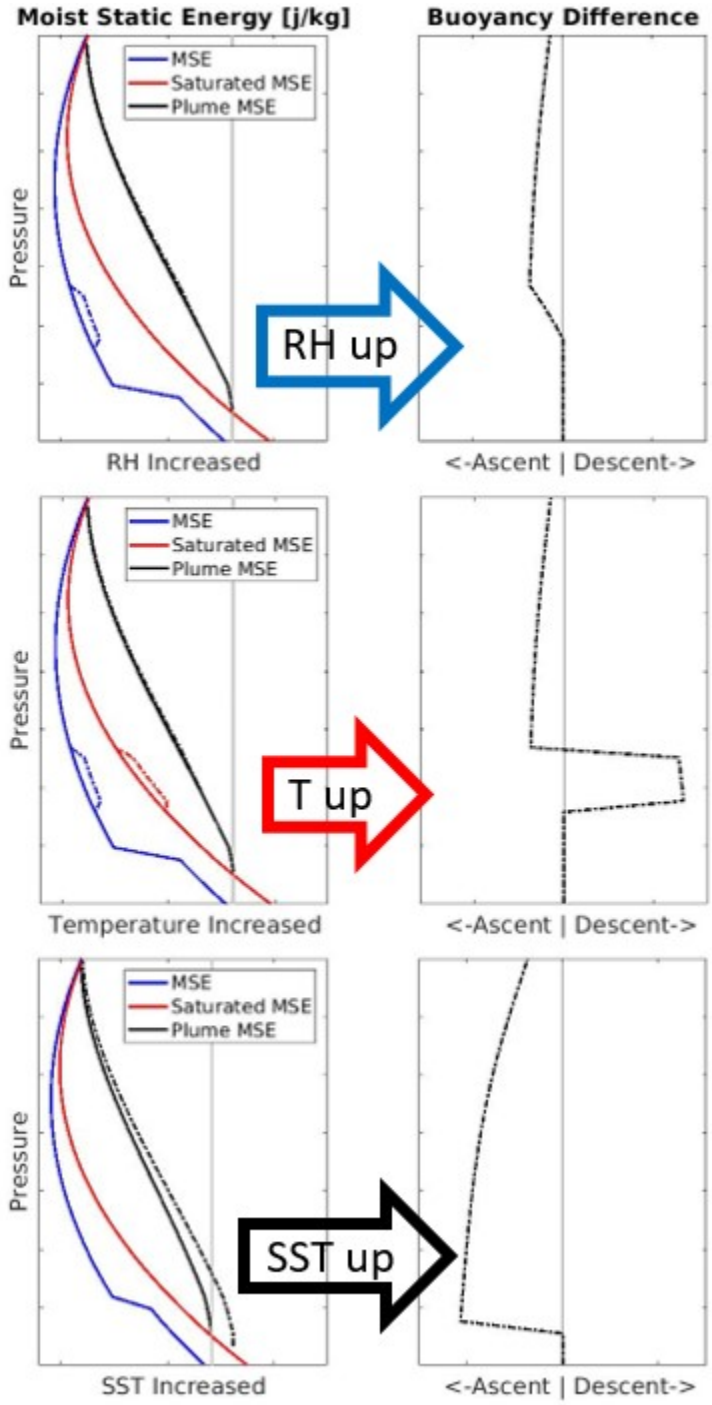

FIGURE 2.8: Figure showing the basic effect that changing the environmental temperature, moisture, or SST have on the buoyancy of an entraining plume. (a.) The Moisture change is created by increasing the MSE that the plume entrains by the equivalent of 2K over a small layer lower in the atmosphere. This change results in a small increase in the buoyancy above the change. (b.) The temperature change shown is also 2K and is over the same short layer lower in the atmosphere. In addition to the moisture change from increasing the temperature and holding the RH constant, there is the local decrease in buoyancy due to the increase in the saturation moisture with the temperature increase.

a complex system. The toy model shows higher SSTs and more environmental moisture increases buoyancy and a positive temperature anomaly leads to a negative buoyancy anomaly. I expect these same relationships to be seen in the real atmosphere, although the toy model offers no predictions to specifics of the relationship.

2.6 Reconciling the two mechanisms

I have shown that I am able to simulate bottom-heavy vertical motion without the imposition of SST gradients or a surface convergence. The sensitivity simulations and entraining plume model revealed that the most important thermodynamic factors were the temperature profile and underlying SST. Combining these facts with the predictive power demonstrated by the dynamic mechanism leads to the natural conclusion that the dynamic mechanism acts through the stability mechanism. In order to join the two mechanisms, I look at how the dynamic mechanism can interact with the stability mechanism via the temperature profile.

The primary way that the two mechanisms interact is through the dependence of the temperature profile, and thus stability, on the SST. Because of large Rossby radius of deformation in the tropics, the temperature profile above the boundary layer is constantly relaxing towards the tropical mean due to the effects of gravity wave propagation. For there to be differences in the temperature profile on climatological scales there must be a consistent source of heating difference that is strong enough to counteract the effects of gravity wave propagation. SST differences are the largest source of heating difference,

which influence the levels closest to the surface the most. The stability of the temperature profile can be simplified by describing it as the slope of the lapse rate between the surface and mid-levels. The mid-level temperature gradients are negligible and the surface temperature variations are predominantly determined by the local SST, so the variance of the temperature profile is controlled by the underlying SST. This can be seen in the temperature differences in figure (2.4), which shows a more stable temperature profile over the cooler SST of the bottom-heavy box.

Next I check the relationship between the stability and SST in our two boxes more broadly. To do this, I utilize the instability index (II) as our measure of stability of the temperature profile and stability. The II has been used previously during research of the stability mechanism and is defined as the difference of the mean saturation moist static entropy between the lower troposphere, defined from 1 to 3 km, and the middle troposphere, defined from 5 to 7 km (Raymond et al., 2015, Sessions et al., 2019). I plot the mean II and SST for every month that comprises our climatology in figure 2.9, where smaller values for the II correspond to more stable profiles. Each marker is shaped according to which box it is from and is colored according to the top-heaviness angle color map in figure (2.1) to show their combined relationship with the monthly top-heaviness angle.

There is a general correlation of higher SSTs, less stable temperature profiles, and top-heavier vertical motion. These trends are strongly dominated by both the behavior within top-heavy boxes along with the relative differences between the two boxes. The

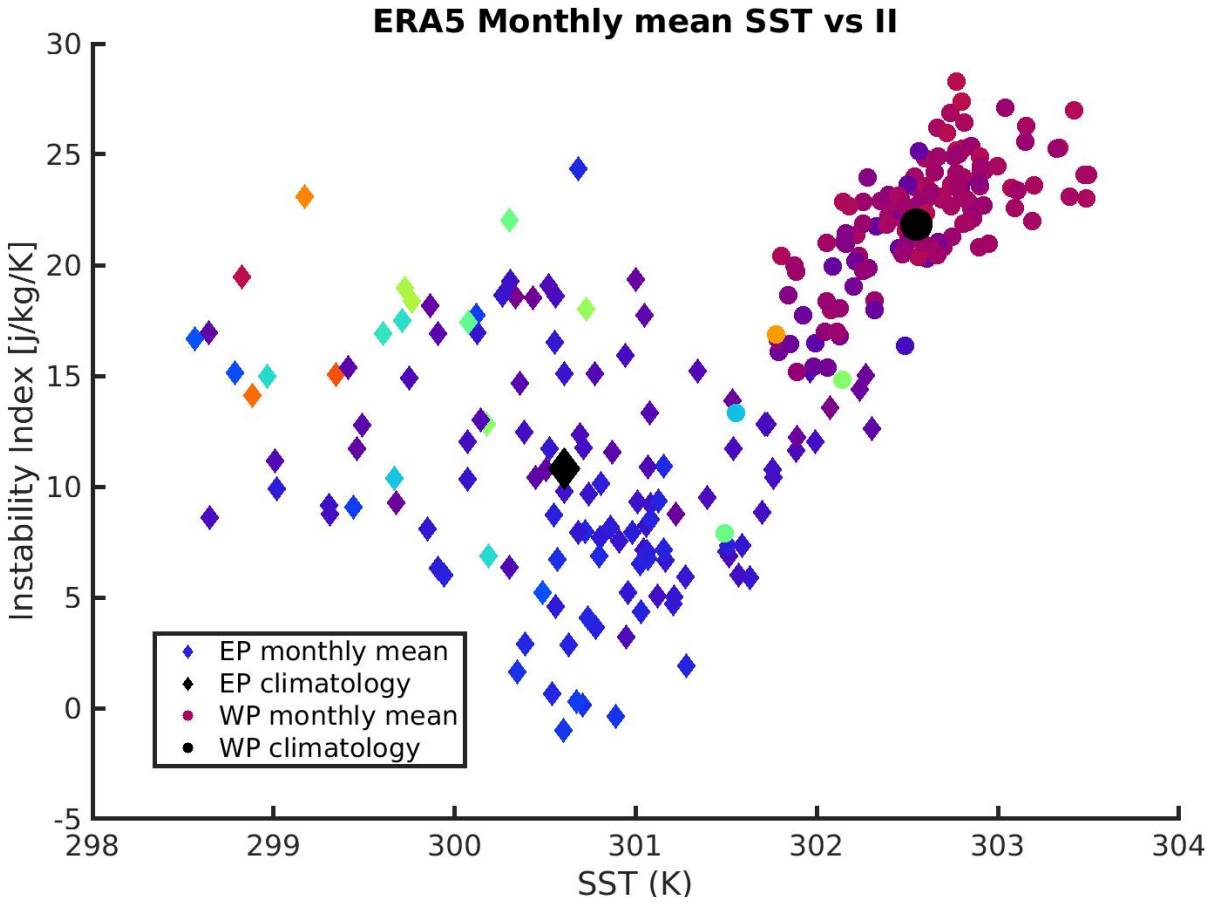

FIGURE 2.9: Comparison of the relationship between the stability and SST in each of our two regions and how these relate to vertical motion shape changes. Scatter plot of the II (a measure of temperature stratification) and SST from ERA5 climatology data. Each point is a monthly mean from the climatology that I use to simulate the East and West Pacific. The East and West Pacific are differentiated with different markers. Each point is colored according to the top-heaviness angle from that month. The legend for top-heaviness angle can be found in figure (1).

correlations between SST and stability as well as between SST and top-heaviness are missing from the bottom-heavy box. However, for each group of SSTs, an increase in the II corresponds to an increase in the top-heaviness. The general trend shows that the stability predicts the top-heaviness and in the top-heavy box the stability, and thus the top-heaviness, is predicted by the SST. Something else appears to be controlling the stability and the top-heaviness in the bottom-heavy box.

I hypothesize that the stability in the bottom-heavy box is influenced by the gradients of SST that are central to the dynamic mechanism's successful prediction of bottom-heavy vertical motion. This process is shown in figure 2.10. The mechanism initially acts as before: SST gradients imprint on the boundary layer creating bent isobars which act in conjunction with surface friction to drive a surface convergence and vertical motion. This vertical motion, because it is driven by SST gradients and not diabatic heating, leads to a relatively cooler temperature over the same magnitude SST with no gradient. Singh et al. (2019b) showed that increasing vertical motion led lower temperatures in a CRM and a bulk plume model. The dynamic mechanism appears to exert its control over the top-heaviness through the stability mechanism and the thermodynamics.

Using the entraining plume framework and reconciling the two mechanisms gives us a description of the controls over the vertical motion profile shape. Starting with the temperature profile in a vacuum, the increased stability in the Central-Eastern Pacific, characterized by a lower lapse rate, leads to bottom-heavy vertical motion because it increases the plume buoyancy near the surface which increases the vertical motion. The lower local magnitude of the SST in the central Eastern Pacific leads to less plume buoyancy and vertical motion relative to the Western Pacific. The relative difference in the SST is important to the stability differences between the two regions because the mid-level temperature across the tropics varies less compared to the surface temperature, which leads to the atmosphere over the warmer SSTs in the Western Pacific to be less stable. Finally, I posit that the SST gradients in the Central-Eastern Pacific, and their associated near surface vertical motion, act to cool and stabilize the temperature profile

beyond what the SST alone would lead to, which also contributes to vertical motion that is more bottom-heavy.

2.7 Horizontal Advection and MQE

A key result in the establishment of the stability mechanism, and the related process of moisture quasi-equilibrium (MQE), is the relationship between column moisture, dry static stability, and top-heaviness (Gjorgjievska and Raymond, 2014, Sentić et al., 2015, Sessions et al., 2015). With this result in mind, first glance would suggest that the occurrence of bottom-heavy vertical motion and stabler temperature profiles would coincide with a higher saturation fraction. As discussed earlier, this is not the case as both the reanalysis and simulations show both boxes have similar amounts of column moisture and rainfall despite their vastly different vertical motion profiles.

The simulations that I ran to validate the stability mechanism in our model also showed no relationship between the column moisture and the top-heaviness of the vertical motion. All three of the validation simulations showed nearly identical column moisture values and similar rain rates along with their drastically different top-heaviness angles. I have validated the stability mechanism and simulated the top and bottom-heavy vertical motion consistent with the stability mechanism, without showing a key relationship of the stability mechanism. The reason for this seeming paradox comes from how I parameterize the horizontal advection of moisture and whether the horizontal advection is determined primarily by local or non-local processes.

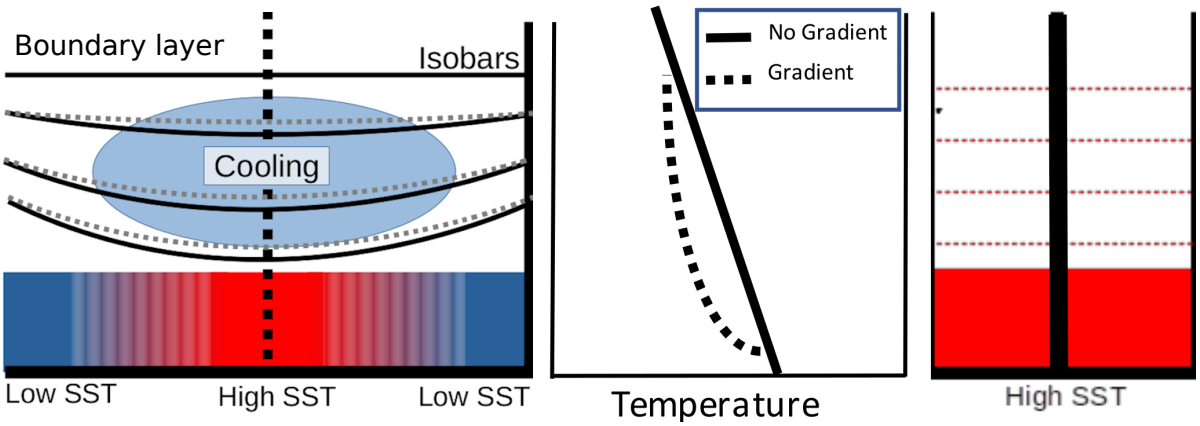

FIGURE 2.10: Schematic of how the dynamic mechanism influences the stability mechanism by changing the stability. The SST gradients in association with friction drive the convergent winds. The mass-continuity associated vertical motion leads to a climatological temperature profile that is cooler than it would be without convergent winds. The vertical motion that is imposed by the SST gradients and friction lead to a temperature profile that is more stable. Also shown is an example of a column that has the same SST but does not have a gradient and the temperatures are relatively higher than the case with a gradient.

The descriptions of the stability-moisture relationship have used vertical motion to explain the mediation, and specifically the horizontal moisture advection due to the divergence field associated with the vertical motion. Wang et al. (2016) showed that, during the DYNAMO campaign, the observed horizontal moisture advection could not be adequately captured by the local divergence field. The lateral entrainment scheme models the moisture advection due to the local divergence field and so they chose to instead parameterize moisture advection by imposing the profile from observation. I similarly choose to impose the profile of moisture advection instead of using a lateral entrainment scheme which differentiates our simulations from those previous which showed the stability moisture relationship.

I do not see the relationship between stability and moisture because the vertical motion

does not have the additional feedback to moisture from the horizontal moisture advection. The stability mechanism, and MQE, describe the relationship between stability and moisture as being moderated by the vertical motion and the net MSE import or export (Raymond et al., 2015). If the role of the vertical motion in forcing the horizontal moisture advection, the connection between stability and moisture is also weakened. The relationship between column moisture and vertical motion shape is dependent upon a strong feedback between them, which is disrupted by a strong non-local source of horizontal moisture advection variability.

2.8 Conclusion

I have, using a spectral WTG approximation, simulated the top and bottom-heavy vertical motion profile shapes from two regions in the Western and Central-Easter Pacific. Through these simulations I have uncovered that:

- The vertical motion shape differences in our regions of interest are a consequence primarily of the temperature profile and SST differences.
- A simple entraining plume model qualitatively demonstrates the stability mechanism's influence over top-heaviness.
- The dynamic mechanism likely acts through the stability mechanism, allowing us to rectify our two mechanisms.

- The correlation between dry static stability and column water vapor in the stability mechanism requires the horizontal moisture advection be primarily determined by local divergence.

I have shown that the most important differences to the top-heaviness between our two boxes are the large-scale temperature profile and the SST. The bottom-heavy vertical motion in the Eastern Pacific is due to a combination of its relatively low SST and high dry static stability, while the top-heavy vertical motion in the Western Pacific can be attributed to its higher SST and its less stable temperature profile.

The two explanations for the controls of top-heaviness, the dynamic mechanism and stability mechanisms, can be reconciled by the dynamic mechanism controlling the top-heaviness through its influence over the stability mechanism. The SST distribution, which lies at the heart of the dynamic mechanism explanation, imparts its control over vertical motion through its influence on the local dry static stability. The magnitude of the local SST sets the local temperature near the surface and that temperature control decreases with height, due to the lack of rotation. The column with the greater SST cools more quickly to reach the same temperature in the mid-levels, which leads to a greater lapse rate and more unstable atmosphere. However, I showed that this does not explain the month-to-month stability differences that I observe in the central Eastern Pacific. I hypothesize that the surface convergence due to SST gradient acts to cool and stabilize the atmosphere, which also leads to an increase in the bottom-heaviness of vertical motion.

I argue that the month-to-month stability variations in the Central-Eastern Pacific are caused by cooling attributed to SST gradient driven surface convergence.

I have also shown that the qualitative vertical motion changes can be captured by the simple model of an entraining plume. The stability validation simulations showed that the differences between the simulated WTG vertical motion profiles looked qualitatively similar to the the plume buoyancy differences that were calculated from the simulation moisture and temperature profiles. Applying a temperature anomaly led to both vertical motion and moisture profile changes. Additionally, the buoyancy differences induced by changing the SST were primarily due to moisture profile differences and not temperature profile differences. This highlights the need to understand the profile of moisture and how it interacts with the top-heaviness of vertical motion.

I have also shown the relationship between stability and column water vapor depends upon the horizontal advection being primarily forced by the local vertical velocity and moisture. When considered narrowly this indicates that the large difference in top-heaviness between our two boxes occurring without large column moisture and precipitation differences is attributed to the differences in the moisture of the surrounding environment. On a broader scale, this means that the stability-moisture relationship from MQE and the stability mechanism is applicable when the moisture advection is primarily driven by the local moisture and divergence fields and requires knowledge of the surrounding moist environments. Such an instance would be large storms in higher absolute vorticity environments, such as the storms undergoing cyclogenesis from Gjorgjievska and

Raymond (2014). Future research is needed to understand where these relations can be safely applied.

The research presented here demonstrates the need to understand the thermodynamic environment in order to predict the vertical motion profile. The temperature profile plays a key role in moderating the relationship between vertical motion and moisture, and the SST distribution enforces vertical motion changes through the temperature profile. I can apply this newly gained understanding to tropical forecasting and modeling efforts in order to diagnose and fix our representations of the important processes.

Chapter 3

Environmental controls of vertical motion shape from OTREC observation

3.1 Introduction

Vertical motion is an essential piece of the tropical atmosphere puzzle, where it plays a role in a wide range of processes, including the evolution of vorticity and divergence (Adames, 2022, Raymond et al., 2014), convective amplification and wave dynamics (Inoue et al., 2020b, Inoue and Back, 2017, Raymond et al., 2015), and precipitation and radiation (Back and Bretherton, 2009a, Yasunaga et al., 2019). Our understanding of the processes that control vertical motion, and the shape of its profile in particular, is incomplete.

This complicates the diagnosis of the biases in our various models, which it has been argued can be addressed by uncovering reliable process oriented diagnostics (PODs) that describe how well models reproduce the relationships of a process. Improving our ability to find the problems is the first step down a path towards improving our ability to forecast weather and project climate change (Maloney et al., 2019).

I investigate observations from a recent field campaign, the organization of tropical East Pacific convection (OTREC), to better understand what controls the shape of vertical motion profiles in order to develop PODs of vertical motion and its associated processes. The OTREC field campaign collected observations of a wide variety of vertical motion profiles and their thermodynamic environments in the Eastern Pacific and Western Caribbean (Fuchs-Stone et al., 2020). Our understanding of these regions is limited, with the shape of the profile of vertical motion having only been established recently (Back and Bretherton, 2006, Back et al., 2017). The regions are prone to observational errors (Rui and Yunfei, 2005), global climate modeling errors (Dai, 2006), and even simple models have trouble properly representing the behavior in the regions (Singh and Neogi, 2022). The OTREC observations provide an opportunity to quantify the vertical motion and its environment to develop a more holistic understanding of tropical convection and large-scale vertical motion.

The top-heaviness of vertical motion is a particularly important aspect whose controls I do not fully understand. The top-heaviness describes whether the altitude of the maximum velocity is in the upper or lower troposphere. Vertical motion is top-heavy when the peak

occurs higher in the atmosphere, and bottom-heavy when its peak is closer to the surface. The top-heaviness changes the energy that moisture advection, moist static energy (MSE) advection, and radiative cooling contribution to the energy budget (Back and Bretherton, 2009a). The vertical motion profile shape also plays a role in the relationship between moisture and precipitation (Masunaga and Mapes, 2020). It has been argued that the ability of a model to represent bottom-heavy vertical motion is statistically related to climate sensitivity (Sherwood et al., 2014). Understanding the top-heaviness distribution is important to understanding the changes to the distribution of precipitation that will come with climate change(Duffy et al., 2020). Top-heaviness also plays a role in tropical cyclogenesis through vorticity convergence (Gjorgjievska and Raymond, 2014, Raymond et al., 2014).

There are several controls of top-heaviness that have been explored in the literature, but the role of the vertical profile of moisture has not been articulated. Recent research has shown that top-heaviness differences, which are driven by large-scale temperature changes, are coincident with important moisture profile differences that were nearly invisible when looking only at the total column moisture (Bernardez and Back, 2023c). The strength of the relationship between the top-heaviness and column moisture is related to how strongly vertical motion and horizontal moisture advection are coupled. This highlights the need to understand the profile of moisture in order to understand the profile of vertical motion.

In this work, I seek to understand how this complicated interlinking clutter of controls operate during OTREC, to incorporate these controls into a more cohesive understanding

of vertical motion, and to develop PODs that can be used to diagnose representations of vertical motion top-heaviness. I will utilize date from the OTREC field campaign as well as the hi-resolution forecasts used during the campaign in order to answer the following questions:

- How does the vertical structure of temperature and moisture relate to the top-heaviness of vertical motion?
- How well does the forecast model capture the observed behavior?
- Can I use a simple entraining plume model to develop a framework that describes the relationship between vertical motion and the large-scale moisture and temperature?

In the next section, I discuss what the observations tell us about the controls of vertical motion profile shape. After this, I use a simple entraining plume model to explore the co-evolution of moisture and vertical motion. I discuss a framework I call vertically resolved moisture quasi-equilibrium (VR-MQE) and how it explains the relationship between vertical motion and moisture moderated through the temperature profile. Finally I analyze a forecast model that was used during the OTREC field campaign, to see how well it replicates the relationships that I see observations.

3.2 Vertical motion and its environment

In this section, I first describe the data that I am using in this investigation. After, I will discuss the top-heaviness angle which describes the vertical motion profile. I will

show what the observations of vertical motion top-heaviness and its controls. Lastly, I will detail how the interactions between the temperature and moisture profile allow us to better understand what controls top-heaviness.

3.2.1 OTREC observations

The OTREC field campaign was an airborne research campaign in the East Pacific and Western Caribbean, created and designed to observe a wide variety of weather conditions that are not biased by choosing where to fly based on the forecast (e.g. MJO event, easterly wave, pre-cyclone or even predicted rainfall) (Fuchs-Stone et al., 2020, Raymond and Fuchs-Stone, 2021). During the field campaign, 22 research flights were flown which sampled one of two boxes in the East Pacific and Western Caribbean respectively. The flights were flown at a height of approximately 14 km and dropped a dropsonde every 1 °in a lawnmower pattern. The dropsondes measured the temperature, moisture, pressure, and horizontal wind profiles as they fell.

These observations were then combined and regridded using the 3DVAR technique (López Carrillo and Raymond, 2011), which smooths, balances, and downscales the measurements to a 0.25°grid by minimizing a penalty cost function. The vertical motion is calculated using the measured horizontal winds and mass continuity, along with an assumption of no vertical wind at the surface and 16 km. For this research I treat each of the downscaled columns as individual data points and I trust the data up to the height where the flights were flown which is just above the 200 hPa level. In the next section I will discuss how I parse through these observations.

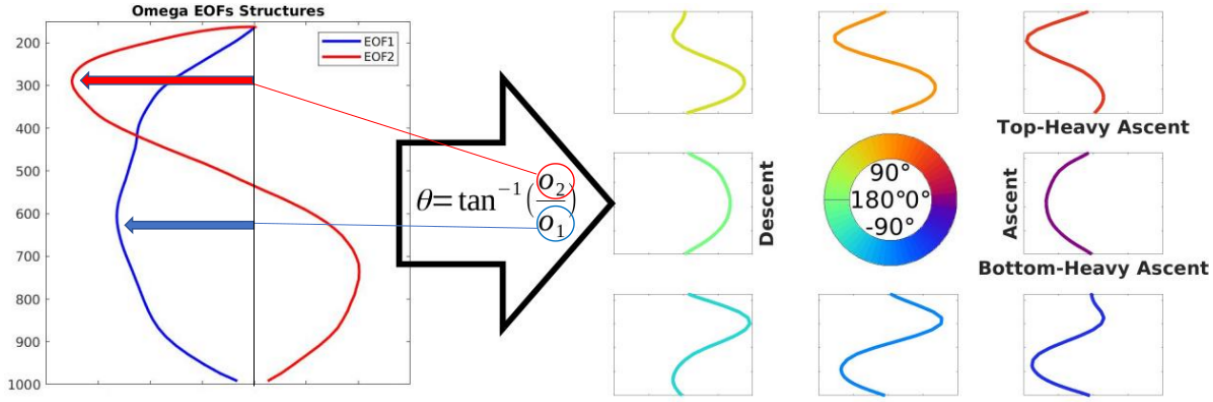

FIGURE 3.1: The empirical orthogonal functions used in this research and how they represent the variability of vertical motion through the top-heaviness angle. The two EOFs are shown on the left. The right shows the top-heaviness angle legend and its relationship to the vertical motion profile.

3.2.2 Quantifying vertical motion profile shape

Before I begin to describe the variability of the vertical motion profile shape, I introduce the metric that I am using, called the top-heaviness angle(Bernardez and Back, 2023c), which is an improved version of the top-heaviness ratio (Back et al., 2017). The top-heaviness angle and ratio calculations utilize the assumption that vertical motion profiles can be represented by the sum of two vertical functions:

$$\omega(x, y, p, t) = o_1(x, y, t)\Omega_1(p) + o_2(x, y, t)\Omega_2(p). \tag{3.1}$$

$o_{(1,2)}$ are the amplitudes of the vertical structure functions $\Omega_{(1,2)}$, which are shown in figure (3.1 a). I find the amplitudes by projecting the vertical motion onto the two structure functions, depicted as the blue and red arrows respectively. The top-heaviness angle is

the arctangent of their ratio:

$$\phi_{TH}(x, y, t) = \arctan(\frac{o_2(x, y, t)}{o_1(x, y, t)}). \tag{3.2}$$

The relationship between this top-heaviness angle and the vertical motion profile can be seen in figure (3.1 b). Angles near zero are ascending while angles near ±180 are descending. The angles that are close to zero and negative are bottom-heavy, while angles that are slightly positive are top-heavy. This angle is the phase angle for a point describing the vertical motion on the phase plane described by the two modes.

I use the first two empirical orthogonal functions (EOFs) from a principal component analysis of vertical motion as a function of pressure using 40 years of daily maritime vertical motion from ERA-5 from 1978-2019. These first two modes of a PCA decomposition have been shown to describe a majority of the variance in vertical motion profile shape (Back et al., 2017), and similar modes have been broadly used in a variety of studies (e.g. Khouider and Majda, 2006, Kuang, 2008, Masunaga and L'Ecuyer, 2014, Peters and Bretherton, 2006).

The observed profiles of vertical motion from the 3Dvar OTREC data that is derived purely from dropsondes are composited by top-heaviness angle and shown in figure (3.2 a), along with the relative frequency of all top-heaviness angles. The observations have been composited based on their top-heaviness into 1°bins angle. The angles that are near 0 °are ascending (shown in blue), with the nearby positive angles being top-heavy and

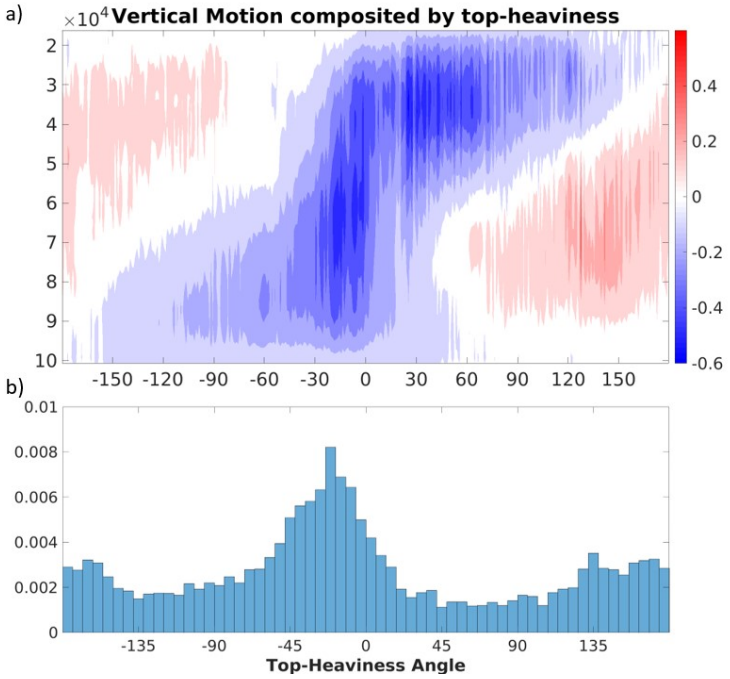

FIGURE 3.2: The vertical motion that was observed during OTREC, composited by the top-heaviness angle. The vertical motion shown is the mean of the vertical motion separated according to the top-heaviness angle into bins 1 °wide. Blue colors show ascent and red colors show descent.

the negative angles being more bottom-heavy, and angles around ±180° are descending. A transition from congestus to deep to stratiform convection is represented by a top-heaviness angle change from negative to positive angles through 0 °, in a transit around the top-heaviness phase plane defined by the two modes. I use the top-heaviness angle in order to explore the thermodynamics relationship to vertical motion in the next section.

3.2.3 Connecting moisture and temperature

The thermodynamics are important to controlling the top-heaviness, specifically the stability contributed by the large-scale moisture and temperature profiles (Raymond and Flores, 2016, Raymond et al., 2015, Sessions et al., 2019). Previous research has found

that a temperature profile with greater dry static stability will tend to have bottom-heavy vertical motion which will tend to be associated with a moister environment and more precipitation (Gjorgjievska and Raymond, 2014, Raymond and Sessions, 2007). The large-scale moisture is associated with the vertical motion through the well known precipitation-moisture relationship (Bretherton et al., 2004, Raymond, 2000). However, the importance of the vertical structure of the moisture profile in driving moist convective instability changes and their affect on top-heaviness has not been clearly demonstrated. Next, I check how the profiles of temperature and moisture vary with the top-heaviness in order to verify already known mechanisms and uncover deeper insights into their relationship.

I look at how the profiles of temperature and moisture vary with the shape of vertical motion by compositing the anomalous relative humidity (RH) and temperature profiles by the top-heaviness angle (see figure 3.3). I calculate the anomalies by removing the mean temperature and moisture profiles from the entire OTREC data set. With this choice, I assume that the mean temperature and moisture profiles are consistent between both domains and are temporally stationary. These assumptions may be overly simplistic and remove important variability; however for the present purposes it is suitable to explore the relationship between top-heaviness and the environment.

Starting with the observations of RH anomaly, figure (3.3 a), I see positive moisture anomalies during ascent and negative anomalies during descent. A small positive RH anomaly seems to start at the surface near $\pm$ 180 $^\circ$ and grows into the troposphere as

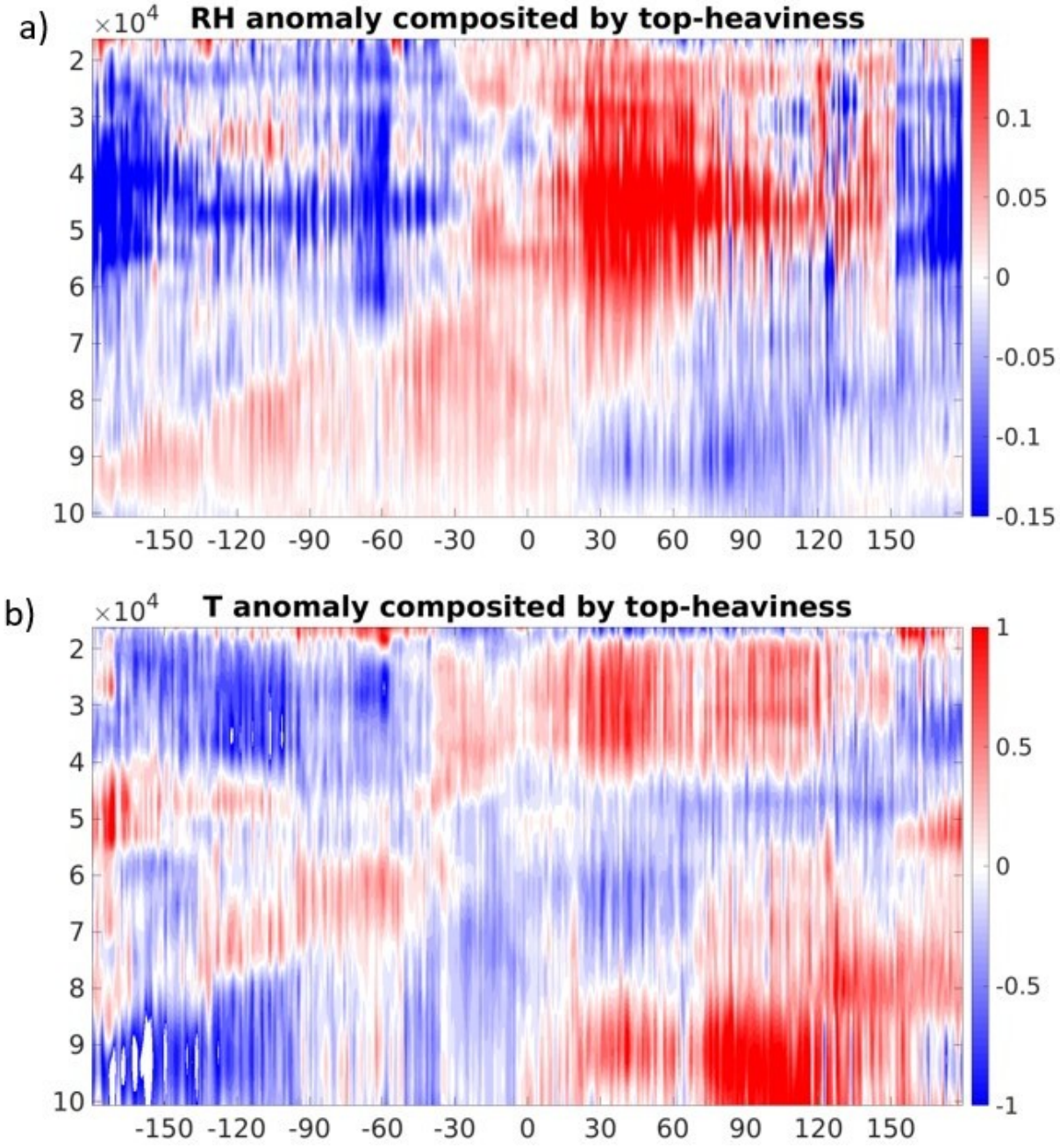

FIGURE 3.3: Observational temperature and moisture anomalies composited by the top-heaviness angle. The temperature anomalies are first sorted into bins 1°wide, then each bin is averaged. Red indicates a positive temperature anomaly, while blue represents a negative temperature anomaly.

the top-heaviness approaches zero. The RH anomaly extends nearly the entire depth of the troposphere after a top-heaviness angle of -30 °, and after a top-heaviness of 30 °the RH anomaly near the surface becomes negative and the RH anomaly in the upper troposphere becomes large. There is a symmetrical negative moisture anomaly that starts near a top-heaviness angle of 0 °, which rises into the troposphere and is associated with column descent when it extends the entire depth of the troposphere. The RH anomalies line up with the vertical motion, where a positive anomaly is correlated with upward vertical motion.

Looking at the temperature anomaly, I see what looks like a negative of the RH anomaly. A negative temperature anomaly starts near the surface and rises as the top-heaviness angle approaches zero. After zero degrees, a positive temperature anomaly forms low in the atmosphere and begins growing upwards. There are some differences between the RH anomalies and the inverse of the temperature anomalies are seen in the upper troposphere. Angles between -180°and -30 °show a negative temperature and moisture anomalies and similarly the angles between 30 °and 150 °shows a positive anomaly where the RH anomaly is also positive.

3.2.4 Moisture profile variability

The thermodynamic variables tend to be less noisy than the vertical motion and are currently more easily observed from our satellite platforms, so compositing by thermodynamic variables rather than the more noisy vertical motion top-heaviness is advantageous.

I choose to composite by moisture profile because it can describe the vertical motion profile variability. The total column moisture anomaly distinguishes ascent versus descent, which is known from previous work on moisture-precipitation relationships. Figure 3 shows a dipole shaped anomaly in the relative humidity which is related to the observed top-heaviness differences.

I use the saturation fraction (SF) to describe the total column moisture anomaly. The SF is also known as the column RH in other research (e.g. Bretherton et al. (2004)) and is the ratio of column moisture to moisture the column could hold if saturated:

$$SF = \frac{\int_{P_{surface}}^{P_{top}} qv \partial p}{\int_{P_{surface}}^{P_{top}} qv^{\star} \partial p}.$$

where qv is the specific humidity, $qv^{\star}$ is the saturation specific humidity, and the integration is over the depth of the troposphere. Previous research has shown that the SF predicts the amplitude of vertical motion. This can be inferred from the non-linear relationship with precipitation (Bretherton et al., 2004, Raymond et al., 2015).

Top and bottom-heavy vertical motion are distinguished in the observed relative humidity anomalies (figure 3.3) by a moisture dipole consisting of a positive (negative) anomaly above a negative (positive) anomaly. I define the moisture dipole coefficient (MDC) in order to measure the dipole anomaly. The MDC is similar to the SF except I calculate the integrated RH for the atmosphere in two layers and instead of adding them, I subtract

the upper layer from the lower layer:

$$MDC = \frac{\int_{P_{surface}}^{P_{middle}} qv\partial p - \int_{P_{middle}}^{P_{top}} qv\partial p}{\int_{P_{surface}}^{P_{top}} qv^{\star}\partial p}.$$

Where the variables are the same as the SF, with the addition of P_{middle}, which is the level that separates the two nodes of the dipole. Larger MDC values have more moisture in the lower atmosphere and smaller values have more moisture in the upper atmosphere.

I define the MDC so that the 600 hPa level separates the lobes of our dipole because it separates the largest moisture anomalies in the top-heavy region well and does a reasonable job distinguishing the dipole for bottom-heavy angles. The level also generally coincides with the freezing level where important processes related to ice are dominant, for example the large radiative heating differences associated with ice (Lin and Emanuel, 2022). Another sensible way to define the dividing level of the atmosphere would be to find the two levels such that both halves have equal integrated saturation moisture. Our results are not sensitive to whether I choose this methodology or the methodology described above, so I choose the simpler method.

I composite/examine vertical motion as a function of SF and MDC in order to examine how well the simple description is able to capture the variance in the vertical motion profile shape. Figure (3.4), shows the vertical motion composited by SF and MDC terciles. The SF varies with the magnitude of the vertical motion, with the highest SF profiles having the greatest magnitude of vertical motion. The MDC controls the top-heaviness with the

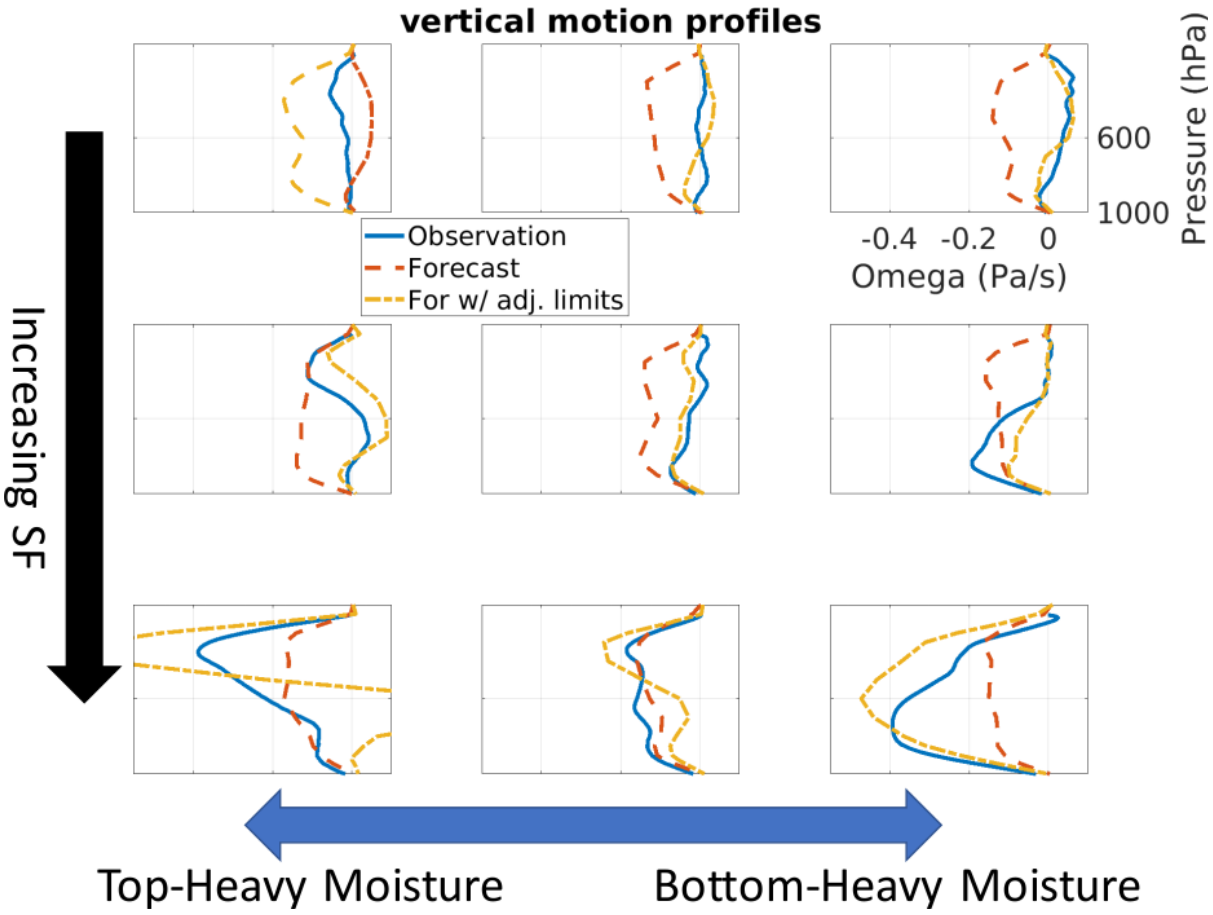

FIGURE 3.4: Vertical motion profiles from OTREC (blue) and the ECMWF 48 hour forecast (orange and yellow) for the same time of day and region as the OTREC flights. Each data set is separated into thirds based on the terciles of both the MDC and the SF and then averaged giving 9 profiles corresponding to the high, medium, and low MDC and SF profiles. The limits of the terciles are relative to the dataset for the blue and orange lines and the yellow line shows the forecast data composited using the observational limits.

most bottom-heavy MDC profiles showing bottom-heavy vertical motion and the most top-heavy MDC profiles showing top-heavy vertical motion.

I believe that the relationship between moisture and vertical motion is a mutual adjustment process which responds to the temperature profile. I hypothesize that a greater moisture anomaly sustains greater precipitation and vertical velocities at those levels through its impact on buoyancy (Schiro and Neelin, 2019). Additionally, the vertical

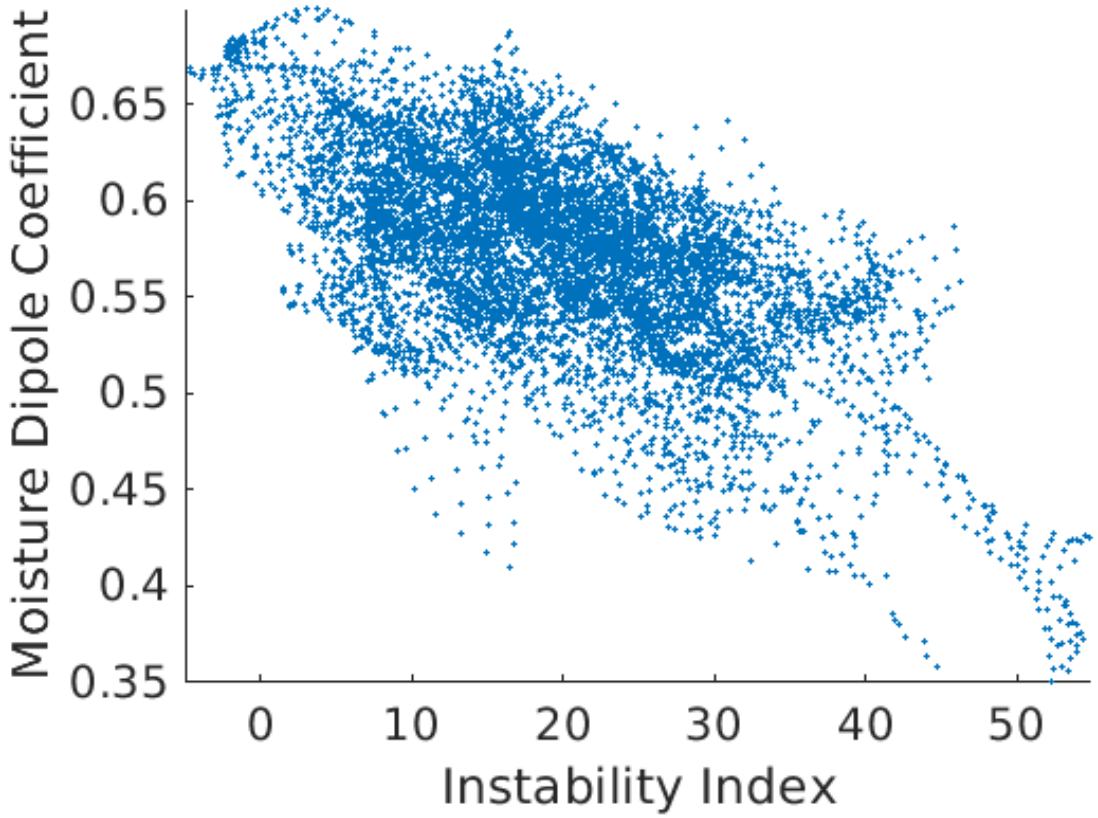

FIGURE 3.5: Correlation of moisture and temperature as a function of height. Each point on the plot represents a correlation between the temperature and moisture at two heights. The temperature has been scaled to moisture units by calculating the saturated mixing ratio and using that in the correlation calculation.

motion affects moisture anomalies through moisture advection and the detrainment of moisture. I next look for how they co-evolve and are related to the temperature profile.

3.2.5 The stability-moisture relationship

The large-scale temperature profile is a good initial guess for what controls vertical motion and moisture, because it adjusts more quickly due to the propagation of gravity waves (e.g. Raymond and Zeng (2005), Sobel and Bretherton (2000), Sobel et al. (2001)). I also know that the temperature and moisture anomalies are transitively related to one another,

owed to their shared relationship to the top-heaviness. Figure 3.3 shows that a bottom-heavy vertical motion profile and bottom-heavy MDC anomaly occur coincidentally with a cool temperature anomaly near the surface and the reverse is true for top-heavy vertical motion and top-heavy MDC anomaly, which coincide with top-heavy vertical motion. The change in dry static stability that I wish to measure is captured by instability index (II), which previous research has used to investigated the connection between temperature, moisture, and vertical motion (Raymond et al., 2015, Raymond and Sessions, 2007). The II provides a compact representation of the difference between lower tropospheric and mid tropospheric temperature (Raymond et al., 2015):

$$II = S_{1-3km} - S_{5-7km}.$$

The S in this context is the dry entropy and the subtext denotes the levels over which the average is taken. I have used entropy to be consistent with previous work, but this could also be defined using dry static energy. A high instability index corresponds to a more dry statically unstable column and usually accompanies more top-heavy vertical motion, while a low instability index is stable and associated with more bottom-heavy vertical motion (Gjorgjievska and Raymond, 2014, Raymond et al., 2014, Raymond and Sessions, 2007, Sessions et al., 2019).

The correlation between moisture and temperature profiles, using the MDC and the II, is shown in figure 3.5. I hypothesize that the close correlation between the stability

and moisture dipole is indicative of a vertically resolved moisture quasi-equilibrium (VR-MQE). Moisture quasi-equilibrium (MQE) is the process of moist convective instabilities controlling column moisture. The convection is controlled by the large-scale instability and controls the import of moisture and thus the precipitation. The process is a "moisture" quasi-equilibrium process because the moisture balances more slowly than the temperature, due to the difference in speed between gravity waves and direct mixing. The temperature profile evolves quickly towards equilibrium and thus the slower evolving moisture feels a constant temperature as any anomalies have been eliminated by the time the moisture can react.

I hypothesize that VR-MQE means that there is a critical moisture profile for each temperature profile that the atmosphere tries to move toward and this is why figure (3.5) shows a strong correlation. I will show our hypothesis for how this process occurs using the simplified framework of an entraining plume model, which is described in the next section.

3.3 VR-MQE through an entraining plume model

3.3.1 The basic model

The relationship between the vertical motion, moisture, and temperature profiles can be explained using a simple entraining plume model along the lines of those used recently in other work (Abbott and Cronin, 2021, Adames et al., 2021, Ahmed and Neelin, 2018, Singh and Neogi, 2022, Singh et al., 2019a). The model describes a plume that is lifted

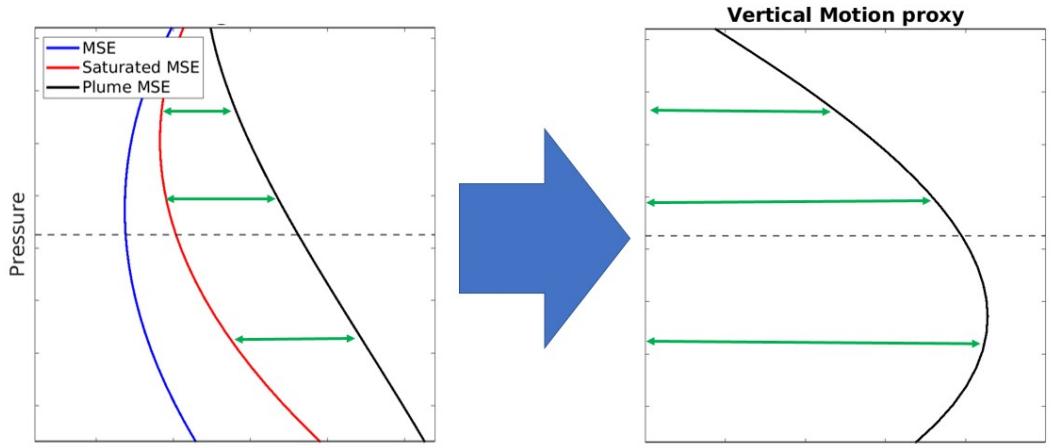

FIGURE 3.6: Diagram that shows how the plume buoyancy is calculated from the plume MSE and environmental saturation MSE. The left side shows the environmental MSE as the blue line, the environmental saturated MSE as the red line, and the plume MSE as the black line. The plume MSE would be a straight line upwards if there were no entrainment. The greater the entrainment rate or the greater the moisture deficit the more the line will bend to the left. When the plume MSE line intersects the environmental saturation MSE, the plume is no longer buoyant. The moisture deficit is represented by the distance between the blue and red lines. The distance between the red and black lines, shown here with green lines, is the plume buoyancy. Subtracting the plume MSE from the environmental saturation MSE gives the plumes excess temperature in units of energy.

from the surface to the lifted condensation level where it begins a buoyancy fueled rise, entraining environmental air and losing energy along its journey, until it finally comes to rest, detraining its moisture into the environment as it rises. The large-scale moisture controls the vertical motion through its effect on buoyancy of an entraining plume and the vertical motion controls the large-scale moisture through its relationship to the detrainment of moisture from the plume. I now work to fill in the details of this summary.

The plume model is built upon the assumption that the plume only loses energy when it entrains lower energy air:

$$\frac{\partial h_p}{\partial z} = -\epsilon(h_p - h_e) \tag{3.3}$$

Where $h = c_p T + gz + L_v q$ is the moist static energy (MSE), c_p is the specific heat capacity of air, T is the temperature, L_v is the latent heat of vaporization of water, q is the specific humidity, g is gravitational acceleration, and z is the height. h_p is the MSE of the plume and h_e is the MSE of the environment. The entrainment rate is given by ϵ, and I choose to make it constant with height with a value of $0.25[km^{-1}]$. I calculate the plume's MSE profile and buoyancy by integrating equation (2) from the lifted condensation level to the top of the atmosphere. I then calculate the plume buoyancy from the difference between the plume's MSE and the environmental saturation MSE. See appendix A for details of the calculation.

I can use the plume buoyancy as a proxy for the convective vertical velocity by assuming that the plume rises in a high friction, high drag environment (Hernandez-Duenas et al., 2019). Under this assumption, the buoyancy of the plume is directly related to the vertical velocity, which contrasts with the traditional view of the plume buoyancy fueling the acceleration of the vertical velocity. I will use the plume buoyancy as a direct proxy for updraft velocity because it simplifies our analysis of how the vertical motion and environment interact and the high friction limit assumption matches observations and is a better fit for some average cloud statistics (Hernandez-Duenas et al., 2019, Romps and Öktem, 2015).

The convective updraft speed is part of the composition of the large-scale vertical motion, with clear air subsidence velocity and area fraction being the other two components:

$$\overline{w} = Aw_u + (1 - A)w_d \tag{3.4}$$

Here $\overline{w}$ is the largescale vertical velocity, w_u is the convective updrafts, and w_d is the between cloud subsidence, and A is the fraction of each level that is occupied by updrafts. The subsidence velocity is determined by the radiational cooling rate which I do not expect to change dramatically, for the purposes of our analysis I will neglect the term $(1 - A)\omega_d$ so I can relate convective vertical velocity to entrainment and detrainment of cloudy air. This leave the area fraction to obfuscate the relationship between the convective updraft velocity and the large-scale vertical motion. I assume that the profile of area fraction will stay constant throughout this chapter.

The entrainment and detrainment rates are also related to the upward convective massflux by way of mass continuity. When vertical motion increases more with height this must either be associated with an increase in the amount of air entrained or decrease the amount of air detrained by the plume. In other words, the slope of the largescale vertical motion is related to the sum of the fractional entrainment or detrainment rates. The equation that describes the relationship between the vertical velocity and the entrainment and detrainment rates, following Romps (2014) and Singh and Neogi (2022), is written as:

$$\frac{1}{A\rho w_u}\frac{\partial A\rho w_u}{\partial z} = \epsilon - \delta \tag{3.5}$$

Here w_u is the convective updraft velocity (units of ms^-1), ρ is the density (units of kgm^3), ϵ is the fractional entrainment rate (units of m^-1), and δ is the fractional detrainment rate (units of m^-1). Because I will choose to use a constant fractional entrainment rate in the calculation of our plume buoyancies only the detrainment can balance variations on the LHS of the equation, which can come from either updraft velocity differences or area fraction differences. Because I have neglected the second term in equation 3.3.1, I can replace the updraft velocity and area fraction with the large-scale vertical velocity, allowing us to to directly relate changes in the detrainment to changes in the large-scale vertical velocity.

The detrainment, in a steady state, controls the large-scale moisture in a balance with subsidence drying (Romps, 2014). If subsidence is the same between two cases, then the detrainment variations will control the largescale moisture variations. The relationship between the vertical motion slope, detrainment, and moisture is illustrated in figure 3.7. This figure shows a sample vertical motion profile and ways the slope could increase or decrease along with how those detrainment changes would affect the largescale moisture. A rightward deflection of the slope, equivalent to an increase in the vertical motion, corresponds to a decrease in detrainment, given entrainment is constant and the profile of area fraction changes is constant. This acts as an anomalous drying source. A leftward deflection of the slope, equivalent to a vertical motion decrease, leads to an increase in detrainment and moistening.

Now that I have conceptually linked the profiles of vertical motion and moisture using

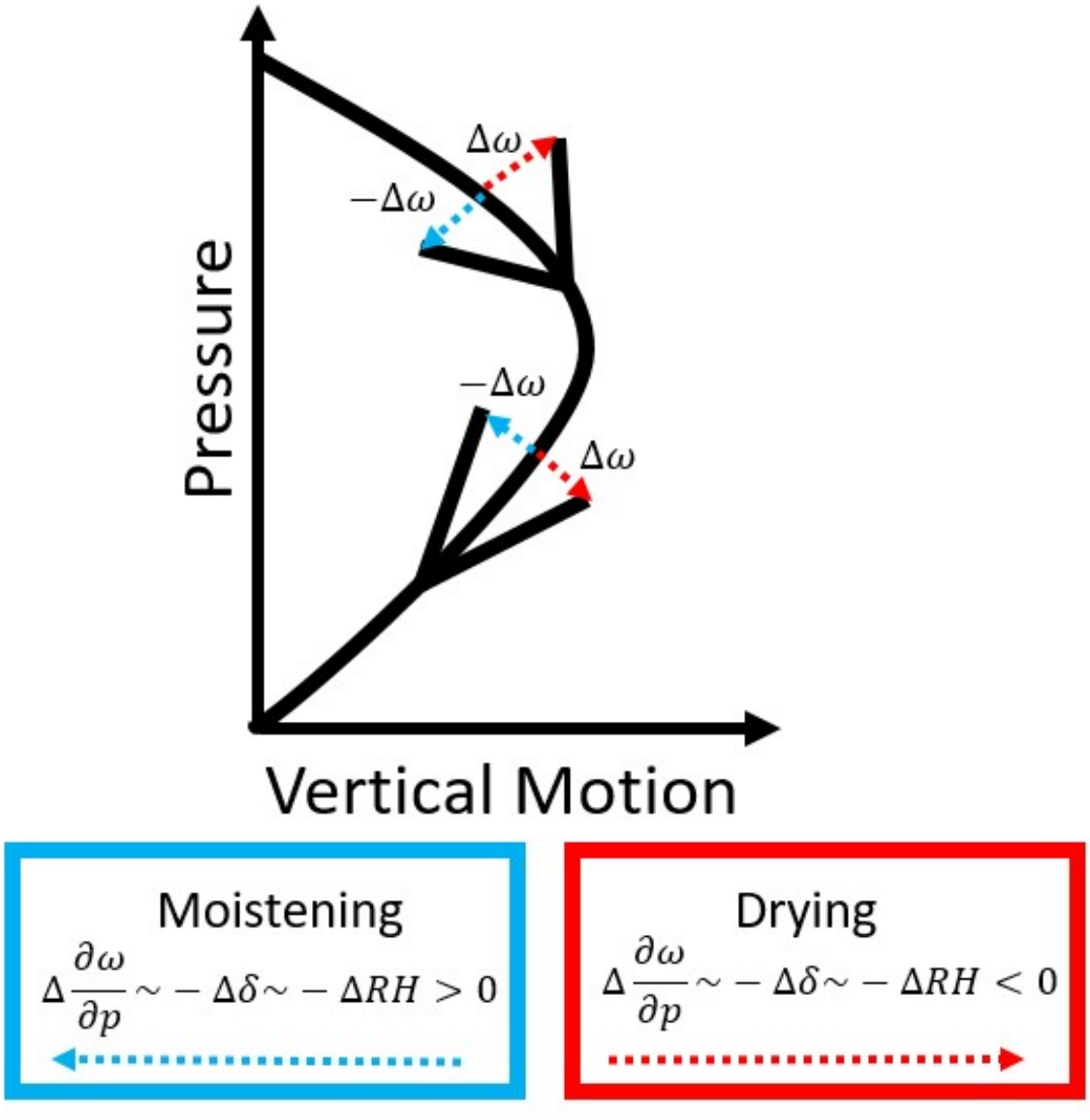

FIGURE 3.7: This schematic shows the effects of changing vertical motion profiles on detrainment and moistening tendency associated with detrainment, under the assumption that entrainment is constant. If the slope of vertical motion tilts further to the right, the associated changes to detrainment will cause a drier profile. If the slope of vertical motion tilts to the left, the detrainment changes will cause a moister profile.

the framework of a simple entraining plume, I turn to the results of the model which demonstrate the principal of VR-MQE.

3.3.2 Moisture and the entraining plume

VR-MQE supposes that there is a critical moisture profile which the atmosphere tries to approach by modifying the vertical motion profile. In order to demonstrate this process I start with an idealized atmosphere, perturb the environmental moisture, and check how the buoyancy responds. The buoyancy changes then give us information about how the vertical motion and its moistening tendency will change.

The idealized atmosphere is constructed starting with a surface temperature which changes at a constant rate with height. The moisture profile is calculated using a constant relative humidity. From the environmental moisture and temperature I calculate the environmental MSE and saturation MSE along with the plume MSE (thin solid lines in figure 3.8 a and d). I then add two different moisture anomalies, one of which increases the SF (top panels) and the other of which increases the MDC (bottom panels), in order to show how the plume buoyancy and vertical motion respond to moisture anomalies. The MDC anomaly is constructed so that it has no effect on the SF (thick dashed lines in figure 3.8 a and d). The red line is the saturation MSE, the blue lines are MSE profiles and the black lines are the plume energy profiles that I calculate.

The plume buoyancy is shown in figure (3.8 b and e) for the anomalous (dash or dot-dash) case and basic (solid) case. When the SF is increased I see an increase in the buoyancy

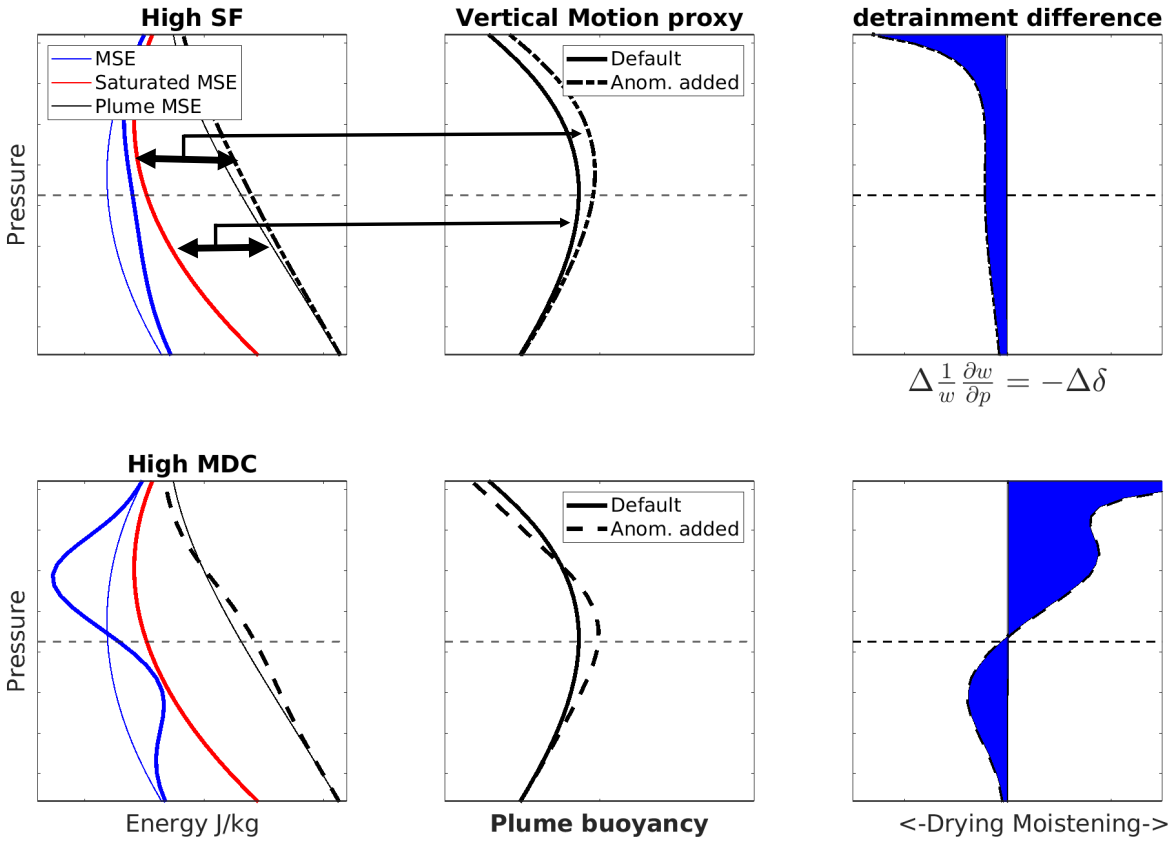

FIGURE 3.8: Schematic showing the effect of a SF anomaly or an MDC anomaly to the plume buoyancy, detrainment, and the associated anomalous moistening or drying. The top set of panels shows the SF anomaly case and the lower set of panels shows the MDC anomaly case. The first column shows the profiles of MSE, saturation MSE, and plume MSE. The thin blue line is the unaltered moisture, which corresponds to the solid plume MSE line. The dashed plume MSE has the moisture anomaly included. The second panel shows the plume buoyancies, which are proportional at each level to the difference between the plume MSE and saturation MSE. The plume buoyancy is our proxy for vertical motion because I am assuming our parcels rise in a high friction environment. The final panel shows the difference between the slopes of the plume buoyancies in solid blue. This represent a qualitative measure of the difference in detrainment between the two vertical motion proxies (neglecting area fraction changes), and therefore the difference in moistening between the two profiles. Negative values indicate anomalous drying and positive values indicate anomalous moistening. This figure demonstrates that for the profiles chosen, a moisture anomaly modifies the plume buoyancy such that the resulting vertical motion and detrainment changes act to get rid of the moisture anomaly.

throughout the vertical levels, while an increase in the MDC leads to a buoyancy anomaly of the same sign but which peaks higher in the atmosphere. The increase or decrease in the plume buoyancy due to an increase or decrease in the moisture at that level and below is a straightforward consequence of the buoyancy losing more or less energy to entrainment as it rises.

I first calculate the slope of the two profiles from the middle panels then subtracting the unperturbed slope from the perturbed slope, which shows the differences in detrainment (neglecting changes in the profile of area fraction) and thus moistening anomaly. The moistening and drying effects by the detrainment differences, which I infer from the buoyancy differences, are shown in figure (3.8 c and f). The area between the detrainment anomaly curve and zero has been filled, when the filled area is positive the buoyancy slope differences imply moistening and vice versa.

In both cases the buoyancy responded in a way that would act to remove the anomaly that I added. In the case of the SF anomaly, there is anomalous drying over the depth of the anomaly. Similarly, the MDC anomaly leads to a moistening and drying tendency that tries to eat away at the MDC anomaly. Over a long timescale, the tendency for the vertical motion to remove moisture anomalies will lead to a moisture profile that is in balance with the environment, specifically the temperature profile, which I hypothesize is why there is a correlation between the MDC and II in figure (3.5. With the idealized case of VR-MQE established, I next check that the explanation fits the observations.

3.3.3 entraining plumes of observations

Next I examine how the buoyancy of entraining plumes is related to the vertical motion profiles and find this is broadly consistent with our hypothesis. The OTREC observations are of an atmosphere that is near balance, which when combined with the simplicity of the entraining plume model, mean I am only looking at the qualitative differences produced by the entraining plume model. In order to focus on MDC differences, I take the moisture and temperature profiles from the top quartile of SF and then divide them into equal bins according to the MDC. I then calculate the plume buoyancies for each of the three bins and for the average of all of the plumes. I take the difference to show the buoyancy effect caused by the temperature and moisture differences in the different MDC environments (figure 3.9 b). The Low MDC case shows an increase in the top-heaviness of the buoyancy while the high MDC case shows a more bottom-heavy buoyancy, which is the same relationship as when comparing MDC to the observed vertical motion profile differences (figure 3.9 a).

I separate the effects of the moisture and temperature on the buoyancy change by substituting the mean RH or temperature profile in when calculating the plume buoyancy (figure 3.9 c or d). The effect due to the moisture variability lines up with the buoyancy variability, as I would expect, with changes in buoyancy that corresponds to the observed vertical motion differences.

I have assumed that the profile of area fraction does not change with changes to the

environment like the moisture anomalies in figure 3.8. This could affect how well I can relate changes in the updraft velocity that are predicted by the entraining plume model to changes in detrainment. There has not been much study on how the updraft area fraction is determined, however a close analogy is the convective cloud fraction which has been studied. Convective cloud fraction is determined by the amount of cloud water in the atmosphere, which is itself related to the amount of moisture (Tiedtke, 1993). This indicates that the area fraction changes and vertical motion changes are correlated, which would act to reinforce the relationship between excess plume buoyancy and its removal by detrainment anomalies that support VR-MQE. This is a question beyond the scope of the present research and merits further investigation.

The temperature effects on buoyancy appear to indicate a moistening tendency which would establish an MDC anomaly, although the effects are less clear and significantly more noisy. Specifically, the case with the top-heavy MDC temperatures shows an increase in buoyancy at the mid-levels and a decrease in the upper levels, which is similar to the anomalous buoyancy shown in figure (3.8 e), which I recall leads to moistening aloft and drying below (see figure 3.8 f). Focusing specifically on the two levels where the plume buoyancy peaks in figure (3.9 d), the difference between the plume buoyancies matches the difference in moisture suggested by the MDC anomaly. The case with the top-heavy MDC temperatures shows an increase in buoyancy at the mid-level and a decrease in the upper levels, which would indicate moistening that establishes the MDC anomaly. The calculated detrainment anomaly from these profiles is too noisy to be qualitatively useful, which is why I have not presented them here. These conclusions are a good

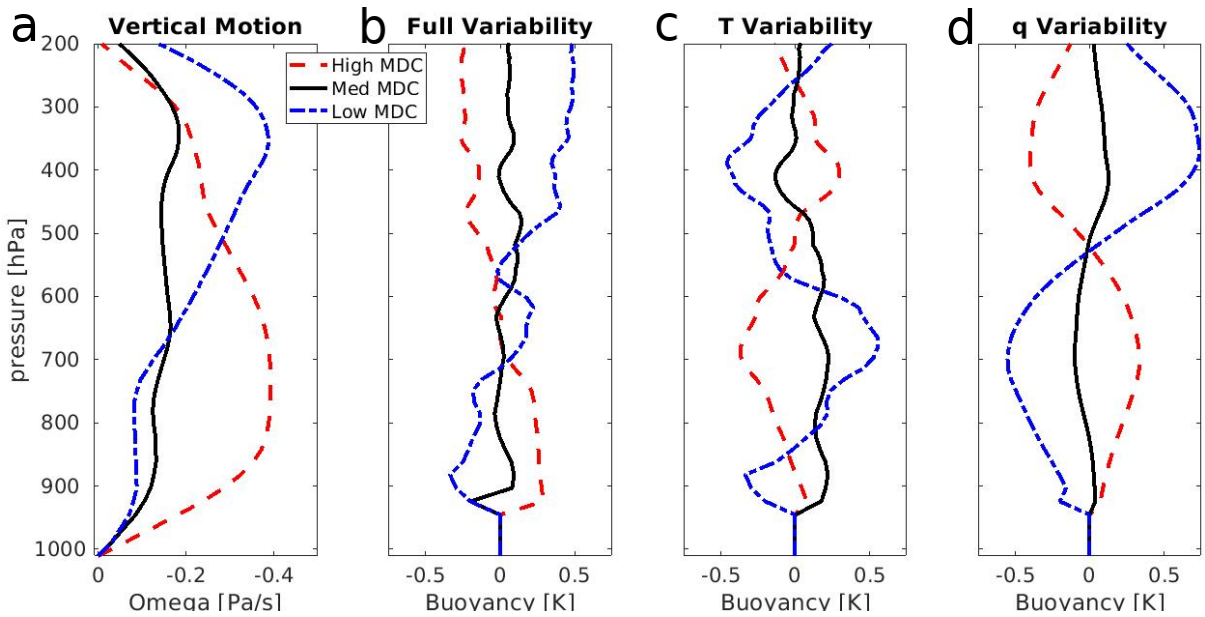

FIGURE 3.9: Plot of the vertical motion profiles and plume buoyancies which were composited and calculated from OTREC observations. First I keep only the top third of profiles based on SF in order to capture the moist profiles. I then divide the remaining data into thirds based on the MDC which gives the three profiles shown. I composite the moisture and temperature profiles in the same way and use these to compute the plume buoyancy profiles. I also calculate the plume buoyancy for the mean of all three MDC bins and subtract that from the plume buoyancies of interest, giving the buoyancy anomaly. a) Shows the vertical motion profiles, which correspond to the the bottom panel of figure 3.4. b) Shows the plume buoyancy anomalies calculated using both temperature and moisture profile. c) Shows the plume buoyancy anomalies calculated using the same RH profile for every case, which highlights the role of temperature in driving the buoyancy anomalies. d) Shows the plume buoyancy anomalies calculated keeping the temperature profile constant to highlight the role of moisture in driving the buoyancy differences.

indication of how the relationship between the moisture and vertical motion is modulated by the stability of the atmosphere. While this explanation is satisfying in its simplicity and efficacy, it is too simple to be definitive proof of the action of VR-MQE. However the observational foundations of VR-MQE, the correlation between the top-heaviness, moisture profile, and instability index, must be correctly captured if a model is going to simulate the important processes related to top-heaviness, making it a valuable POD.

3.4 The Forecast Model Perspective

The daily forecasts of the OTREC regions are a good set of simulations to test the presence of VR-MQE. The data the I use is from the European Center for Medium Range Forecasting (ECMWF) Integrated Forecasting System (IFS, version CY47R1). I use the 48 hour forecast model output of flight take-off, which is 6 AM local time, because this is a long enough lead that I expect the output to be significantly impacted by the free running model so that our results are expected to reflect model bias. I limit the geographic extent of the forecast model data I use to the flight boxes and I include the data from both boxes for every day of the field campaign. I do not distinguish between which box is which, because the processes that I seek to understand should operate similarly in both boxes and I wish to include as much information as possible to maximize the confidence in our conclusions.

I first recreate figure (3.3) with the forecast data (figure 3.10) to show the structure of the temperature and moisture anomalies associated with top-heaviness differences. The immediate difference that I see between the forecast moisture anomalies and the observations is the lack of moisture dipole in favor of a strong correlation between upward vertical motion, regardless of top-heaviness, and positive column anomalies. There is a small asymmetry between the top and bottom-heavy moisture anomalies, but it does not show the dipole as well, the boundary layer moistening seen in the transition from descent to bottom-heavy ascent is not seen, and the dry anomaly in the top-heavy region near 30 $^{\circ}$is absent.

The forecast temperature anomalies are more similar to the observations, although the magnitude of the anomaly is much smaller. In common, I see a cool anomaly that starts near the surface and rises in association with a change from bottom to top-heavy vertical motion. Outside of the mid-levels the differences are greater: the boundary layer temperature anomalies seem to be flipped for top and bottom-heavy vertical motion, with a cool anomaly under top-heavy vertical motion and a warm anomaly under the bottom-heavy vertical motion. In the upper levels, the cool anomaly penetrates too deeply.

It is clear from figure (3.10 a) that forecast model cannot distinguish thermodynamic profiles between the top and bottom-heavy ascending motion. I have also plotted the forecast vertical motion composited by the SF and MDC, using the tercile limits from both observation (orange line) and forecast (yellow line) in figure 3.4. The profiles of vertical motion that are composited by the observational limits do not show much difference and do not distinguish top or bottom-heavy vertical motion. I must use the bin-limits calculated from the forecast data in order to see a relationship between the moisture profile and vertical motion profile. These composites look more similar to the composited observational vertical motion profiles, especially for the larger SF cases, which correctly distinguishes top and bottom-heavy vertical motion, though the forecast model profiles are significantly too top-heavy in all MDC terciles.

The forecast model does not capture the correct relationship between top-heaviness and MDC but shows a strong correlation between SF and vertical motion which indicates that the model may be overly tuned to the relationship between precipitation and CWV

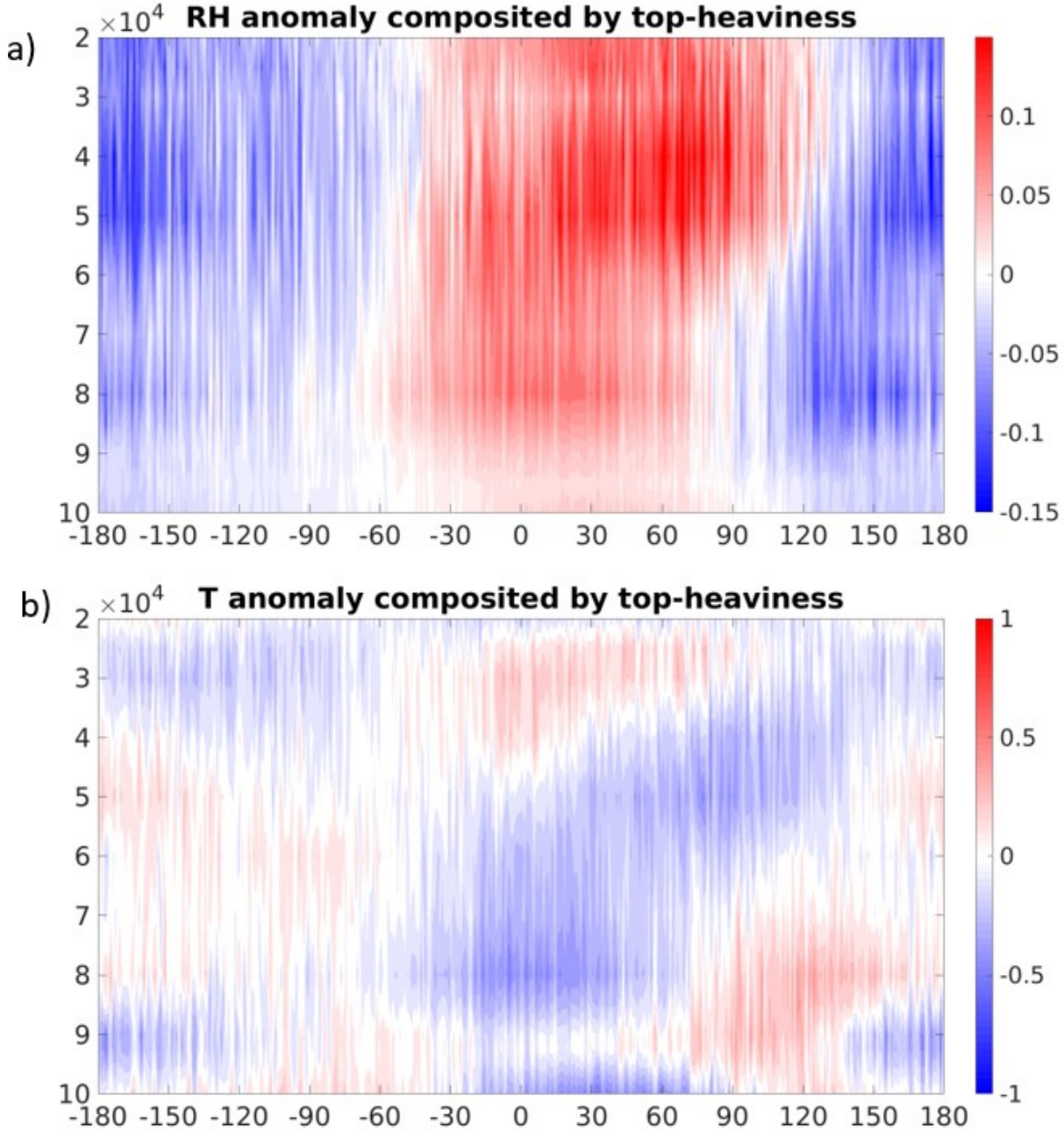

FIGURE 3.10: Forecast temperature and moisture anomalies composited by the top-heaviness angle. The anomalies are sorted into bins 1°wide and averaged. Red indicates a positive temperature or moisture anomaly. Blue represents a negative temperature anomaly.

to the detriment of other processes. For instance, the lack of correlation between the moisture and vertical motion also changes the relationship between vertical motion and radiative heating differences, because radiative heating differences are primarily due to cloud variations, which are associated with moisture variations. Observations suggest that the heating differences contributed by vertical motion and radiation tend to balance each-other and the radiation and vertical advection being out of phase could have large impacts on the energy budget and convective large-scale interactions (Back and Bretherton, 2009b, Inoue et al., 2020c).

I have used a 48 hour forecast in order to allow the model influence to dominate the effects that I see, however I should be cognizant of the errors that could be caused by initializing the model. The East Pacific is more poorly captured by remote sensing products like GPCP. Adler et al. (2012) found relative bias error estimates as high as 20% in the Eastern Pacific. Sentić et al. (2022) showed that assimilating the observations from OTREC into the forecast model led to an improvement in the forecast. Further research is needed to understand why the relationship between moisture and vertical motion is not capture as well as how prevalent of a bias it is.

3.5 Conclusion

In this research, I have used observations from the OTREC field campaign to investigate the moisture and temperature profile controls of the vertical motion profile shape, specifically the top-heaviness of the profile. I have found that ascent is associated with

a positive moisture anomaly and a negative temperature anomaly at a given level. The bottom-heavy vertical motion that is common to the area tends to occur when there is a cool and moist anomaly at low levels.

In order to describe these results, I have also introduced a new metric, the moisture dipole coefficient (MDC), which measures the presence of a relative humidity dipole, information normally lost to column integration. The MDC is able to describe the variability of the moisture profile when combined with the SF, which I have shown is enough to describe the observed variability of the vertical motion profile shape, from ascent to descent and from top to bottom-heavy. The MDC is also strongly correlated with the stability of the temperature profile, which I show using the II, a measure of the dry static stability. The correlation between the temperature, moisture, and vertical motion profiles is evidence of a quasi-equilibrium process between the profiles of moisture and vertical motion whose response is moderated by the stability of the temperature profile, which I call VR-MQE.

I use a simple entraining plume model in order to demonstrate a theoretical basis for and to provide a qualitative description of VR-MQE. The model calculates the buoyancy of a theoretical plume from the environmental temperature and moisture, which I relate to the vertical motion and the moistening tendency and therefore the moisture. Increasing the moisture at a given level increases the plume buoyancy and vertical motion, which are related to changes in detrainment, which controls the largescale moisture. The relationship between plume buoyancy and detrainment is currently predicated on the assumption that changes in the profile of area fraction can be ignored. Detrainment

from moist plumes helps to determine the moisture balance, therefore the differences in detrainment are related to anomalous largescale moistening differences. A moisture anomaly, in the entraining plume framework, leads to a detrainment anomaly that act to remove the excess moisture and move the moisture towards some critical value which is set by the large-scale temperature.

The relationship between the vertical motion and moisture profiles, which is captured through the top-heaviness angle and MDC, is a promising process oriented diagnostic for modelling the tropics. I showed that the forecast model, which was used during the OTREC campaign, did not capture the relationship between the moisture and vertical motion which I observed. Future work is needed to establish the relationship between moisture and vertical motion more generally and to understand what aspects of the model need to be tuned or modified to better represent the observed relationships.

Chapter 4

Vertical moisture modes in steady state WTG simulations investigated using a two-model

4.1 Introduction

The weak temperature gradient (WTG) framework is foundational to understanding the tropical atmosphere, to accurate weather forecasting, and to climate prediction (Adames, 2022, Charney, 1963, Sobel and Bretherton, 2000). The WTG framework is the basic assumption that horizontal temperature gradients, due to fast gravity wave redistribution, are small enough to be ignored which causes vertical advection to be the primary balance of diabatic heating. The WTG framework has been used to study a range of tropical

problems, from understand the MJO (Sentić and Sessions, 2017, Wang et al., 2016), to understand the interactions between moist convection and the large-scale environment (Neogi and Singh, 2022, Singh and Neogi, 2022, Sobel and Bretherton, 2000), as well as the evolution of slower developing systems like tropical waves (Adames, 2022). Perhaps the most practically useful implementation of the WTG framework is as a parameterization of large-scale vertical motion in cloud resolving models as in Raymond and Zeng (2005), Sobel et al. (2001).

Models which use a WTG parameterization display an important behavior, called multiple equilibria, where the model will enter either a dry or moist equilibrium depending on the initial conditions of the model (Sessions et al., 2010, Sobel et al., 2007). The moist equilibrium, as the name would suggest, is characterized by high column water vapor, consistent precipitation, and ascending vertical motion. The dry equilibrium, on the other hand, is characterized by low column moisture, a lack of rain and general descending motion. The dry and moist equilibria are thought to correspond to the dry and moist areas that arise due to convective aggregation (Raymond et al., 2009). Generally the dry equilibrium is discarded and avoided because research is primarily interested in the moist convection and the dry equilibrium can become non-physically dry. For example, realistic values for the dry region of the atmosphere are 20-40 mm of column water vapor (CWV) (Mapes et al., 2018). Values around 10 mm are seen rarely seen in the far tropics and the dry equilibrium simulations have values around 6 mm of CWV, so it is generally good practice to disregard and avoid the dry equilibrium.

A model will enter the moist or dry equilibrium depending on the model's reaction to the convective forcing and whether there will be an export or import of energy. A simulation will enter and stay in the moist equilibrium if it is able to import enough moisture to sustain deep convection. The prevalence of multiple equilibria and whether or not a simulation will enter a particular equilibrium depends on the specifics of the model. For instance the choice of radiation and horizontal moisture transport parameterizations are important for the existence of multiple equilibria (Sessions et al., 2015, 2016). I also know that whether a particular simulation will enter the dry equilibrium is impacted by the initial conditions of the model; by increasing the initial moisture I can move a model into the moist equilibrium (Sessions et al., 2015, 2010).

I avoid problems with interpreting the dry-equilibrium by nudging the model towards the moist equilibrium by increasing the moisture in the column. This is precisely what I were attempting when I discovered a new twist in the story of WTG multiple equilibria, a new kind of equilibrium state.

In recent SWTG simulations of climatological vertical motion profile shape, Bernardez and Back (2023b) had unpublished early simulations which entered into the dry equilibrium. They modified the initial moisture profile in order to get a moist equilibrium state and the model entered into a new kind of equilibrium where the model state, primarily the moisture and vertical motion, underwent an steady state oscillation of convective amplification and decay (figure 4.1). These were simulations that had constant imposed

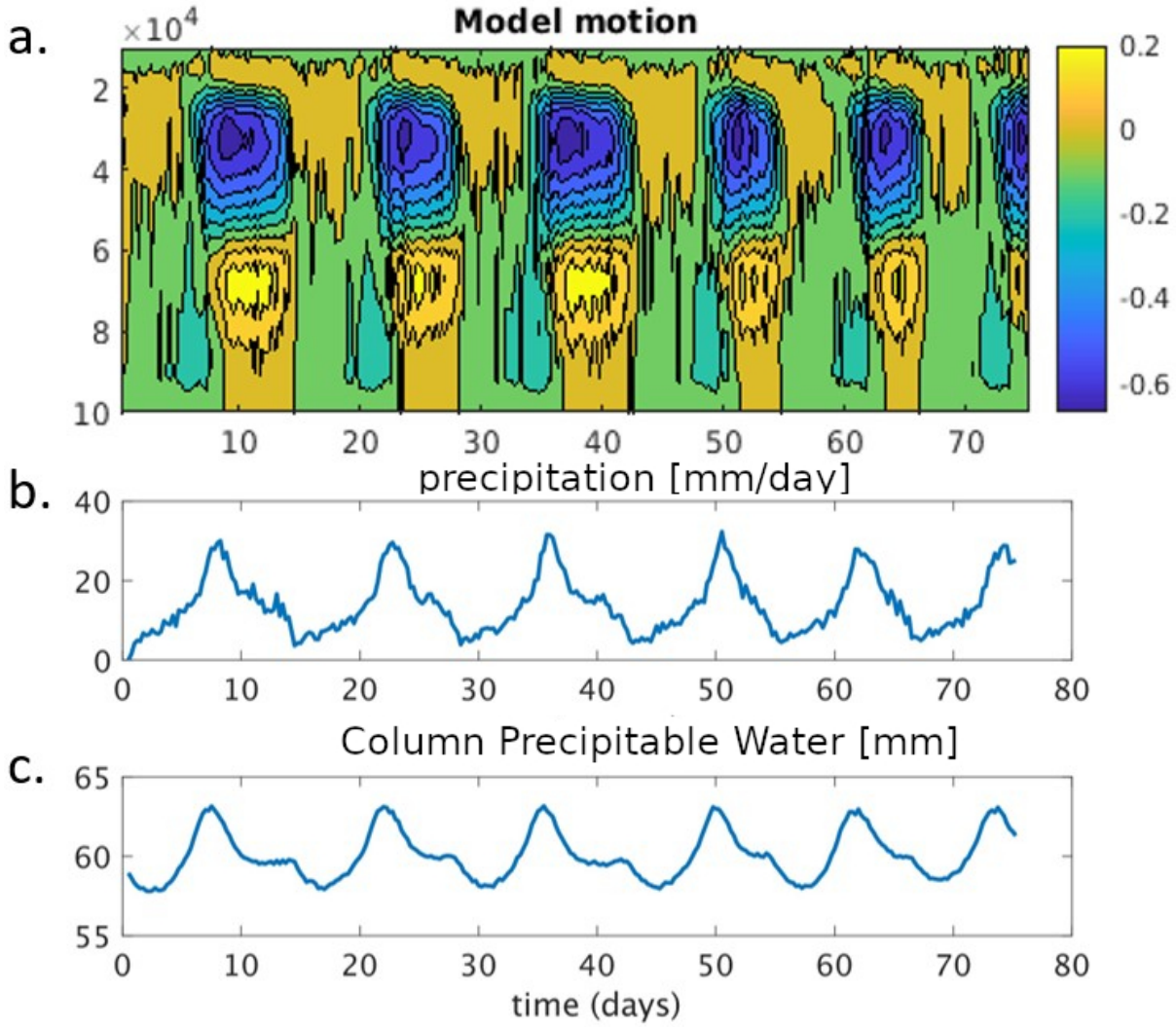

FIGURE 4.1: Description of the periodic equilibrium. Panel (a) shows The contour of the SWTG vertical velocity produced by the model in units of [pa/s] with a contour interval of .01 [pa/s], panel (b) The precipitation produced by the model, and panel (c) The time series of column water vapor (CWV).

horizontal advection and no time-dependence to drive the variability. The oscillation appears as an emergent phenomenon from the internal interactions of the model.

Through the rest of the chapter, I will go over the model and simulations which produced the periodic equilibrium. Afterwards, I will discuss the oscillation and its features. Next, I will show how the model is a moisture mode where vertical advection drives the oscillations

and go over a two-mode model that is able to capture the oscillation. Finally I will discuss what our results mean to our understanding of vertical motion in the tropics.

4.2 Weak Temperature Gradient model

The periodic equilibrium was initially discovered in a simulation from the preliminary work of Bernardez and Back (2023b), which used the weather research and forecasting model (WRF) (version 3.5.1) (Skamarock et al., 2008) as the small scale cloud resolving model (CRM) and the spectral WTG parameterization from Wang et al. (2016), as the specific WTG parameterization. The boundaries of the model are comprised of a constant single value of SST for the lower boundary condition, doubly periodic lateral boundaries and an imposed horizontal moisture advection for the horizontal, and a momentum damping scheme acts as the upper boundary (Klemp et al., 2008). The simulation had a domain size of 64x64x23 km, with a horizontal grid size of 1km and a vertical grid size set such that there are 60 stretched levels and 10 occur in the lowest kilometer of the atmosphere.

The model domain has its winds relaxed back to the original profile with a relaxation rate that matches the characteristic. I use the Morrison two-moment scheme to parameterize the microphysics(Morrison et al., 2009) and the RRTMG long-wave scheme and the Goddard shortwave scheme to parameterize the radiation (Chou and Suarez, 1999, Iacono et al., 2008, Matsui et al., 2007, Shi et al., 2010). The solar insolation is set to a constant value of $370w/m^2$, so that I do not have a diurnal cycle. I parameterize subgrid scale eddies using the three-dimensional Smagorinsky first-order closure scheme and an implicit

vertical diffusion scheme is used to ensure numerical conservation of moisture. Everything else that I have not mentioned is kept the same as Bernardez and Back (2023b). The data that I use is sourced from ERA-5 reanalysis of a region in the Central-Eastern Pacific (Hersbach et al., 2019b). I take the surface temperature, SST, winds, and moisture values along with the profiles of temperature, wind, and moisture. The temperature, SST, and wind profiles go directly into the initializing the model and the moisture profiles are used to calculate the horizontal moisture advection which I impose. I construct our data by averaging daily data from 2008-2018 in the region bounded by 7.5-10°N 120-140°E.

The SWTG parameterization relaxes the domain mean temperature profile towards a specific reference profile. I cannot directly use the reanalysis temperature profile because of the differences between real world physics and model representation, so I must obtain a temperature profile consistent with the model. I use an equilibrium model state known as either radiative convective dynamic equilibrium (RCDE) (Singh et al., 2019a) or radiative convective advective equilibrium (RCAE) Romps (2021), which I call the driven equilibrium (DE).

I create the DE simulations by imposing the vertical motion profile that I wish to emulate and allowing the model to evolve to equilibrium. The mean temperature profile of the DE simulation, because of the finite relaxation timescale, still has a temperature anomaly that has yet to be relaxed and needs to be removed (See Bernardez and Back (2023b) for a complete description). The corrected DE temperature profile is used as the reference profile for calculating the SWTG vertical velocity.

The initial simulation is initialized with the reference temperature profile and an initial moisture profile that is taken from the DE simulation. The simulation is initialized with the wind profile, SST and imposed horizontal moisture advection from reanalysis as well (see (Bernardez and Back, 2023b)). The first simulation went to the dry equilibrium and, in order to nudge the model towards the moist equilibrium, I set the moisture profile so that it had a uniform relative humidity of 85 % and ran the model again. This simulation entered into a new kind of equilibrium where the model state undergoes a steady state periodic oscillation, which I describe in the next section.

4.3 The Periodic Equilibrium: a Moisture Mode

I were successfully able to force the model to leave the dry equilibrium by setting the moisture to 85 % RH, at which point it entered a new kind of equilibrium where the moisture and vertical motion fields show a distinct steady state oscillation. The basic features of the oscillation are shown in figure 4.1 using the WTG vertical motion, the column integrated water vapor (CWV), and the precipitation reported by the model. The simulation and oscillation begin with a period of shallow bottom-heavy vertical motion which acts to slowly decrease the CWV while the precipitation slowly increases. The Precipitation and moisture then rapidly increase as the vertical motion becomes deeper and extends through the depth of the column. After precipitation and CWV peak, the vertical motion becomes stratiform and both the precipitation and CWV start decreasing. The stratiform vertical motion ends when the moisture and precipitation reach a minimum and the cycle is restarted. The period of the oscillation is approximately 14 days, although

the lack of diurnal cycle makes comparison to days in the real atmosphere somewhat dubious.

Upon first discovering the new equilibrium, I tested several different aspects of the model, in order to figure out how, why, and when the periodic equilibrium appears. I were only able to obtain a periodic oscillation when I used an interactive radiation scheme and an imposed horizontal moisture advection. Doubling or halving the characteristic WTG relaxation time-scale doubled/halved the period of the oscillation. Changing to the SST, temperature, moisture, or wind profiles would sometimes excite the periodic equilibrium, however I were not able to determine a perceptible pattern from the basic tests that I conducted. All of the periodic equilibrium simulations are consistent with the results that I report here, so I only show the results from the first simulation which displayed the oscillatory behavior.

The oscillations has many of the markers of a moisture mode, which is a dynamical mode which acts through the prognostic moisture (Adames et al., 2019, Ahmed et al., 2021, Fuchs and Raymond, 2007). Recent research has started to reveal the importance of moisture modes to the tropical atmosphere and the implication that they are emergent in SWTG models is attractive. Understanding the periodic equilibrium could provide a crucial tool to understand and correctly parameterize moisture mode behavior.

The work by Adames et al. (2019) and Ahmed et al. (2021) established three criteria for determining a moisture mode, which I show in figure (4.2). These criteria are (a) a strong correlation between precipitation and the total column water, (b) a leading order WTG

balance in the dry static energy (DSE) budget, and (c) variations in MSE anomalies are dominated by moisture anomalies.

The first criteria, seen in panel (a), is a strong correlation between the precipitation and column water vapor anomaly. In figure (4.2), each dot is a model output time step, which are separated by 6 hours. The color of each dot corresponds to the top-heaviness angle, although here it is used only for clarity. There is a broadly linear relationship between the two and a clear hysteresis between the two. The section of the period with the greater slope occurs during the amplification phase and the section with the lesser slope occurs during the contraction phase.

The second criteria is a leading order WTG balance in the dry static energy (DSE) budget:

$$\omega \frac{\partial s}{\partial p} = Q_{rad} + L_v P + Q_{sh}. \tag{4.1}$$

Here $s = c_p T + gz$ is the DSE, ω is the pressure velocity, Q_{rad} is the column radiative heating, P is the rain rate, and Q_{sh} is the surface sensible heat flux (panel b). This criteria is forced by the SWTG parameterization and the nature of the model and the figure confirms this.

The final criteria is for variations in the moist static energy (MSE), which is the sum of the DSE and the latent heat $h = s + l_v q_v$, are dominated by moisture variations (panel c). This criteria is also enforced partially by the SWTG parameterization, and would be enforced fully using a strict implementation of WTG. With all three criteria for a

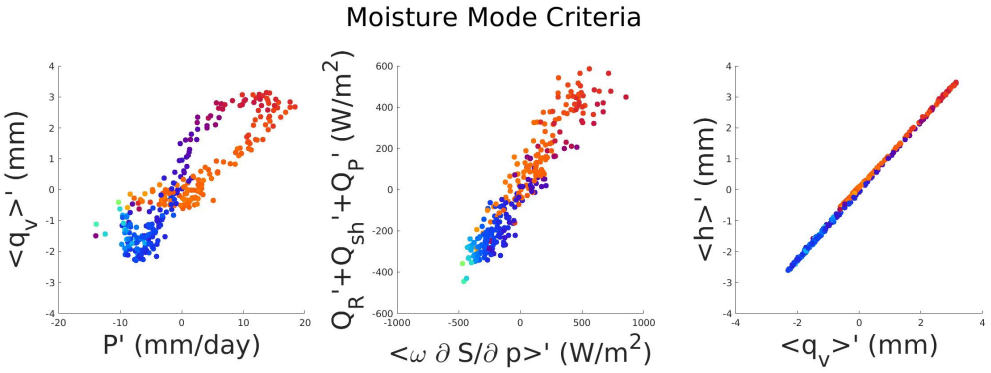

FIGURE 4.2: Moisture mode criteria for the periodic equilibrium. a) The relationship between the column water vapor (CWV) anomaly and the precipitation anomaly, b) the relationship apparent heating and vertical advection of DSE, and c) the relationship between column MSE anomalies and column moisture anomalies. Each point is colored based on the vertical motion profile shape called the top-heaviness angle for clarity.

moisture mode satisfied by the periodic equilibrium and I can call it a vertical motion moisture mode.

The column MSE budget is a useful tool for studying moisture modes because of its relationship to moisture and precipitation. The equation for the column energy budget is:

$$\frac{\partial \langle h \rangle}{\partial t} = \langle \omega \frac{\partial h}{\partial p} \rangle + Q_{hadv} + Q_{rad} + Q_{lh} \tag{4.2}$$

Here h is the MSE, defined as $h = c_p T + gz + L_v q_v$, where T is the temperature, z is the height, q_v is the specific humidity, and c_p, g, and L_v are the constants of specific heat of air, gravitational acceleration, and latent heat of vaporization. Q_{hadv} is the column horizontal MSE advection, which in our case is the imposed horizontal moisture advection, and Q_{lh} is the surface latent heat flux. $\langle\rangle$ represent a mass weighted integral over the depth of the troposphere. The surface sensible heat flux is small enough in our cases that I ignore it.

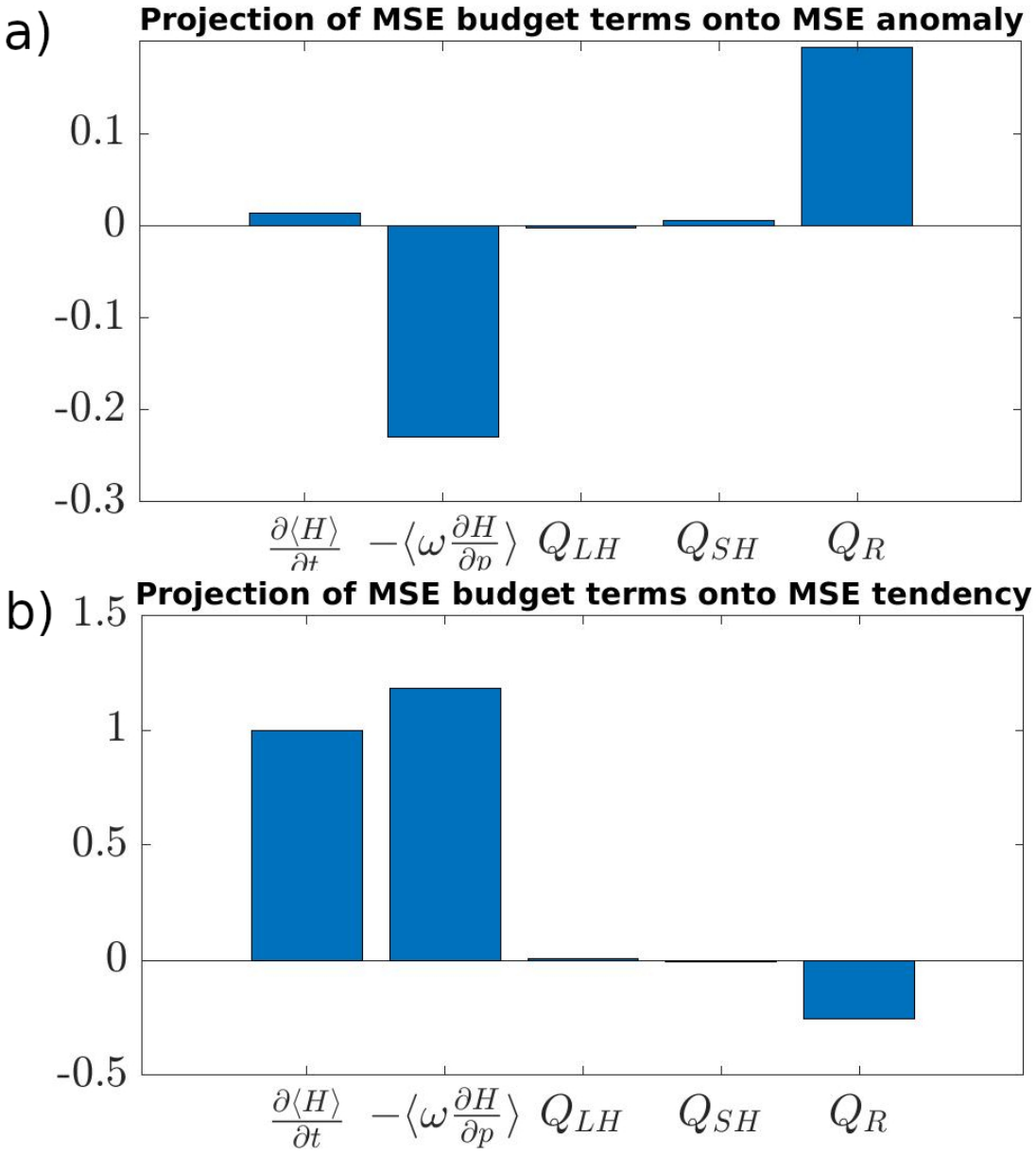

FIGURE 4.3: Projection of MSE budget terms onto the column MSE anomaly (a) and the column MSE tendency (b), which shows the relative contribution of each term to the maintenance of the moisture mode (a) and propagation of the moisture mode (b).

A prevalent way of investigating moisture modes is to use the MSE budget to investigate how each MSE budget term contributes to the amplitude and the period of the wave (Adames, 2017, Andersen and Kuang, 2012, Mayta et al., 2022). The time series of MSE anomaly measures the amplitude of the wave and I can measure how each term in the MSE budget contributes to the maintenance of the amplitude by projecting MSE anomalies onto the time-series of each budget term (figure 4.3 a). I call this the maintenance term, because it shows what contributes to maintaining the amplitude of the wave.

The MSE anomaly projection, shown in figure (4.3 a), shows how much each term wants to either amplify or weaken the moisture mode oscillation. The two most important terms in the energy budget are the radiation and MSE advection, which is essential the combination of moisture and vertical motion variability. The radiative cooling tries to amplify the wave and increase the column MSE over time while the MSE advection tries to damp the wave and decrease and it is only their balance that leads to the steady state oscillation that I observe.

The projection of the MSE tendency onto the time series of the budget terms gives us the propagation term, which shows how much each term contributes to the period of the oscillation. The contribution of the budget terms to the propagation of the moisture mode is shown in figure (4.3 b). I see again that the most important terms are the MSE advection and the radiation, although this time the radiation is relatively less important. The majority of the work is being done by the vertical MSE advection trying to increase the propagation of the wave and the radiative heating slowing it down.

Generally, vertical advection and radiation changes are coupled together in the atmosphere. They also tend to balance energetically such that their combined effect on convection is to neither amplify or decay (Back et al., 2017, Inoue et al., 2020b). I see the same balance through the maintenance terms. I need to dig deeper to understand how the radiation and vertical advection are interacting to generate the moisture mode variability while still maintaining a steady state. I do this by decomposing the vertical motion and radiation into two-modes of vertical variability which explain the variance of the moisture mode the best. In the next section, I will discuss the derivation of the simplified model and go over what it tells us about the oscillation.

4.4 Two-mode Framework

4.4.1 Vertical Advection

two-mode models are common in the field in part because the vertical velocity profile variability tends to be dominated by the first two-modes of variability. When principal component analysis is used to look at how vertical motion profiles vary, I find that two-modes explain in excess of 85 % of the variance (Back et al., 2017). I rewrite the vertical motion as:

$$\omega(x, y, p, t) = o_1(x, y, t)\Omega_1(p) + o_2(x, y, t)\Omega_2(p) \tag{4.3}$$

Here o_i are the amplitudes of Ω_i the vertical modes that are used to decompose the vertical motion. I can calculate the specific modes I use in a number of ways including solving the anelastic equations (Wang et al., 2016), using a Fourier transform (Herman

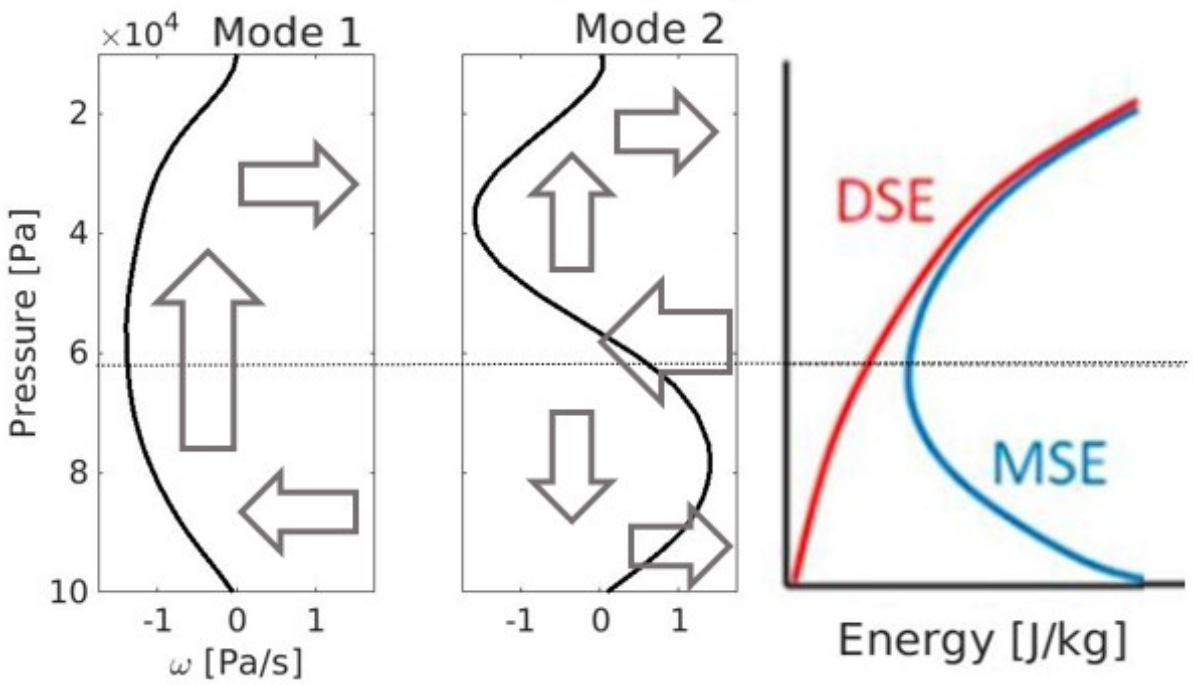

FIGURE 4.4: Simplified examples of the first and second mode of vertical motion along with an example profile of MSE and DSE. The arrows indicate the direction of advection, when they are pointed to the left energy is entering the column and when they are pointed to the right air is leaving the column. Both cases have the energy of the profile shown on the left.

and Raymond, 2014), or using principal component analysis (PCA) to find the vertical structures which explain the most variance (Back et al., 2017). I choose to use vertical modes calculated from PCA of 40-year climatology of reanalysis data, which Bernardez and Back (2023a) used to describe vertical motion. I have verified that the results of the following section were not sensitive to this choice by repeating the analysis using the vertical modes calculated using PCA of the domain mean vertical motion. I apply the vertical decomposition to the vertical motion and keep only the first two-modes based upon the criteria of (North et al., 1982).

The distinct vertical shapes of the two-modes means they interact with the MSE and

DSE budgets differently. A simplified version of the two vertical modes that I use are shown in figure (4.4), along with simplified profiles of DSE and MSE, which haven been taken from (Inoue et al., 2020b). The arrows indicate the circulation associated with each mode and horizontal lines show where the profiles import or export air and thus energy, with an export of energy indicated by a rightward arrow. The thin black line shows the approximate MSE minimum to aid in visualization.

I can see that the first mode has a strong influence over the DSE budget due to the very different energies that it is importing versus exporting, but has a much smaller impact on the MSE budget. The second mode will have very little affect on the DSE budget while having a much larger impact on the MSE budget. The first mode should have a strong impact on the DSE budget, and thus the precipitation, but should not affect the MSE budget, and thus convective amplification or decay. The second mode, on the other hand, should show little effect on the precipitation, while having a much stronger effect over convective amplification.

To confirm this is shown, I apply the two-mode simplification to the projection of MSE anomalies and tendency I can calculate the fraction of the propagation and maintenance that is contributed by each mode (figure 4.5 a and b). In order to do this I calculated the advection contributed by each mode, along with the residual, and I project the MSE tendency and anomaly onto those time-series as I did with the full vertical advection. The first panel shows how each modes' contribution to the vertical advection maintains the steady state oscillation and it is apparent that the second first mode does not have a large

impact. The second panel shows the contribution of each mode to vertical affections' role in setting the period of the wave and again I see that the second mode is significantly important while the first mode is not. The oscillation variability occurs primarily in the MSE budget, which the first mode does not have much of an ability to affect, so the lack of contribution to the vertical motion moisture mode matches the expectations I had from the simplified picture of our two-modes above. Next, I apply the same decomposition to the radiation.

4.4.2 Radiation

The contribution of the radiation to the two-mode model is found by assuming that the radiative heating variability is controlled by the vertical motion variability. I do this using the following linear regression model which I solve using a least squares approach:

$$Q_{rad} = r_0 + o_1 r_1 + o_2 r_2 + \epsilon_r \tag{4.4}$$

Where r_0 is the mean column radiative heating, and $r_{1,2}$ are the column radiative heating rate constant associated with each mode and the product of this constant with its corresponding mode gives the portion of radiative heating contributed by that mode. When I do this with the periodic data I find an R-square statistic of (0.901) and a large F-statistic which indicates the variables are well separated.

The fraction of radiation contributed to the maintanence and propagation can be seen in the middle panels of figure (4.5 c and d). In short, the radiative heating tries to increase

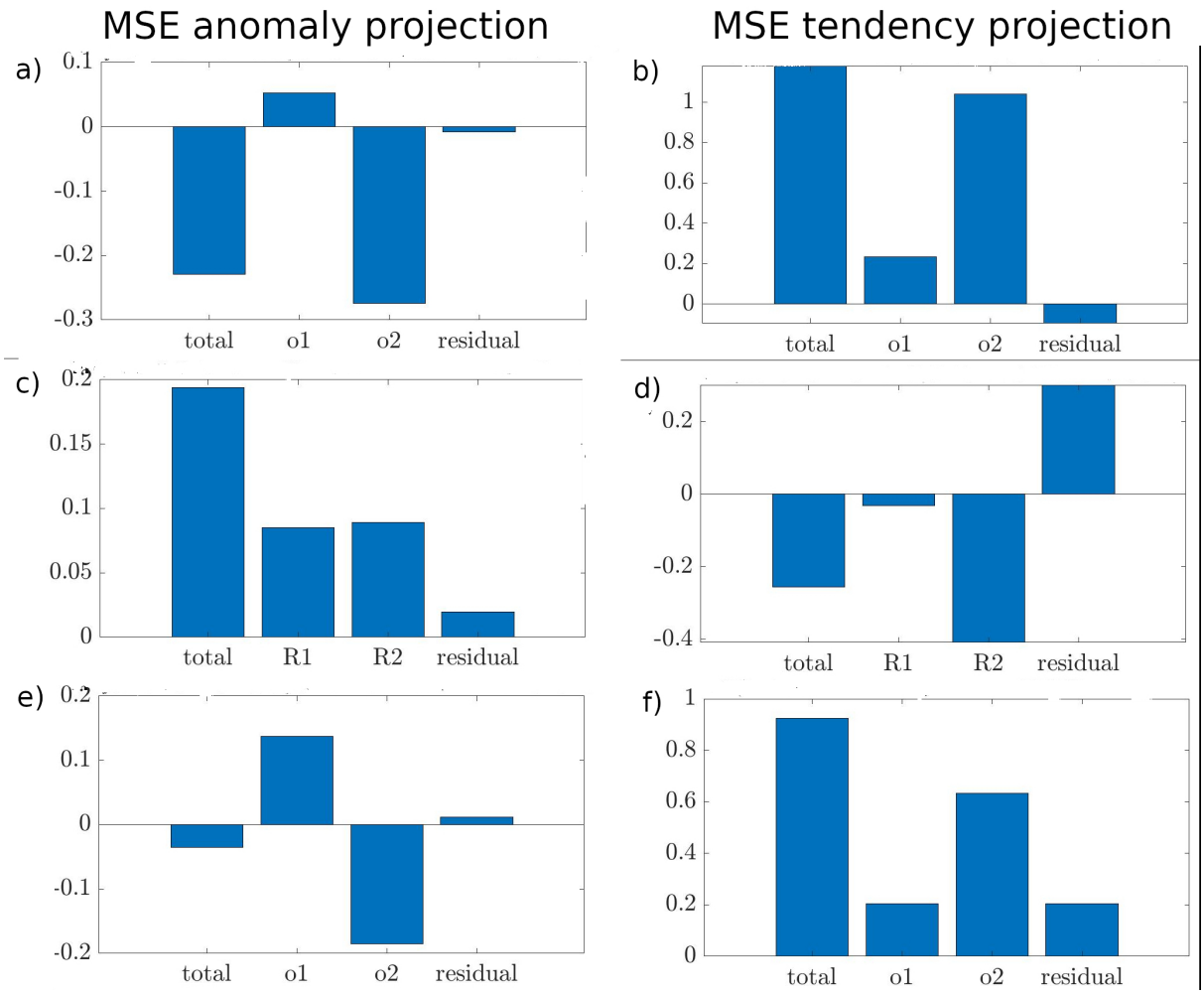

FIGURE 4.5: Projection of the column MSE anomaly (a,c,e) and the column MSE tendency (b,d,f) onto the MSE budget terms, which shows the relative contribution of each term to the maintenance of the moisture mode and propagation of the moisture mode. The top panel (a,b) shows the relative contribution of the two-modes to the vertical advection of MSE. the middle panels (c,d) show the relative contribution of each mode to the column radiative heating. The bottom panels (e,f) show the contribution of each mode to the combination of the MSE advection and column radiation, which means it is the top panel subtracted from the bottom-panel.

the amplitude of the oscillation and both modes contributes about equally to that goal. The propagation of the oscillation by the radiation is contributed primarily by the second mode and the radiative differences associated with the first mode are not important to the propagation of the oscillation.

The residual of radiation, the part of the radiative heating that is not explained by the two-mode approximation, is also important for wave propagation. The radiation residual driving propagation is the largest effect that a residual displays, which indicates the two-mode model does a good job of explaining the oscillation. I now move on to understanding how the combined effects of radiation and vertical advection control the oscillation.

4.4.3 Combined Effects

The sum of the vertical advective and radiative effects is shown in the bottom panels of (figure 4.5 e and f). It shows the maintenance of the oscillation is accomplished by a balance of both modes, with the first mode trying to amplify the wave and the second mode trying to reduce the wave. The first mode is primarily due to the radiation while the second mode is due to mostly to the vertical advection. The propagation of the moisture mode is primarily accomplished by the second mode and within the second mode the vertical advection drives the oscillation and the radiation attempts to diminish the propagation. To summarize, the second mode is responsible for the propagation of the oscillation and the balance between the two-modes is responsible for the steady state nature of the oscillation.

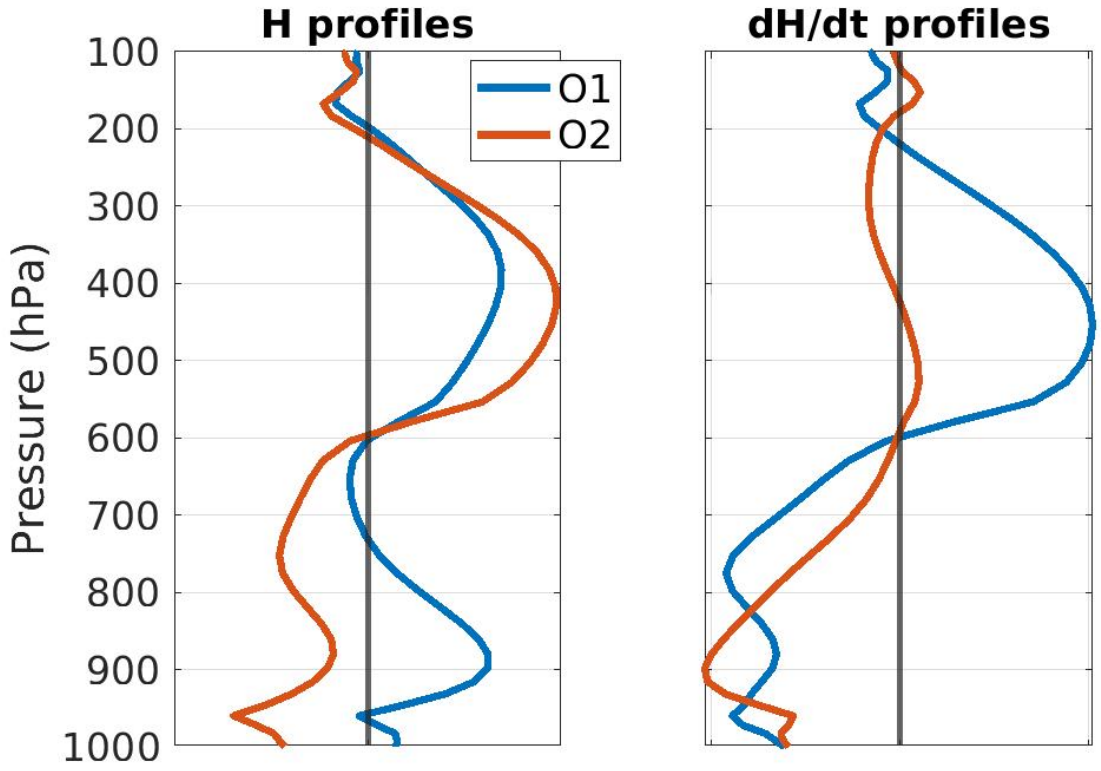

FIGURE 4.6: Profiles projecting the MSE anomalies and the MSE tendency onto each of the two-modes individually. The first panel shows the MSE profiles that correlate and excite the two-modes (blue and orange) that I get by projecting the MSE anomalies onto each mode. The second panel shows the MSE anomaly that each of the modes tends to excite, which is given by projecting the MSE tendency onto each of the two-modes.

The interaction between the radiation and vertical advection which leads to the oscillation and is captured by our two-mode model is complex, however I can simplify with more linear regression, this time focused on looking at understanding the vertical variability. I project the MSE anomalies and tendency onto each of our two-modes individually, shown in figure (4.6). These profiles are the level by level correlation between each mode and the MSE anomaly and tendency and they represent how the MSE excites the vertical motion and how the vertical motion excites MSE anomalies, respectively. The previous section showed that the two-mode model explains the contributions of both the radiation

and the vertical advection, which means these correlations represent the combined effects of both the radiation and vertical advection on the MSE.

The first panel shows MSE anomaly profiles, which represent the MSE anomaly that tends to correlate or excite each mode. A positive first mode, which corresponds to general ascending motion, is excited by either a lower or upper tropospheric MSE anomaly, with the lower tropospheric anomaly being more powerful in excitation. This means that the first mode is generally excited by a column relative humidity (CRH) anomaly:

$$CRH = \frac{\int_{P_{surface}}^{P_{top}} qv\partial p}{\int_{P_{surface}}^{P_{top}} qv^{\star}\partial p}.$$

Here qv is the specific humidity, $qv^{\star}$ is the saturation specific humidity.

The second mode is excited by a dipole structure of MSE with a positive second mode response, which corresponds to a top-heavy vertical motion profile shape, correlating with a negative MSE anomaly in the lower troposphere and a positive anomaly in the upper troposphere. The separation point between the positive and negative lobes appears around 600 hPa or the approximate freezing level. This anomaly can be tracked by a metric called the moisture dipole coefficient, which is defined as:

$$MDC = \frac{\int_{P_{surface}}^{P_{middle}} qv\partial p - \int_{P_{middle}}^{P_{top}} qv\partial p}{\int_{P_{surface}}^{P_{top}} qv^{\star}\partial p}.$$

The middle pressure level is set at 600 hPa. The two-modes are generally excited by an MSE anomaly that is of a similar vertical shape, next I look at how each of the modes

generates MSE anomalies.

The second panel shows the projection of the MSE tendency onto each of the modes individually. The correlation between each mode and the tendency of MSE shows how each mode tends to generate MSE anomalies. The first mode excites a dipole MSE anomaly structure, with a positive MSE anomaly lobe in the upper troposphere and a negative MSE anomaly in lower troposphere. The second mode tends to excite a negative MSE anomaly response in only the lower troposphere.

I can now put together the story of the oscillation through our understanding of the vertical provided by figure 4.6. The first mode tends to correlate with a CRH anomaly and tends to excite a negative MDC anomaly. Meanwhile, the second mode tends to correlate with a negative MDC anomaly and tends to excite a negative SF anomaly. The authors could at this point leave the solution as an exercises to the reader, I will be more thorough in our discussion.

I start by writing down the correlations from the first panel of 4.6 in equation form gives:

$$\begin{aligned} CRH &\approx a_1 o_1 \\ MDC &\approx -a_2 o_2. \end{aligned} \tag{4.5}$$

The second panel gives the correlation with the tendency of MSE, and shows that the first mode correlates with an MDC anomaly tendency and the second mode correlates

with a CRH anomaly tendency:

$$\begin{aligned} \frac{\partial CRH}{\partial t} &\approx -a_3 o_2 \\ \frac{\partial MDC}{\partial t} &\approx a_4 o_1. \end{aligned} \tag{4.6}$$

Which solves to the series of first order linear differential equations:

$$\begin{aligned} \frac{\partial o_1}{\partial t} &\approx -\frac{a_3}{a_1} o_2 \\ \frac{\partial o_2}{\partial t} &\approx -\frac{a_4}{a_2} o_1. \end{aligned} \tag{4.7}$$

When I calculate the coefficients, either finding the area under the curves in figure 4.6 or by directly calculating the correlations in the above equations directly using the CRH and MDC, and solve the system of equations I get an elliptical solution that matches the oscillation. I have not shown the scatter plot of the oscillation with the solution to the set of equations above because it is not informative and have instead opted for a more descriptive diagram in figure (4.7).

The state of the model at any given time is shown as the red dot and the oscillation is shown as the black ellipse. The two sets of axis are the basis formed by the two-mode model and the moisture variables plotted on top of each other. Visualizing both the sets of axis is important because if I were to look only at the two-mode phase plane the tilted ellipse is puzzling, and by laying the moisture phase plane it becomes clear why it is so aligned. The moisture axis is shifted so that it is centered at the mean values which define our anomalies. The axis is rotated relative to the vertical motion axis because

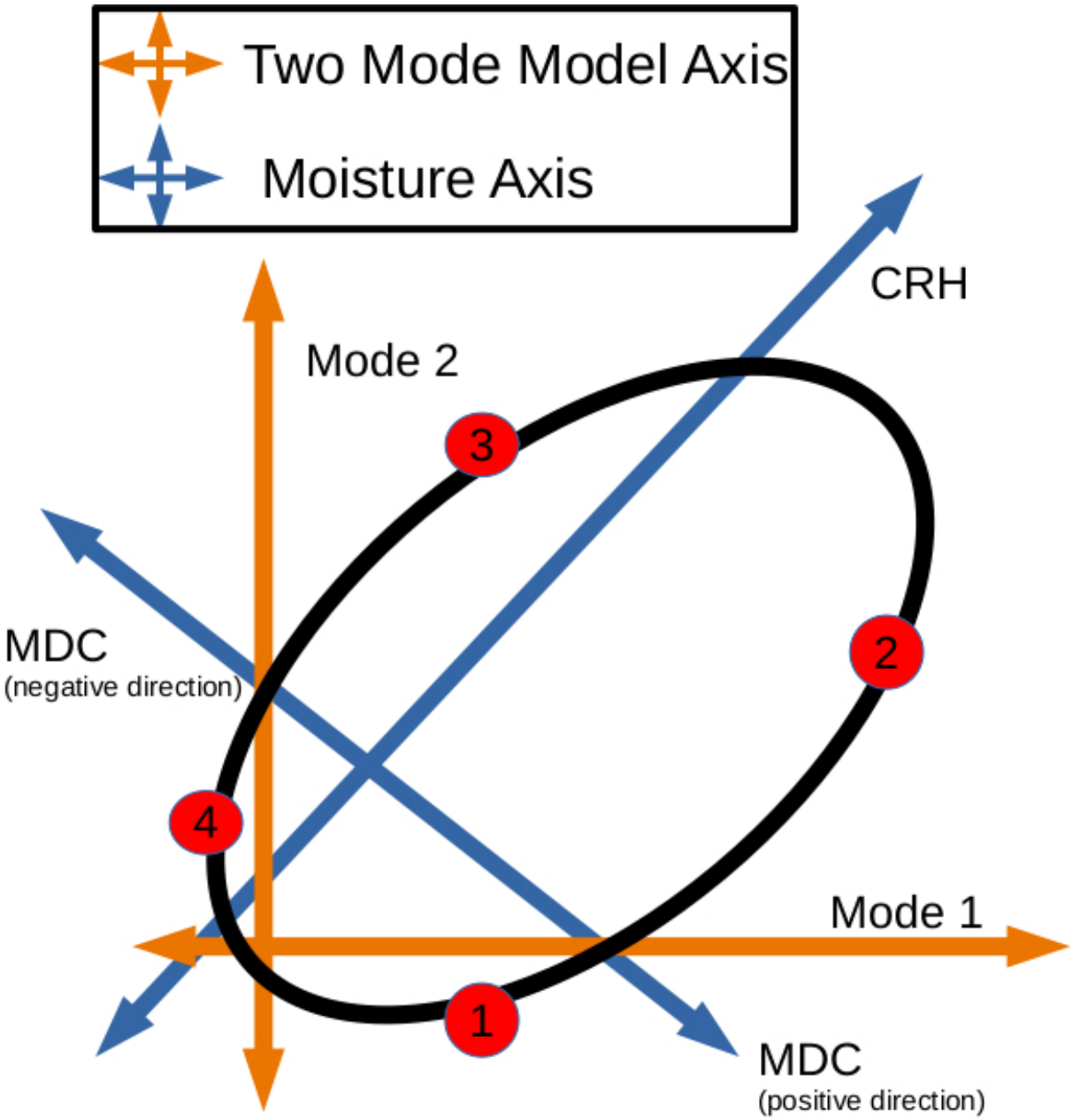

FIGURE 4.7: Schematic of the periodic oscillation viewed on the two-mode and moisture phase planes. The orange axis is the two-mode model basis and the blue axis is for the moisture basis. The moisture axis are defined using the CRH and the MDC so that a decrease in MDC correlates with an increase in mode 2. The model state at any moment is shown as the red dot and the path that it takes during an oscillation is shown as the black line.

of the asymmetric nature of how the two-modes interact with each other and the MSE budget.

A period begins, point 1, with bottom-heavy lightly ascending air, high MDC, and low CRH. The column moistens throughout the column driving an increase in both modes moving the dot towards point 2. The vertical motion is deep and slightly top-heavy, the CRH is nearing its maximum and the MDC is starting to decrease. The first mode continues to effectively move MSE from the lower to upper troposphere while the second mode removes moisture from the lower troposphere, leading us around the curve as the second mode becomes stronger than the first and the CRH begins to decrease depositing us at point 3. The vertical motion at this point is stratiform and the moisture is primarily concentrated in the upper troposphere. The first mode becomes smaller and has less of an effect, while the second mode slowly removes moisture from the lower troposphere driving us to point 4 where the atmosphere is near its driest and the first mode becomes slightly negative which begins to increase the lower tropospheric moisture and decrease the upper tropospheric moisture, increasing the MDC. When the upper troposphere has dried enough the second mode becomes negative and begins to increase the lower tropospheric moisture and MDC even further catapulting the oscillation to begin the journey again at the start.

The two-mode model provides a qualitative description of our oscillation, in the next section I will discuss the implications of the model and what conclusions may be drawn from our results.

4.5 Discussion

The two-mode model acts as a kind of predator-prey system, with the two-modes generating and consuming each other through the MSE anomalies captured through the CRH and MDC. This is a particularly attractive possibility because of the substantial mathematical foundation that exists to understand systems of this type. I could provide a more complex description by expanding the correlations so that both modes affect each of the upper and lower tropospheric moisture or MSE and adding the constant forcing term from surface fluxes, moisture advection, and radiation. This would add more coefficients to equation (7), which would allow the two mode model to fit the data better, the current description is quite satisfactory for the present explanatory purposes of this research. If I were able to obtain the sets of coefficients in equation (7) for either level of complexity *a priori*, I could determine which equilibrium the simulation will fall into before running the SWTG simulation.

The coefficients are also important because of their relation to how the moisture and two-mode axis are translated and rotated relative to each other and why the oscillation appears. They are a linearization of the functional relationship between the MSE and DSE budgets of moist convection. The functional relationship is moderated by factors like the radiation-moisture relationship, moisture-precipitation relationship, fractional entrainment and detrainment rates. A better understanding of how these coefficients are determined and if they are predictable could shed light on better ways of parameterization moist convection.

While the details of how the two axis are related would be helpful, the schematic diagram using them is still a good tool for understanding the oscillation and the multiple equilibria phenomena more generally. On the two-mode phase plane, both the moist and dry equilibrium states move towards a very particular equilibrium point and stay in the neighborhood of it while randomly jiggling around it. Taking the average over a long time highlights this equilibrium point and removes the random variability of the jiggling around. As shown the periodic equilibrium settles into a limit cycle.

In this way it is also good for showing how the oscillation, while a steady state equilibrium, is fundamentally different from the other two equilibria because the mean behavior does not represent the important variability. The time average of the periodic equilibrium will give a point inside of the orbit which the model state never actually reaches. Compared to the dry and moist equilibria which settle into a spot defines the mean. This can be important when asking questions like "do the radiation and vertical MSE advection balance?" They balance if you ask the column integrated MSE anomaly, but not if you ask the column integrated MSE tendency.

4.6 Conclusion

I have discovered a new kind of WTG multiple equilibrium state which is characterized by a periodic oscillation in the vertical motion and moisture. This oscillatory state is a vertical motion moisture mode according to the criteria from (Mayta et al., 2022). The

moisture mode results from an environment that is laterally homogeneous and constant in time and is due to radiation and vertical advection and their interaction.

I can describe the vertical motion moisture mode as a closed elliptical loop on a set of axis defined by either a two mode decomposition of the vertical motion or moisture. The vertical motion axis describe whether vertical motion is ascending or descending and top or bottom-heavy and are sourced from PCA of a 40-year climatology of daily vertical motion data, which are also used in Bernardez and Back (2023a). The moisture axis are defined using the CRH and MDC because they capture the moisture variability related to the oscillation well. I can solve for the ellipse using by relating changes in each of the two axis to each other, with moisture variations driving vertical motion changes and vice versa. The oscillation act as a sort of predator prey dynamic between the moisture and vertical motion anomalies, forming a limit cycle on the phase planes of moisture and vertical. I can solve the set of equations and get a solution that qualitatively matches the oscillation.

The existence of the oscillation, and multiple equilibria, in WTG models is contingent on many particular factors. The large-scale temperature and initial moisture profiles, wind profiles, SST, and parameterizations of radiation and horizontal moisture transport are some of the factors that I found to be important to which equilibrium state the model settles into and the existence of the periodic oscillation. While I have provided a description of the oscillation and know many of the factors that control it, I do not have an explanation for its emergence. A deeper understanding of how the periodicity

emerges from moist convective processes is needed to fully understand the oscillation. The existence of the periodic equilibrium and the potential for the advances in understanding that they can help with is fascinating and compelling.

Chapter 5

Conclusion

5.1 Summary of key results

5.1.1 Chapter 2

The first research chapter looked into how the two proposed explanations of top-heaviness, the dynamic and stability mechanism, are able to explain the top-heaviness difference between the Eastern and Western Pacific. I showed that climatological vertical motion shape and top-heaviness can be explained through thermodynamics without explicitly imposing SST gradients or surface convergence, and that aspects of both mechanisms are important for explaining the top-heaviness difference that we see. I used a small domain CRM, which parameterized the vertical motion using the WTG approximation, in order to simulate the vertical motion from two regions with distinctly top and bottom-heavy

vertical motion. We are able to simulate the vertical motion profiles from the environmental thermodynamics, with the most important variables being the magnitude of the underlying SST and the large-scale temperature profile, which the WTG parameterization relaxes the column towards. I then demonstrate how this process can be explained using a simple entraining plume model, which is the first such direct explanation of the stability mechanism.

Aspects of both mechanisms explain the results that we see, which hints at a reconciliation between the two Mechanisms. The dynamic mechanism predicts vertical motion shape as a consequence of the underlying SST distribution and I find that in the Western Pacific the stability and SST are correlated with higher SSTs driving higher instability and more top-heavy vertical motion, consistent with the predictions of the dynamic mechanism. In the Eastern Pacific the stability is not correlated with the SST, which indicates that something else is controlling the variability. The proposed explanation links the dynamic and stability mechanism by positing that the SST gradients drive surface convergence, which alters the stability of the atmosphere and drives greater stability and more top-heavy vertical motion.

Previous research on the stability mechanism has seen a correlation between the stability, top-heaviness, and column moisture with greater stability correlating with bottom-heavy vertical motion and greater column moisture. Through this research, I have shown that this relationship is dependent upon how the horizontal advection of moisture couples to vertical motion. When vertical motion and horizontal moisture advection are tightly

coupled, there is a strong correlation between the top-heaviness and the column moisture that has been seen during previous research. When the horizontal moisture advection is unconstrained by the vertical motion the relationship between top-heaviness and column moisture is coincidental. This means that generally the column moisture is not a reliable tool for estimating the top-heaviness. The Next Chapter provides a better metric.

5.1.2 Chapter 3

The second research chapter focuses on the results of the OTREC field campaign which took observations from the Eastern Pacific and Western Caribbean, a region that has climatological bottom-heavy vertical motion and a history of being difficult to forecast and simulate. The goal of this research is to better characterize the observed vertical motion in these regions, further our understanding of what controls vertical motion in observations, and develop process oriented diagnostics which can be used to improve future modeling efforts. The research flights and dropsondes observed a range of vertical motion profiles which span the spectrum of top-heaviness angles, the dominant vertical motion being bottom-heavy ascent.

I demonstrated coherent patterns in the observed temperature and moisture anomalies that correlate with the top-heaviness differences. Ascent correlates with an increase in the RH and negative temperature anomalies. Bottom-heavy and top-heavy vertical motion can be distinguished using dipole shaped moisture anomalies. I introduced a new metric for measuring the variability of the profile of moisture, called the moisture dipole coefficient, which as the name suggests measures the presence of a dipolar moisture

anomaly centered at the approximate freezing level. The MDC, along with a measure of the total column moisture, is able to distinguish the range of vertical motion profiles from bottom to top-heavy .

Connecting this to the previous chapter, which showed that the temperature profile helps control the vertical motion, and the connection between temperature and vertical motion in the observations presented here, we show that the MDC and the instability index are correlated. I then use the simple entraining plume model to hypothesize a causal reason for the relationship between moisture and vertical motion. The entraining plume model uses the temperature and moisture to calculate the buoyancy of a hypothetical plume which correlates with the updraft vertical velocity and large-scale vertical velocity. The entraining plume differences relate to detrainment differences, which are important to controlling the large-scale moisture. When the atmosphere is anomalously moistened, the entraining plume buoyancy changes and vertical motion responds leading to an anomalous moistening tendency. This moistening tendency acts to remove the added moisture anomaly, which supports the existence of a process called vertically resolved moisture quasi-equilibrium. VR-MQE describes that tropical atmosphere as trying to achieve some critical profile of moisture which is determined by the profile of temperature. When an anomaly of column moisture or MDC anomaly is generated, by things like horizontal moisture advection or surface heat fluxes, the vertical motion will adjust in order to remove that moisture anomaly. The close correlation between vertical motion, moisture, and stability is due to the atmosphere operating near the balance state characterizing the quasi-equilibrium nature. In the next chapter, I investigated an extreme

example of vertical motion and moisture evolving near a balanced state.

5.1.3 Chapter 4

The final chapter unveil the existence of a new equilibrium state within the multiple equilibrium phenomena that models parameterized with the WTG approximation express. This new kind of equilibrium shows a periodic oscillation of vertical motion, moisture, and precipitation that matches the characteristics of a moisture mode and is emergent from uniform and unchanging boundary conditions. Through many simulations which were not shown, I identified several model conditions that are necessary for the periodic equilibrium, among these are interactive radiation, imposed horizontal moisture advection, and wind shear. There was no obvious pattern to the conditions that are needed for the model to fall into the periodic equilibrium.

The vertical moisture mode can be captured by a simple two mode model which is based on the same decomposition of vertical motion that is used to calculate the top-heaviness angle. The two mode model reveals that the column acts as two separate reservoirs of MSE in the upper and lower troposphere which interact through moist convection and the action of vertical advection. The transition from bottom-heavy to top-heavy vertical motion during an oscillation follows a transition from bottom-heavy to moisture, which is strikingly similar to the MDC results from the second paper.

The story of vertical motion and moisture that is told by this research, as I understand it, is one of a partnered dance that is directed by the temperature and convective forcing.

The temperature profile sets a critical profile of moisture, which vertical motion acts to drive the atmosphere towards, depending upon the current profile of moisture. Added on top of this is the convective forcing, including horizontal advection of moisture, driving the atmospheric moisture in a pseudo stochastic manner. Starting with an atmosphere that is too dry to drive deep convection, bottom-heavy vertical motion and shallow cumulus begin to moisten the atmosphere as moist packets of air leave the boundary layer in a buoyancy driven rise until they deposit their moisture through detrainment. When the free troposphere has moistened enough for moist plumes to reach from the surface to the upper troposphere, deep convection begins. As convection deepens and precipitation increases, a greater amount of moisture is needed to sustain the convection. Meanwhile, moisture and ice are building in the upper troposphere driving large radiational changes. When the convective forcing stops supplying an adequate supply of moisture for the ever increasing needs of deep convection, deep convection ceases and is replaced by very top-heavy stratiform vertical motion as the convective processes related to the moisture in the upper troposphere continue. As the moisture in the upper troposphere is no longer able to support stratiform convection we return to general descent and moistening of the boundary layer and lower troposphere by shallow cumulus. The balance between radiation and vertical advection leads to an overall redistribution of moisture and an adjustment of the MDC to be in line with the stability, however it does not lead to a large change in the overall moisture or MSE budget and thus does not amplify convection over longer time scales. Over shorter timescales, the imbalance between radiation and vertical advection may be essential to how convection behaves.

The first research chapter showed that the climatological top-heaviness is determined by the temperature profile through the stability mechanism, which is in turn influenced by the distribution of SST. The second chapter showed the profile of moisture is important to the profile of vertical motion and top-heaviness which can be explained by a process called vertically resolved moisture quasi-equilibrium. The third chapter presented a new kind of WTG equilibrium that demonstrates vertical moisture mode behavior. The rewards from the combined efforts of computation simulations, observational field work, and simple analytic modeling are two new analysis metrics, in the top-heaviness angle and MDC, a more extensive and cohesive explanation of the stability mechanism provided by the entraining plume model, and an explanatory framework for the evolution of vertical motion and moisture profiles in the form of VR-MQE.

5.2 Implications and Future Research

Vertical motion in the tropics is incredibly complicated and intersects with almost every aspect of the weather system. Disconnecting the vertical motion from this complicated mess of causation in order to constrain its behavior. While the research provided here helps to improve our understanding of vertical motion behavior, there is still much we do not understand and more research is needed. The research presented here provides an explanation for the controls of top-heaviness, but does not explicitly lay out a way to improve our representations of deep convection. The next steps are to establish that the controls of vertical motion presented are applicable in a broader context, investigate how

our current modeling efforts do not properly represent the processes of deep convection, and develop new parameterizations which are better suited.

The first step that is needed is a thorough investigation of the predictability and applicability of the MDC-II relationship, the relationship between the profile of moisture and vertical motion, and VR-MQE. The initial confirmation can be done simply by calculating the various metrics and checking the correlation between them and, if confirmed, further analysis looking at the differences between the good and bad representations across a range of data types and sets. Observational field campaign data provides the most accurate picture of the weather as it is taken in situ. Satellite and remote sensing products provide an excellent data source in terms of coverage and breadth, but have downsides including issues related to temporal and spatial extent and overlap. Reanalysis is also an excellent source of data in terms of coverage, however it is biased by the data that is assimilated. By computing and comparing the correlations between each of these data sources we can better understand what the current forecast models and GCMs do well and where they can be improved. In addition to showing where current models have poor realizations of convection, the research presented here can also be used to improve the convective parameterizations.

The simple two mode model presented in the third research chapter could be generalizable, which would provide a tremendously useful tool for predicting the behavior of vertical motion. The coefficients of the model represent the functional relationship between moisture and vertical motion of moist convection. For any given atmospheric state,

if the coefficients can be determined from the environmental conditions, beforehand, then the trajectory on the phase planes, and thus convective evolution, can be calculated and we have a, hopefully, simple parameterization of convection. This seems like a possibility because of the inherent geometry in the column integrated vertical advection, which is simply the inner product of vertical motion and the vertical derivative of moisture. How strongly the vertical derivative of moisture projects onto each mode, along with the strength of each mode, determines the advection by each mode. If we also decompose the moisture into a set of orthogonal modes, the vertical moisture advection is defined as a series of constants multiplied by the amplitude of the respective moisture and vertical motion modes. Depending on the construction of the modes that decompose the moisture, most of these could be small enough to ignore which would let us construct a limited set of solvable differential equations.

The research presented here was designed to ignore the diurnal cycle and to understand the variability in its absence. The WTG modeling that we conducted explicitly removed the diurnal cycle and the OTREC observational flights all occurred at the same time of day to remove diurnal variability. We can also establish if this framework performs for vertical motion over land where the diurnal cycle has a much greater impact, there are substantially more aerosols and cloud condensation nuclei, and the atmosphere is more often moisture limited. These differences lead to substantially faster vertical motion, among other differences, which VR-MQE would have to predict to be applicable over land. Both of these could be tested using analysis of field campaign or satellite data to confirm the correlations between the analysis metrics in order to see if they are consistent

or predictable. Additionally these could both be tested using the WTG framework, by modifying the surface conditions or adding a diurnal cycle and verifying that we can produce vertical motion profile shapes that are consistent with the real world and VR-MQE.

Another exciting possibility worth testing is the role of this process in tropical cyclogenesis. (Gjorgjievska and Raymond, 2014) used field campaign data to show that greater stability, associated with bottom-heavy vertical motion, led to intensification of the cyclone. The stability changes were due to a balanced potential vorticity response. VR-MQE can explain some parts of the process of cyclogenesis. As a convective MCS deepens, and vertical motion becomes more top-heavy, the level of the atmosphere where convergence is occurring rises higher into the atmosphere. Convergence acts on the ambient vorticity concentrating it closer to the storm, and like a ballerina tucking their arms, the spinning increases and a vorticity anomaly is generated at the mid-level. This vorticity anomaly pairs itself with a temperature anomaly to form the balanced potential vorticity response that occurs due to the thermal wind law. The temperature anomaly is a dipole with warming above the vorticity anomaly and cooling below, which acts to stabilize the atmosphere. VR-MQE hypothesizes that this temperature change leads to a change in the critical moisture profile, which leads the vertical motion to become bottom-heavy, which is essential for concentrating convergence near the surface in order to generate the surface cyclone which establishes the cyclone's fuel supply. This could be confirmed using a large data set of intensifying and non-intensifying tropical cyclones by looking to see how consistent this series of events is, whether there is a predictable critical moisture profile that

changes consistently, and finally if we can predict whether and how fast intensification will occur.

The periodic oscillation from the third research chapter still has many unanswered questions which could shed light on our ignorance of the real world. Which equilibrium will a WTG simulation fall into? Can this be determined before running the model? Are there more kinds of equilibria? Will a vertical decomposition of the moisture and vertical motion be able to describe the gamut of equilibria? How does periodic equilibrium relate to the dynamics of the real atmosphere? What are the necessary and sufficient conditions for the periodic oscillation to appear? What happens when we say periodic equilibrium into the mirror three times? All of these, save one which has been tested, need further investigation. They could be answered by developing the simple analytic model so that it will make a prediction about the equilibrium state of a WTG simulation and testing the prediction. If the functional relationship that is convection can be linearized and the coefficients of the simple model solved, the model should be able to capture the multiple equilibria behavior.

Appendix A

Plume Buoyancy Calculation

We calculate the buoyancy of the plume by assuming that the plume rises with the saturation moisture relative to its temperature. We start with the difference between the plume MSE, rising at saturation, and the plume saturation MSE:

$$h_p - h^*_{env} = c_p(T_p - T_{env}) + L_v(q^*_p - q^*_{env}) \tag{A.1}$$

The the p and env underscores denote the plume and environmental values.

The difference in saturation specific humidity values is a function of the difference in temperatures, which we can bring out by using a Taylor series approximation around the environmental saturation specific humidity, which we truncate after the second term:

$$q_p^* = q_{env}^* + (T_p - T_{env})\frac{(17.63 \cdot 243.0)}{(T_{env} + 243.0)^2} q_{env}^* \tag{A.2}$$

Here we have used the Magnus form approximation of the saturation vapor pressure in order to calculate the derivatives. We plug this approximation into the difference in equation (3) to get:

$$h_p - h_{env}^* = (T_p - T_{env}) \left(c_p + L_v q_{env}^* \frac{(17.63 \cdot 243.0)}{(T_{env} + 243.0)^2} \right) \tag{A.3}$$

The saturation MSE difference between the plume and the environment is directly correlated to the temperature difference, scaled by the factor in parenthesis on the right. As T gets small and qv^* goes to zero, this factor converges to the specific heat. At the higher values of T and qv^*, for instance a surface temperature of $30C^\circ$ and surface pressure of 1000 hPa, the factor has a value of 5x C_p, meaning the buoyancy due to the MSE difference is smaller at the surface than in the upper troposphere.

Bibliography

Abbott, T. H. and T. W. Cronin, 2021: Aerosol invigoration of atmospheric convection through increases in humidity. *Science*, **371**, 83–85, doi:10.1126/science.abc5181.

Adames, Á. F., 2017: Precipitation budget of the Madden-Julian oscillation. *Journal of the Atmospheric Sciences*, **74**, 1799–1817, doi:10.1175/JAS-D-16-0242.1.

— 2022: The Basic Equations under Weak Temperature Gradient Balance: Formulation, Scaling, and Types of Convectively-coupled Motions. *Journal of the Atmospheric Sciences*, **79**, 2087–2108, doi:10.1175/JAS-D-21-0215.1.

Adames, Á. F., D. Kim, S. K. Clark, Y. Ming, and K. Inoue, 2019: Scale analysis of moist thermodynamics in a simple model and the relationship between moisture modes and gravity waves. *Journal of the Atmospheric Sciences*, **76**, 3863–3881, doi:10.1175/JAS-D-19-0121.1.

Adames, Á. F., S. W. Powell, F. Ahmed, V. C. Mayta, and J. D. Neelin, 2021: Tropical Precipitation Evolution in a Buoyancy-Budget Framework. *Journal of the Atmospheric Sciences*, **78**, 509–528, doi:10.1175/JAS-D-20-0074.1.

URL https://journals.ametsoc.org/view/journals/atsc/78/2/jas-d-20-0074.1.xml

Adler, R. F., G. Gu, and G. J. Huffman, 2012: Estimating climatological bias errors for the global precipitation climatology project (gpcp). *Journal of Applied Meteorology and Climatology*, **51**, 84 – 99, doi:10.1175/JAMC-D-11-052.1.

URL https://journals.ametsoc.org/view/journals/apme/51/1/jamc-d-11-052.1.xml

Ahmed, F., J. David Neelin, and Á. F. Adames, 2021: Quasi-equilibrium and weak temperature gradient balances in an equatorial beta-plane model. *Journal of the Atmospheric Sciences*, **78**, 209–227, doi:10.1175/JAS-D-20-0184.1.

Ahmed, F. and J. D. Neelin, 2018: Reverse engineering the tropical precipitation-buoyancy relationship. *Journal of the Atmospheric Sciences*, **75**, 1587–1608, doi:10.1175/JAS-D-17-0333.1.

Anber, U., P. Gentine, S. Wang, and A. H. Sobel, 2015: Fog and rain in the Amazon. *Proceedings of the National Academy of Sciences of the United States of America*, **112**, 11473–11477, doi:10.1073/pnas.1505077112.

Andersen, J. A. and Z. Kuang, 2012: Moist static energy budget of MJO-like disturbances in the atmosphere of a zonally symmetric aquaplanet. *Journal of Climate*, **25**, 2782–2804, doi:10.1175/JCLI-D-11-00168.1.

Arakawa, A. and W. H. Schubert, 1974: Interaction of a Cumulus Cloud Ensemble with the Large-Scale Environment, Part I. *Journal of the Atmospheric Sciences*, **31**, 674–701, doi:10.1175/1520-0469(1974)031¡0674:IOACCE¿2.0.CO;2.

URL `http://journals.ametsoc.org/doi/10.1175/1520-0469(1974)031%3C0674:IOACCE%3E2.0.CO;2`

Back, L. E. and C. S. Bretherton, 2006: Geographic variability in the export of moist static energy and vertical motion profiles in the tropical Pacific. *Geophysical Research Letters*, **33**, 1–5, doi:10.1029/2006GL026672.

— 2009a: A simple model of climatological rainfall and vertical motion patterns over the tropical oceans. *Journal of Climate*, **22**, 6477–6497, doi:10.1175/2009JCLI2393.1.

— 2009b: On the relationship between SST gradients, boundary layer winds, and convergence over the tropical oceans. *Journal of Climate*, **22**, 4182–4196, doi:10.1175/2009JCLI2392.1.

Back, L. E., Z. Hansen, and Z. Handlos, 2017: Estimating Vertical Motion Profile Top-Heaviness: Reanalysis Compared to Satellite-Based Observations and Stratiform Rain Fraction. *Journal of the Atmospheric Sciences*, **74**, 855–864, doi:10.1175/jas-d-16-0062.1.

Bechtold, P., M. Köhler, T. Jung, F. Doblas-Reyes, M. Leutbecher, M. J. Rodwell, F. Vitart, and G. Balsamo, 2008: Advances in simulating atmospheric variability with the ecmwf model: From synoptic to decadal time-scales. *Quarterly Journal of the Royal*

Meteorological Society: A journal of the atmospheric sciences, applied meteorology and physical oceanography, **134**, 1337–1351.

Bernardez, M. and L. Back, 2023a: Environmental controls of vertical motion shape from OTREC observation, 1–12.

— 2023b: Integrating thermodynamic and dynamic views on the control of the top-heaviness of convection in the Pacific ITCZ with weak temperature gradient simulations, 1–33. doi:doi.org/10.1002/essoar.10512628.1.

— 2023c: On the controls of vertical motion top-heaviness, 1–33. doi:doi.org/10.1002/essoar.10512628.1.

Bony, S. and K. A. Emanuel, 2005: On the role of moist processes in tropical intraseasonal variability: Cloud-radiation and moisture-convection feedbacks. *Journal of the Atmospheric Sciences*, **62**, 2770–2789, doi:10.1175/JAS3506.1.

Bretherton, C. S., M. E. Peters, and L. E. Back, 2004: Relationships between water vapor path and precipitation over the tropical oceans. *Journal of Climate*, **17**, 1517–1528, doi:10.1175/1520-0442(2004)017¡1517:RBWVPA¿2.0.CO;2.

Charney, J. G., 1963: A note on large-scale motions in the tropics. *Journal of the Atmospheric Sciences*, **20**, 607–609.

Chou, M.-D. and M. J. Suarez, 1999: A solar radiation parameterization for atmospheric studies. Technical report.

Ciesielski, P. E., H. Yu, R. H. Johnson, K. Yoneyama, M. Katsumata, C. N. Long, J. Wang, S. M. Loehrer, K. Young, S. F. Williams, et al., 2014: Quality-controlled upper-air sounding dataset for dynamo/cindy/amie: Development and corrections. *Journal of Atmospheric and Oceanic Technology*, **31**, 741–764.

Dai, A., 2006: Precipitation characteristics in eighteen coupled climate models. *Journal of Climate*, **19**, 4605–4630, doi:10.1175/JCLI3884.1.

Dai, A. and C. E. Bloecker, 2019: Impacts of internal variability on temperature and precipitation trends in large ensemble simulations by two climate models. *Climate dynamics*, **52**, 289–306.

Daleu, C. L., R. S. Plant, S. J. Woolnough, S. Sessions, M. J. Herman, A. Sobel, S. Wang, D. Kim, A. Cheng, G. Bellon, P. Peyrille, F. Ferry, P. Siebesma, and L. Van Ulft, 2015: Intercomparison of methods of coupling between convection and large-scale circulation: 1. Comparison over uniform surface conditions. *Journal of Advances in Modeling Earth Systems*, **7**, 1576–1601, doi:10.1002/2015MS000468.

Duffy, M. L., P. A. O'Gorman, and L. E. Back, 2020: Importance of Laplacian of Low-Level Warming for the Response of Precipitation to Climate Change over Tropical Oceans. *Journal of Climate*, **33**, 4403–4417, doi:10.1175/JCLI-D-19-0365.1. URL `https://journals.ametsoc.org/jcli/article/33/10/4403/345259/Importance-of-Laplacian-of-LowLevel-Warming-for`

Edman, J. P. and D. M. Romps, 2015: Self-consistency tests of large-scale dynamics parameterizations for single-column modeling. *Journal of Advances in Modeling Earth*

Systems, **7**, 320–334, doi:10.1002/2014MS000378.

URL https://onlinelibrary.wiley.com/doi/10.1002/2014MS000378

Emanuel, K. and F. Zhang, 2016: On the predictability and error sources of tropical cyclone intensity forecasts. *Journal of the Atmospheric Sciences*, **73**, 3739 – 3747, doi:https://doi.org/10.1175/JAS-D-16-0100.1.

URL https://journals.ametsoc.org/view/journals/atsc/73/9/jas-d-16-0100.1.xml

Fuchs, Ž. and D. J. Raymond, 2007: A simple, vertically resolved model of tropical disturbances with a humidity closure. *Tellus A: Dynamic Meteorology and Oceanography*, **59**, 344–354, doi:10.1111/j.1600-0870.2007.00230.x.

URL https://www.tandfonline.com/doi/full/10.1111/j.1600-0870.2007.00230.x

Fuchs-Stone, Ž., D. J. Raymond, and S. Sentić, 2020: OTREC2019: Convection Over the East Pacific and Southwest Caribbean. *Geophysical Research Letters*, **47**, 0–2, doi:10.1029/2020GL087564.

URL https://onlinelibrary.wiley.com/doi/10.1029/2020GL087564

Gjorgjievska, S. and D. J. Raymond, 2014: Interaction between dynamics and thermodynamics during tropical cyclogenesis. *Atmospheric Chemistry and Physics*, **14**, 3065–3082, doi:10.5194/acp-14-3065-2014.

Hagos, S., C. Zhang, W. K. Tao, S. Lang, Y. N. Takayabu, S. Shige, M. Katsumata, B. Olson, and T. L'ecuyer, 2010: Estimates of tropical diabatic heating profiles: Commonalities and uncertainties. *Journal of Climate*, **23**, 542–558, doi:10.1175/2009JCLI3025.1.

Handlos, Z. J. and L. E. Back, 2014: Estimating vertical motion profile shape within tropical weather states over the oceans. *Journal of Climate*, **27**, 7667–7686, doi:10.1175/JCLI-D-13-00602.1.

Herman, M. J. and D. J. Raymond, 2014: WTG cloud modeling with spectral decomposition of heating. *Journal of Advances in Modeling Earth Systems*, **6**, 1121–1140, doi:10.1002/2014MS000359.

Hernandez-Duenas, G., L. M. Smith, and S. N. Stechmann, 2019: Weak- and strong-friction limits of parcel models: Comparisons and stochastic convective initiation time. *Quarterly Journal of the Royal Meteorological Society*, **145**, 2272–2291, doi:10.1002/qj.3557.

Hersbach, H., P. Bell, B. Berrisford, G. Biavati, A. Horányi, J. Muñoz Sabater, J. Nicolas, C. Peubey, R. Radu, I. Rozum, D. Schepers, A. Simmons, C. Soci, D. Dee, and J.-N. Thépaut, 2019a: Era5 monthly averaged data on pressure levels from 1979 to present. copernicus climate change service (c3s) climate data store (cds). Accessed: 2019-06.

— 2019b: Era5 monthly averaged data on pressure levels from 1979 to present. copernicus climate change service (c3s) climate data store (cds). Accessed: 2019-06.

— 2019c: Era5 monthly averaged data on single levels from 1959 to present. copernicus climate change service (c3s) climate data store (cds). Accessed: 2019-06.

Iacono, M. J., J. S. Delamere, E. J. Mlawer, M. W. Shephard, S. A. Clough, and W. D. Collins, 2008: Radiative forcing by long-lived greenhouse gases: Calculations with the aer radiative transfer models. *Journal of Geophysical Research: Atmospheres*, **113**.

Inoue, K., A. F. Adames, and K. Yasunaga, 2020a: Vertical Velocity Profiles in Convectively Coupled Equatorial Waves and MJO : New Diagnoses of Vertical Velocity Profiles in the Wavenumber-Frequency Domain.

Inoue, K., Á. F. Adames, and K. Yasunaga, 2020b: Vertical velocity profiles in convectively coupled equatorial waves and mjo: New diagnoses of vertical velocity profiles in the wavenumber–frequency domain. *Journal of the Atmospheric Sciences*, **77**, 2139–2162.

Inoue, K. and L. Back, 2015a: Column-integrated moist static energy budget analysis on various time scales during TOGA COARE. *Journal of the Atmospheric Sciences*, **72**, 1856–1871, doi:10.1175/JAS-D-14-0249.1.

Inoue, K. and L. E. Back, 2015b: Gross moist stability assessment during TOGA COARE: Various interpretations of gross moist stability. *Journal of the Atmospheric Sciences*, **72**, 4148–4166, doi:10.1175/JAS-D-15-0092.1.

— 2017: Gross Moist Stability Analysis: Assessment of Satellite-Based Products in the GMS Plane. *Journal of the Atmospheric Sciences*, **74**, 1819–1837, doi:10.1175/JAS-D-16-0218.1.

URL http://journals.ametsoc.org/doi/10.1175/JAS-D-16-0218.1

Inoue, K., M. Biasutti, and A. M. Fridlind, 2020c: Evidence that horizontal moisture advection regulates the ubiquitous amplification of rainfall variability over tropical oceans. *Journal of the Atmospheric Sciences*, 1–19, doi:10.1175/JAS-D-20-0201.1.

URL https://journals.ametsoc.org/doi/10.1175/JAS-D-20-0201.1

Johnson, R. H. and P. E. Ciesielski, 2000: Rainfall and radiative heating rates from toga coare atmospheric budgets. *Journal of the atmospheric sciences*, **57**, 1497–1514.

— 2013: Structure and properties of madden–julian oscillations deduced from dynamo sounding arrays. *Journal of the Atmospheric Sciences*, **70**, 3157–3179.

Kang, S. M., D. M. Frierson, and I. M. Held, 2009: The tropical response to extratropical thermal forcing in an idealized GCM: The importance of radiative feedbacks and convective parameterization. *Journal of the Atmospheric Sciences*, **66**, 2812–2827, doi:10.1175/2009JAS2924.1.

Khouider, B. and A. J. Majda, 2006: A Simple Multicloud Parameterization for Convectively Coupled Tropical Waves. Part I: Linear Analysis. *Journal of the Atmospheric Sciences*, **63**, 1308–1323, doi:10.1175/JAS3677.1.

URL https://journals.ametsoc.org/doi/10.1175/JAS3833.1https://journals.ametsoc.org/doi/10.1175/JAS3677.1

Klemp, J. B., J. Dudhia, and A. D. Hassiotis, 2008: An upper gravity-wave absorbing layer for nwp applications. *Monthly Weather Review*, **136**, 3987 – 4004, doi:https://doi.org/10.1175/2008MWR2596.1.

URL https://journals.ametsoc.org/view/journals/mwre/136/10/2008mwr2596.1.xml

Kuang, Z., 2008: A moisture-stratiform instability for convectively coupled waves. *Journal of the Atmospheric Sciences*, **65**, 834–854, doi:10.1175/2007JAS2444.1.

Lin, J. and K. Emanuel, 2022: Stratospheric Modulation of the MJO through Cirrus Cloud Feedbacks. *Journal of the Atmospheric Sciences*, 1–30, doi:10.1175/jas-d-22-0083.1.

Lindzen, R. S. and S. Nigam, 1987: On the Role of Sea Surface Temperature Gradients in Forcing Low-Level Winds and Convergence in the Tropics. *Journal of the Atmospheric Sciences*, **44**, 2418–2436, doi:10.1175/1520-0469(1987)044¡2418:otross¿2.0.co;2.

López Carrillo, C. and D. J. Raymond, 2011: Retrieval of three-dimensional wind fields from Doppler radar data using an efficient two-step approach. *Atmospheric Measurement Techniques*, **4**, 2717–2733, doi:10.5194/amt-4-2717-2011.

URL https://amt.copernicus.org/articles/4/2717/2011/

Madden, R. A. and P. R. Julian, 1971: Detection of a 40–50 day oscillation in the zonal wind in the tropical pacific. *Journal of Atmospheric Sciences*, **28**, 702–708.

Maithel, V. and L. Back, 2022: Moisture recharge–discharge cycles: A gross moist stability–based phase angle perspective. *Journal of the Atmospheric Sciences*, **79**, 2401–2417.

Maloney, E. D., A. Gettelman, Y. Ming, J. Davidneelin, D. Barrie, A. Mariotti, C. C. Chen, D. R. Coleman, Y. H. Kuo, B. Singh, H. Annamalai, A. Berg, J. F. Booth, S. J. Camargo, A. Dai, A. Gonzalez, J. Hafner, X. Jiang, X. Jing, D. Kim, A. Kumar, Y. Moon, C. M. Naud, A. H. Sobel, K. Suzuki, F. Wang, J. Wang, A. A. Wing, X. Xu, and M. Zhao, 2019: Process-oriented evaluation of climate and weather forecasting models. *Bulletin of the American Meteorological Society*, **100**, 1665–1686, doi:10.1175/BAMS-D-18-0042.1.

Mapes, B. E., 1993: Gregarious tropical convection. *Journal of Atmospheric Sciences*, **50**, 2026–2037.

Mapes, B. E., E. S. Chung, W. M. Hannah, H. Masunaga, A. J. Wimmers, and C. S. Velden, 2018: The Meandering Margin of the Meteorological Moist Tropics. *Geophysical Research Letters*, **45**, 1177–1184, doi:10.1002/2017GL076440.

Masunaga, H., C. E. Holloway, H. Kanamori, S. Bony, and T. H. M. Stein, 2021: Transient Aggregation of Convection: Observed Behavior and Underlying Processes. *Journal of Climate*, **34**, 1685–1700, doi:10.1175/JCLI-D-19-0933.1.

URL `https://journals.ametsoc.org/view/journals/clim/34/5/JCLI-D-19-0933.1.xml`

Masunaga, H. and T. S. L'Ecuyer, 2014: A mechanism of tropical convection inferred from observed variability in the moist static energy budget. *Journal of the Atmospheric Sciences*, **71**, 3747–3766, doi:10.1175/JAS-D-14-0015.1.

Masunaga, H. and B. E. Mapes, 2020: A mechanism for the maintenance of sharp tropical margins. *Journal of the Atmospheric Sciences*, **77**, 1181–1197, doi:10.1175/JAS-D-19-0154.1.

Matsui, T., W. Tao, and R. Shi, 2007: Goddard radiation and aerosol direct effect in goddard wrf. *NASA/UMD WRF Workshop*.

Mayta, V. C., Á. F. Adames, and F. Ahmed, 2022: Westward-Propagating Moisture Mode Over the Tropical Western Hemisphere. *Geophysical Research Letters*, **49**, 1–10, doi:10.1029/2022GL097799.

Morrison, H., G. Thompson, and V. Tatarskii, 2009: Impact of cloud microphysics on the development of trailing stratiform precipitation in a simulated squall line: Comparison of one-and two-moment schemes. *Monthly weather review*, **137**, 991–1007.

Neelin, J. D. and I. M. Held, 1987: Modeling Tropical Convergence Based on the Moist Static Energy Budget. **115**, 3–12, doi:10.1175/1520-0493(1987)115¡0003:MTCBOT¿2.0.CO;2.

Neogi, S. and M. S. Singh, 2022: Understanding Changes in the Tropical Circulation under Global Warming Using a Cloud-Resolving Model and a Conceptual Model. *Journal of Climate*, **35**, 5855–5868, doi:10.1175/JCLI-D-21-0854.1.

North, G. R., T. L. Bell, R. F. Cahalan, and F. J. Moeng, 1982: Sampling Errors in the Estimation of Empirical Orthogonal Functions. *Monthly Weather Review*, **110**, 699–706, doi:10.1175/1520-0493(1982)110¡0699:SEITEO¿2.0.CO;2.

URL http://journals.ametsoc.org/doi/10.1175/1520-0493(1982)110%3C0699:SEITEO%3E2.0.CO;2

Peters, M. E. and C. S. Bretherton, 2006: Structure of tropical variability from a vertical mode perspective. *Theoretical and Computational Fluid Dynamics*, **20**, 501–524, doi:10.1007/s00162-006-0034-x.

Raymond, D. J., 2000: Thermodynamic control of tropical rainfall. *Quarterly Journal of the Royal Meteorological Society*, **126**, 889–898, doi:10.1002/qj.49712656406.

URL http://adsabs.harvard.edu/cgi-bin/nph-data_query?bibcode=2000QJRMS.126..889R&link_type=EJOURNAL%5Cnpapers2://publication/doi/10.1002/qj.49712656406

Raymond, D. J. and M. M. Flores, 2016: Predicting convective rainfall over tropical oceans from environmental conditions. *Journal of Advances in Modeling Earth Systems*, **8**, 703–718, doi:10.1002/2013MS000595.

Raymond, D. J., Ž. Fuchs, S. Gjorgjievska, and S. L. Sessions, 2015: Balanced dynamics and convection in the tropical troposphere. *Journal of Advances in Modeling Earth Systems*, **7**, 1093–1116, doi:10.1002/2013MS000467.

Raymond, D. J. and Fuchs-Stone, 2021: Weak Temperature Gradient Modeling of Convection in OTREC. *Journal of Advances in Modeling Earth Systems*, **13**, doi:10.1029/2021MS002557.

Raymond, D. J., G. S, S. S, F. Z, S. Gjorgjievska, and S. Sessions, 2014: Tropical Cyclogenesis and Mid-Level Vorticity. *Australian Meteorological and Oceanographic Journal*, **64**, 1–30.

Raymond, D. J. and S. L. Sessions, 2007: Evolution of convection during tropical cyclogenesis. *Geophysical Research Letters*, **34**, 1–11, doi:10.1029/2006GL028607.

Raymond, D. J., S. L. Sessions, A. H. Sobel, and Ž. Fuchs, 2009: The Mechanics of Gross Moist Stability. *Journal of Advances in Modeling Earth Systems*, **1**, n/a–n/a, doi:10.3894/james.2009.1.9.

Raymond, D. J. and X. Zeng, 2005: Modelling tropical atmospheric convection in the context of the weak temperature gradient approximation. *Quarterly Journal Of The Royal Meteorological Society*, **131**, 1301–1320, doi:10.1256/qj.03.97.
URL `http://doi.wiley.com/10.1256/qj.03.97%5Cnpapers2://publication/doi/10.1256/qj.03.97`

Riehl, H., 1950: On the role of the tropics in the general circulation of the atmosphere. *Tellus*, **2**, 1–17.

Riehl, H. and J. S. Malkus, 1958: On the heat balance of the equatorial trough zone. *Geophysica*, **6**, 503–538.

Romps, D. M., 2014: An analytical model for tropical relative humidity. *Journal of Climate*, **27**, 7432–7449, doi:10.1175/JCLI-D-14-00255.1.

— 2021: Ascending columns, WTG, and convective aggregation. *Journal of the Atmospheric Sciences*, **78**, 497–508, doi:10.1175/JAS-D-20-0041.1.

Romps, D. M. and Z. Kuang, 2010: Do undiluted convective plumes exist in the upper tropical troposphere? *Journal of the Atmospheric Sciences*, **67**, 468–484.

Romps, D. M. and R. Öktem, 2015: Stereo photogrammetry reveals substantial drag on cloud thermals. *Geophysical Research Letters*, **42**, 5051–5057, doi:10.1002/2015GL064009.

Rui, L. and F. Yunfei, 2005: Tropical precipitation estimated by gpcp and trmm pr observations. *Advances in atmospheric Sciences*, **22**, 852–864.

Schiro, K. A. and J. D. Neelin, 2019: Deep convective organization, moisture vertical structure, and convective transition using deep-inflow mixing. *Journal of the Atmospheric Sciences*, **76**, 965–987, doi:10.1175/JAS-D-18-0122.1.

Schumacher, C., R. A. Houze, and I. Kraucunas, 2004: The tropical dynamical response to latent heating estimates derived from the TRMM precipitation radar. *Journal of the Atmospheric Sciences*, **61**, 1341–1358, doi:10.1175/1520-0469(2004)061¡1341:TTDRTL¿2.0.CO;2.

Sentić, S., P. Bechtold, v. Fuchs-Stone, M. Rodwell, and D. J. Raymond, 2022: On the impact of dropsondes on the ecmwf integrated forecasting system model (cy47r1)

analysis of convection during the otrec (organization of tropical east pacific convection) field campaign. *Geoscientific Model Development*, **15**, 3371–3385, doi:10.5194/gmd-15-3371-2022.

URL https://gmd.copernicus.org/articles/15/3371/2022/

Sentić, S. and S. L. Sessions, 2017: Idealized modeling of convective organization with changing sea surface temperatures using multiple equilibria in weak temperature gradient simulations. *Journal of Advances in Modeling Earth Systems*, **9**, 1431–1449, doi:10.1002/2016MS000873.

URL https://onlinelibrary.wiley.com/doi/10.1002/2016MS000873

Sentić, S., S. L. Sessions, and Ž. Fuchs, 2015: Diagnosing DYNAMO convection with weak temperature gradient simulations. *Journal of Advances in Modeling Earth Systems*, **7**, 1849–1871, doi:10.1002/2015MS000531.

URL http://doi.wiley.com/10.1002/2015MS000531

Sessions, S. L., M. J. Herman, and S. Sentić, 2015: Convective response to changes in the thermodynamic environment in idealized weak temperature gradient simulations. *Journal of Advances in Modeling Earth Systems*, **7**, 712–738, doi:10.1002/2013MS000282.Received.

Sessions, S. L., S. Sentic, and M. J. Herman, 2016: The role of radiation in organizing convection in weak temperature gradient simulations. *Journal of Advances in Modeling Earth Systems*, **8**, 244–271, doi:10.1002/2015MS000587.

Sessions, S. L., S. Sentić, and D. J. Raymond, 2019: Balanced Dynamics and Moisture Quasi-Equilibrium in DYNAMO Convection. *Journal of the Atmospheric Sciences*, **76**, 2781–2799, doi:10.1175/jas-d-18-0173.1.

Sessions, S. L., S. Sugaya, D. J. Raymond, and A. H. Sobel, 2010: Multiple equilibria in a cloud-resolving model using the weak temperature gradient approximation. *Journal of Geophysical Research*, **115**, D12110, doi:10.1029/2009JD013376.
URL `http://www.agu.org/pubs/crossref/2010/2009JD013376.shtml`

Sherwood, S. C., S. Bony, and J. L. Dufresne, 2014: Spread in model climate sensitivity traced to atmospheric convective mixing. *Nature*, **505**, 37–42, doi:10.1038/nature12829.

Shi, J. J., W.-K. Tao, T. Matsui, R. Cifelli, A. Hou, S. Lang, A. Tokay, N. Wang, C. Peters-Lidard, G. Skofronick-Jackson, et al., 2010: Wrf simulations of the 20–22 january 2007 snow events over eastern canada: Comparison with in situ and satellite observations. *Journal of Applied Meteorology and Climatology*, **49**, 2246–2266.

Singh, M. S. and S. Neogi, 2022: On the Interaction between Moist Convection and Large-Scale Ascent in the Tropics. *Journal of Climate*, **35**, 4417–4435, doi:10.1175/JCLI-D-21-0717.1.

Singh, M. S. and P. A. O'Gorman, 2013: Influence of entrainment on the thermal stratification in simulations of radiative-convective equilibrium. *Geophysical Research Letters*, **40**, 4398–4403, doi:10.1002/grl.50796.

Singh, M. S., R. A. Warren, and C. Jakob, 2019a: A Steady-State Model for the Relationship Between Humidity, Instability, and Precipitation in the Tropics. *Journal of Advances in Modeling Earth Systems*, **11**, 3973–3994, doi:10.1029/2019MS001686.

— 2019b: A Steady-State Model for the Relationship Between Humidity, Instability, and Precipitation in the Tropics. *Journal of Advances in Modeling Earth Systems*, **11**, 3973–3994, doi:10.1029/2019MS001686.

Skamarock, W. C., J. B. Klemp, J. Dudhia, D. O. Gill, D. M. Barker, M. G. Duda, X.-Y. Huang, W. Wang, and J. G. Powers, 2008: A Description of the Advanced Research WRF Version 3. Technical report, University Corporation for Atmospheric Research, note NCAR/TN-468+ STR.

Sobel, A. H., G. Bellon, and J. Bacmeister, 2007: Multiple equilibria in a single-column model of the tropical atmosphere. *Geophysical Research Letters*, **34**, 1–5, doi:10.1029/2007GL031320.

Sobel, A. H. and C. S. Bretherton, 2000: Modeling tropical precipitation in a single column. *Journal of Climate*, **13**, 4378–4392, doi:10.1175/1520-0442(2000)013¡4378:MTPIAS¿2.0.CO;2.

Sobel, A. H. and J. D. Neelin, 2006: The boundary layer contribution to intertropical convergence zones in the quasi-equilibrium tropical circulation model framework. *Theoretical and Computational Fluid Dynamics*, **20**, 323–350, doi:10.1007/s00162-006-0033-y.

Sobel, A. H., J. Nilsson, and L. M. Polvani, 2001: The Weak Temperature Gradient Approximation and Balanced Tropical Moisture Waves*. *Journal of the Atmospheric Sciences*, **58**, 3650–3665, doi:10.1175/1520-0469(2001)058¡3650:TWTGAA¿2.0.CO;2.

Tiedtke, M., 1993: Representation of clouds in large-scale models. *Monthly Weather Review*, **121**, 3040–3061.

Tompkins, A. M., 2001: Organization of tropical convection in low vertical wind shears: The role of cold pools. *Journal of the atmospheric sciences*, **58**, 1650–1672.

Wang, S. and A. H. Sobel, 2012: Impact of imposed drying on deep convection in a cloud-resolving model. *Journal of Geophysical Research Atmospheres*, **117**, 1–14, doi:10.1029/2011JD016847.

Wang, S., A. H. Sobel, and Z. Kuang, 2013: Cloud-resolving simulation of TOGA-COARE using parameterized large-scale dynamics. *Journal of Geophysical Research Atmospheres*, **118**, 6290–6301, doi:10.1002/jgrd.50510.

Wang, S., A. H. Sobel, and J. Nie, 2016: Modeling the MJO in a cloud-resolving model with parameterized large-scale dynamics: Vertical structure, radiation, and horizontal advection of dry air. *Journal of Advances in Modeling Earth Systems*, **8**, 121–139, doi:10.1002/2015MS000529.

Yanai, M., S. Esbensen, and J.-H. Chu, 1973: Determination of Bulk Properties of Tropical Cloud Clusters from Large-Scale Heat and Moisture Budgets. *Journal of the Atmospheric Sciences*, **30**, 611–627, doi:10.1175/1520-0469(1973)030¡0611:DOBPOT¿2.0.CO;2.

Yasunaga, K., S. Yokoi, K. Inoue, and B. E. Mapes, 2019: Space-time spectral analysis of the moist static energy budget equation. *Journal of Climate*, **32**, 501–529, doi:10.1175/JCLI-D-18-0334.1.